

# IWT SBO PROJECT 120003 “SEARCH”

## Archaeological heritage in the North Sea

Development of an efficient assessment methodology and approach towards a sustainable management policy and legal framework in Belgium.

### *Archeologisch erfgoed in de Noordzee*

*Ontwikkeling van een efficiënte evaluatiemethodologie en voorstellen tot een duurzaam beheer in België.*



## Scientific results on (sub-) seafloor offshore imaging

### WP 1.3.4

Responsible partners: UG-RCMG, Deltares

Authors: O. Zurita Hurtado, T. Missiaen

June 2016

## Contents

|   |    |
|---|----|
| 1. Introduction.....  | 3  |
| 2. Technical Specifications.....  | 4  |
| 2.1. <i>Seismic Sources</i> .....   | 4  |
| 2.2. <i>Receivers</i> .....   | 5  |
| 2.3. <i>Data acquisition</i> .....  | 7  |
| 2.4. <i>Data processing</i> .....   | 8  |
| 3. Test sites and field work summary .....  | 10 |
| 4. Tests results .....  | 13 |
| 4.1. <i>Comparative tests of different seismic sources at the Ostend Valley</i> ..... | 13 |
| 4.1.1. <i>Single-channel data results</i> .....                                       | 15 |
| 4.1.2. <i>Multi-channel data results</i> .....  | 22 |
| 4.2. <i>Comparative tests of different seismic sources at the Thornton Bank</i> ..... | 27 |
| 4.2.1. <i>Single-channel data results</i> .....                                       | 28 |
| 4.3 <i>Gas research - Zeebrugge Valley</i> .....                                      | 31 |
| 4.3.1. <i>Test results</i> .....  | 32 |
| 4.4. <i>Gas research – Ostend Valley long offset tests</i> .....                      | 38 |
| 4.4.1. <i>Long offset principle and problems</i> .....                                | 38 |
| 4.4.2 <i>Long offset test results</i> .....   | 42 |
| 5. Summary.....   | 56 |
| 6. References .....   | 57 |
| Appendix A (Technical specifications on the seismic sources used) .....               | 58 |
| Appendix B (SC data demultiple results) .....   | 61 |
| Appendix C (Navigations systems specifications) .....                                 | 65 |

## 1. Introduction

In the framework of the SEARCH project more than 1300 km of 2D high and very high resolution seismic reflection data have been acquired in the Belgian part of the North Sea. The purpose of these seismic investigations was twofold: (1) to test different seismic source and receiver combinations for their suitability in the detection and identification of buried palaeo-landscapes, and (2) to assess the archaeological potential of the Quaternary deposits in the Belgian part of the North Sea.

Marine seismic imaging is an ideal tool to obtain detailed information of the subsurface below the seafloor. Due to its accuracy and resolving power, seismic methods have increasingly become a major investigation tool in marine archaeological studies. Until now, however, no efficient survey methodology exists that is particularly aimed at archaeological assessment studies. Standard geophysical techniques, such as marine seismic reflection, are mainly used on an *ad hoc* basis (if at all) and these techniques are often not well adapted for archaeological investigations. Moreover these acoustic techniques are ineffective in large parts of the nearshore zone due to the presence of biogenic gas in the sediments (areas of fast accumulation of fine-grained muddy sediments rich in organic matter provide ideal environments for the production of this biogenic methane), and generally cannot be applied appropriately in intertidal areas.

The main goal of this work package WP1.3.4 is to supply a flexible, generic acoustic survey methodology through the comparison of different high-resolution seismic source/receiver configurations in different geological settings of the Belgian Continental Shelf (BCS). This should allow a cost-efficient and accurate assessment of the archaeological potential of the seafloor and sub-seafloor environment. In this specific work package we focus on 2D seismic techniques for the offshore and nearshore area.

## 2. Technical Specifications

The main objective of very high resolution (VHR) seismic investigations is to image the shallow sedimentary sequence (in the range of 100 metres below the seafloor) with the highest possible detail. One of the main requirements for successful VHR seismic imaging is a high vertical resolution. The latter has implications for the type of seismic source that is used.

### 2.1. Seismic Sources

Seismic sources can be classified on the basis of the frequencies and strengths of the emitted acoustic energy. These two parameters affect the performance of the instrument, which is largely defined by the (vertical) resolution and penetration depth of the signal into the seafloor.

The resolution is the ability to differentiate closely spaced layers (or objects) and is mostly dependent on the frequency content of the signal. In general, low frequency sources like (air- or water-) guns have a low vertical resolution (> 5m) but can penetrate several hundred meters and more into the seafloor. Medium frequency sources like boomers or sparker can penetrate to depths of a few tens of metres up to a hundred meters with a relative good resolution (0.5 to 5m). Finally, high frequency sources like pingers, chirps and echosounders provide detailed information (< 0.5m) of the shallow subsurface down to a few tens of meters below the seafloor.

The signal repeatability of the source will also have an effect on the vertical resolution. A seismic event can be identified more reliably from one trace to another and its location in time or depth becomes less ambiguous as the acoustic pulse becomes more repeatable. Sparker sources generally have a relatively low repeatability, whereas boomers and transducer sources (Chirp, echosounder) have a good repeatability.

Penetration, on the other hand, is controlled by the strength of the emitted signal. Increasing the power of the acoustic signal allows for greater penetration into the substrate. Penetration depth is also affected by the type of sediments present at the seafloor. In general, penetration increases for soft sediments as silts and clays but decreases for hard(er) and coarse sediments like sands and gravels. Increasing the energy of the source when working in areas with a sandy seafloor is counterproductive because it causes more acoustic signal to be reflected back off the seafloor, leading to unwanted noise in the data.

A total of eleven different seismic sources were tested for the project, covering a range of frequencies as wide as possible. Four sources belong to UGent-RCMG: SIG sparker 1200, UGent-RCMG's in-house developed Centipede sparker, IKB Seistec boomer, and Kongsberg Geopulse echosounder; four sources appertain to Deltares: I/O Sleeve gun, Design Projects 300J boomer, Design Projects 500J boomer, and Edgetech X-Star chirp; two sources were made available by Geophysical Services Offshore NV (GSO): Geo-Source 200 sparker and GSO 360 sparker; and one source was supplied by the University of Delft (TUDelft): Innomar SES-2000 parametric echosounder. An overview of the different sources is given in Table 1.

|    | Seismic Source                 | Frequency Range (Hz) | Vertical resolution (m) | Penetration (m) |
|----|--------------------------------|----------------------|-------------------------|-----------------|
| 1  | I/O Sleeve gun-IB              | 150-250              | > 1                     | < 1000          |
| 2  | SIG sparker 1200               | 800 – 900            | > 0.50                  | < 200           |
| 3  | Geo-Source 200 sparker         | 800 – 1200           | < 0.50                  | < 200           |
| 4  | GSO 360 sparker                | 800 – 1200           | < 0.50                  | < 200           |
| 5  | RCMG Centipede sparker         | 1000 – 1200          | > 0.35                  | < 50            |
| 6  | IKB-Seistec boomer             | 1000 – 5000          | > 0.25                  | < 20            |
| 7  | Design Projects 500J boomer    | 1000 – 4000          | > 0.35                  | < 50            |
| 8  | Design Projects 300J boomer    | 3500 – 7000          | > 0.25                  | < 30            |
| 9  | Kongsberg Geopulse pinger      | 3500                 | > 0.25                  | < 50            |
| 10 | Edgetech X-Star chirp          | 500 – 12000          | > 0.20                  | < 15            |
| 11 | Innomar parametric echosounder | 6000 – 12000         | > 0.15                  | < 15            |

*Table 1 – Comparative table of the performance of the seismic sources used (for more information on each source see Appendix A)*

## **2.2. Receivers**

The acoustic energy generated by the seismic sources (and reflected by the seabed and sub bottom layers) was recorded with two different receivers (streamer or receiver cables) simultaneously, a single-channel (SC) streamer and a multi-channel (MC) streamer. The SC streamer consists of a number of closely spaced hydrophones grouped into one channel that generate one summed (stacked) signal per shot. The MC streamer comprises an array of receiver channels (each comprising a number of closely spaced hydrophones) that are separated by a fixed distance (in our case 3,125 m). One shot is represented by a series of signals (traces) equalling the number of receiver channels in the array (shot gather). Shooting several times along a profile will generate a set of shot gathers.

|                      | No. of channels | Hydrophones per group | Distance between hydrophones | Distance between channels |
|----------------------|-----------------|-----------------------|------------------------------|---------------------------|
| SIG SC streamer      | 1               | 10                    | 30 cm                        | N.A.                      |
| Teledyne MC streamer | 24 / 48         | 4                     | 40 cm                        | 3.125m                    |

*Table 2 – Comparative table of the performance of the receivers used*

Single-channel data involve relatively low processing requirements and therefore offer a rapid way to image the structure of the substrate beneath the seafloor at a relative low cost. However, these data often present a low signal-to-noise ratio, which may lead to misinterpretation or simply to the impossibility to interpret the data. Advanced processing techniques can be applied in order to improve the quality of the data but because of the intrinsic nature of the single-channel system not all processing techniques are effective.

In multi-channel data the different traces belonging to the same common subsurface location of a defined bin-size will be summed up (i.e. stacked), which results in a better signal-to-noise ratio compared to single-channel data. However, for the stacking to be advantageous the signal needs to be repeatable (if this is not the case the signal-to-noise ratio will not improve and it may even deteriorate). Additionally, the positions of the source and receivers must be known accurately for correct calculation of the common reflection points. Multi-channel data involve more advanced processing (and therefore higher costs), and as a consequence has only recently started to be used in shallow surveys. Additionally, in busy waterways the use of a long multi-channel streamer can be very difficult.

The ability of a streamer for correct and accurate imaging of the subsurface structures with the highest possible lateral and vertical resolution depends on several parameters. However we will focus on three in particular:

a) Streamer depth

The streamer is towed at a fixed depth behind the vessel. The deeper the streamer is towed, the greater the immunity to swell and ambient noise. However, deep towing the streamers enhances the low frequencies but attenuates the high frequencies due to the constructively or destructively interference between the ghost reflections (the result of reflections from the sea surface) with the primary reflections. On the contrary, when the streamer is towed at shallow depths it boosts the high-end frequency content needed for high resolution but attenuates the low-end frequency content required for deep penetration. Shallow towing also makes the seismic data susceptible to swell noise.

b) Distance between channels

The horizontal resolution of the seismic section and the capacity of imaging dipping reflectors depends on the distance between channels of the streamer cable. This distance has to be decided depending on the maximum expected reflector dip, the velocity of the propagating media and the maximum desired recoverable frequency. This relation can be summarized by the following expression

$$F_{max} = \frac{v}{2d_x \sin(\theta)}$$

where  $F_{max}$  is the maximum recorded frequency without spatial aliasing,  $d_x$  is the distance between channels,  $\vartheta$  is the dip of the reflector and  $v$  is the velocity of the medium. The steeper the dip or the bigger the distance between channels, the lower the frequency at which spatial aliasing occurs. Spatial aliasing has serious effects on the performance of multi-channel processes such as  $f - k$  filtering and migration. Because of spatial aliasing, these processes can perceive events with steep dips at high frequencies as different from what they actually are and, hence, do not treat them properly.

c) Maximum cable length

The maximum offset should be as large as possible to aid velocity analysis and multiple attenuation. At the same time, it must be small enough so that the most important reflection arrives just below the mute zone applied during processing (see tests below). Additionally, it must be small enough to avoid wide angle reflection distortions (reflections with angle of incidence near or greater the critical angle). As a rule of thumb, the distance between the source and the furthest receiver's should be equal to that of the target's depth.

### 2.3. Data acquisition

Data acquisition took place on board of the RV Belgica and the RV Simon Stevin. Both vessels are well equipped to carry out shallow geophysical investigations. The draught of the vessels however does not allow to deploy them in very shallow waters (< 5 m). The vessels sailed on electrical propulsion to reduce the amount of acoustic noise introduced by the engine and the speed of the vessels was kept between 3 and 4 knots.

The sleeve gun, sparker and boomer sources were towed behind the vessels. The parametric echosounder and the Geopulse pinger were attached to a specifically designed mounting pole at the port side of the vessel, while the X-star chirp was towed along the starboard side of the ship (see Figure 1). The streamers were towed behind the vessel. The single-channel streamer was towed at port side whereas the multi-channel streamer was positioned in the middle or at starboard side of the stern. Relevant data was recorded simultaneously with both streamers and when possible different sources were used at the same time.

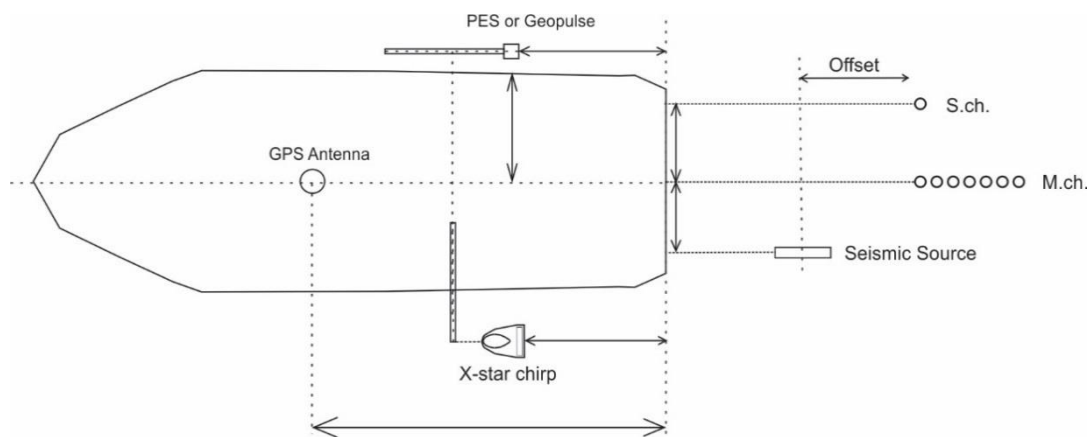


Figure 1 – Sketch of the vessel illustrating the equipment configuration.  
SC = Single-channel streamer; MC = Multi-channel streamer.

All navigation information was obtained from the vessel's navigation systems. Navigation log files contained GPS position and UTC time for each field record. On the RV Belgica, positioning was acquired with two built-in GNSS (Global Navigation Satellite System) receivers:

- MGBTECH with SEPTENTRIO AsteRx2eH RTK heading receiver (cm accuracy)
- Furuno GP-150 EGNOS DGPS receiver (m accuracy (relative: 1m, absolute: 5m))

On the RV Simon Stevin, positioning was acquired using:

- MGBTECH RTK GPS (cm accuracy)
- DGPS JRC JLR 7800 (m accuracy (relative: 1m, absolute: 5m))

Technical specifications of these systems can be found in Appendix C.

All single-channel data (sleeve gun, sparkers, boomers and pinger) were recorded using UGent-RCMG's DELPH seismic analogue acquisition unit; all multi-channel data (sleeve gun, sparkers and boomers) were recorded using Deltares' Geometrics Geode system. Chirp and parametric echosounder were recorded using their own built-in recording system. The data were recorded in standard SEG-Y format (except for the parametric echosounder which uses its own (SES) data format). Only times, not coordinates, were input into the SEG-Y trace headers. Data quality was monitored during acquisition on the data acquisition PC.

## 2.4. Data processing

The **single-channel data** was processed with *Deco Geophysical* seismic processing software *RadExPro* using the following flow:

1. Common Mid-Point (CMP) binning – Navigation information is added to the seismic data. In this project, all the navigation information corresponded to the x and y positions of the GPS of the vessel. Source and receivers were assumed to lie at a constant distance on a linear path behind the vessel allowing us to calculate the source, receiver and reflection point locations in a simple way. The error introduced by this assumption is minimal and avoids placing extra positioning systems on the actual streamer (which would increase costs significantly)
2. Data editing – noisy and/or dead traces are edited or simply deleted.
3. Deconvolution – signal wavelet is compressed in order to increase resolution.
4. Noise Attenuation – removal of noisy frequencies.
5. Seabed picking - the seafloor reflector was highlighted and the arrival time stored in order to be used by other processes such as muting, swell correction, tidal corrections, multiple attenuation, etc.
6. Swell correction – A swell filter was applied to attenuate heave effects. This helps to flatten the seabed and the subsequent horizons.
7. High amplitude noise attenuation – removal of local narrow frequency band noises observed as vertical stripes on the seismic record.
8. Spatial noise removal – removal of side scattered noise and spatially random noise.
9. Amplitude correction – gain was applied to increase the amplitudes of the data at greater depth (later arrivals) when compared to the earlier arrivals.
10. Multiple attenuation – Multiples are delayed reflections that interfere with the “primary” reflections we want to image. The delay occurs because the reflection energy has taken a more complex and longer ray path from source to receiver, reverberating between two layers that are highly reflective. While any two layers with high reflectivity can create a multiple, in general it is energy reverberating in the water column (i.e. between the seafloor and the sea surface) that is the most important (so-called seafloor multiple). In single-channel data, seafloor multiple reflections are quite strong due to the incapacity of these systems to discriminate between events based on their arrival time or direction of arrival. When working in very shallow water, they hide primary reflections and therefore it is desirable to attenuate them as much as possible. Advanced processing techniques can be applied in order to improve the quality of the data and overcome some of these issues but because of the intrinsic nature of the single-channel system most demultiple techniques are not as efficient on SC data as on MC data.
11. Muting – Data above water bottom was removed.
12. Tidal correction – tidal changes introduce time variant shifts to the seismic trace that need to be corrected.
13. Data archive – data was exported in SEG-Y format so it could be later read on most interpretation software's.

**Multi-channel data** was processed with the same software using the following flow (some processing steps are common to both acquisition geometries and are indicated below with a \*)

1. Common Mid-Point binning – navigation information for each source, channel and reflection location are calculated from the supplied x and y positions of the GPS of the vessel. Source and receivers were assumed to lie at a constant distance on a linear path behind the vessel.
2. Data editing \*
3. Deconvolution \*
4. Noise Attenuation \*
5. High amplitude noise attenuation \*
6. Velocity analysis every 250 CDP's – creates a model of the seismic velocities in the sub-surface. It is performed in the CDP domain, where the assumption of hyperbolic move-out of reflections is often reasonable. The aim of the velocity analysis is to find the velocity that flattens a reflection hyperbola and thus provides the best result when stacking is applied (Yilmaz, 2001).

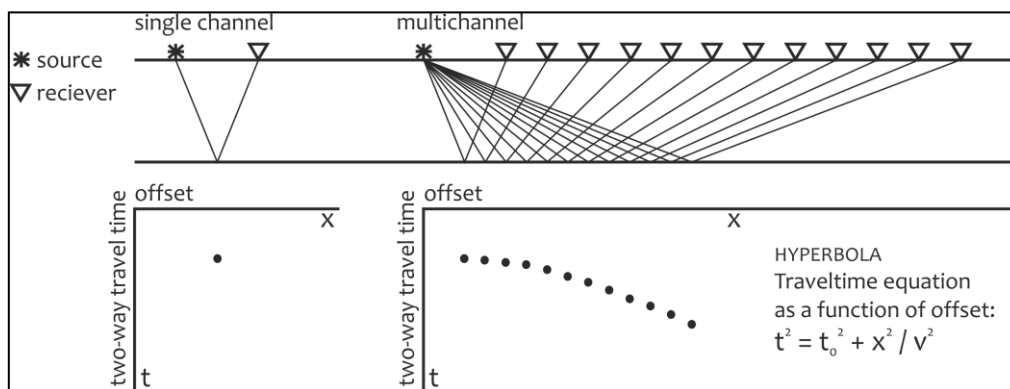


Figure 22 – The two-way travel times of a horizontal reflection in single-channel and multi-channel seismic data recording (after Toth, 2013)

7. Data sorting – sort the data from common shot point (CSP) to common midpoint (CMP) gathers.
8. Normal move-out (NMO) correction – When the distance between the source and receiver increases, the travel time also increases. On the seismogram the effect of this delay in travel time is visible as a hyperbolic curve. The NMO correction is applied to correct for this effect.
9. Muting – Frequency distortion occurs as a result of NMO correction, particularly at shallow depths and large source-receiver offsets. A stretch mute is applied (manually picked or based on angle of reflection) to remove sections that are affected by NMO stretching.
10. Stacking – All the traces from the same common midpoint (CMP) are summed up into one trace, generating a pseudo zero-offset section (similar to the one obtained with a single-channel streamer).
11. Spatial noise removal \*
12. Amplitude correction \*
13. Multiple attenuation \*
14. Muting \*
15. Tidal correction \*
16. Data archive \*

### 3. Test sites and field work summary

Several test sites were selected for this study. The selection was based on different criteria such as availability of information and in-situ ground-truth data, expected archaeological features and economic importance. In total, five main test sites were chosen: (1) Ostend Valley: buried river valley, potential for prehistoric habitation, sand extraction area; (2) Thornton Bank: numerous archaeological finds, windfarm area; (3) Vlakte van de Raan: drowned islands at the mouth of the Scheldt estuary; (4) Yser Valley: small buried river valley well known onshore but location unknown offshore; and (5) Middle and Offshore platforms, suspected fluvial sediments on the Middle and Offshore Scarp, presumed to be ancient river terraces from the Meuse and Rhine rivers.

Data acquisition took place during five campaigns:

#### 1) October 2013 (7 - 9)

Conducted on board of the RV Simon Stevin, this survey covered the Ostend Valley located 10 km offshore the city of Ostend (Figure 2). The water depth of the study area ranges from 5 to 15m, with the lowest value corresponding to sandbanks. The goal of the survey was to obtain more precise information on the complex geological layering of the Ostend Valley. A test line that crossed the entire width of the valley was therefore defined. Seismic profiles were obtained over the same line using seven different seismic sources (Centipede sparker, SIG sparker, Seistec boomer, 300J boomer, X-Star chirp, Geopulse pinger and parametric echosounder); data were recorded with a single-channel (SC) streamer and a 24 channel MC streamer simultaneously. The seismic campaign had to be stopped after three days because of bad weather. For more details on this campaign, we refer to report SBO120003\_WP1.2.3\_A.

#### 2) April 2014 (22 - 25)

Carried out on board of the RV Belgica, the survey focused on the Thornton area, roughly 30-50 km offshore of Zeebrugge (Figure 2). The main objective of the survey was to perform conventional seismic profiling in order to obtain more precise information on the geological layering of the areas around the Thornton and the Northern Valley, as well as the connection between these two valleys. The water depth in the area ranges from 10 to 30m. A test line that crossed the entire width of the Thornton Bank was defined. This test line was covered using four different seismic sources (SIG sparker, Centipede sparker, Seistec boomer and Parametric Echosounder) and the goal was to test different sources and receiver configurations in order to image the structure of the sandbank. Data was recorded with a single-channel and a 12 channel MC streamer simultaneously. Unfortunately, the MC streamer was defective and half of channels did not record any data. For more details on this campaign, we refer to report SBO120003\_WP1.2.3\_C.

#### 3) May 2014 (12 - 16)

Conducted on board of the RV Simon Stevin, the study area covered two different valley structures, the Ostend Valley and the Yser Valley (Figure 2). The latter is a smaller valley to the west of the Ostend Valley near the Belgian-French border. The area had a low density of seismic lines and therefore the main goal of the survey was to perform conventional seismic profiling to complete the existing seismic database. Additionally, further tests were performed on the test line defined during the 2013 campaign in order to compare with the sources already tested. The water depth in the surveyed area ranges from 5 to 15m. Different seismic sources were used during the campaign: Centipede sparker, SIG sparker, 500J boomer, Geopulse and Parametric Echosounder. Data was recorded with two different streamers simultaneously (a SC streamer and a 24 channel MC streamer). In addition to the seismic equipment, a Hydrochart was used. This device is a combination of multibeam and side-scan sonar to image the seafloor and objects. For more details on this campaign, we refer to report SBO120003\_WP1.2.3\_B.

#### 4) March 2015 (23 - 27)

Conducted on board of the RV Belgica, the study covered the area between the Ostend Valley (offshore the city of Ostend) and the Vlakte van de Raan (near the Dutch border). The water depth of the study area ranges from 5 to 10m. In total, more than 120km of 2D high resolution seismic reflection data were acquired during this survey using five different seismic sources: (1) Sleeve gun, (2) Centipede sparker, (3) SIG sparker, (4) Geo-Source 200 sparker and (5) GSO 360 sparker. When applicable, two different types of receivers were used to register the data; a single-channel streamer (SC) and a multi-channel streamer (MC; 48 channels).

During this campaign, special attention was paid to areas known for the presence of biogenic gas in the subsurface. The main goal was to test the capacity of different seismic equipment to penetrate the gassy sediments and image the shallow layers as well as the top-Palaeogene surface and the underlying Tertiary deposits. The shallow gas tests were carried out in three different zones, respectively located on the western and eastern side of the harbour of Zeebrugge and in a deeper part of the Ostend Valley (so-called Sepia Pits). In the latter location long-offset acquisition configurations were tested using two vessels simultaneously, one vessel acting as source vessel (RV Belgica) and the other as receiver vessel (RV Simon Stevin), resulting in offsets of more than 300 meters. The idea behind these long-offset test was to image the sediments below the gas horizon.

In addition, a couple of profiles were recorded over the test line across the Ostend Valley using two different seismic sources that hadn't been tested previously, the Sleeve gun and the Geo-Source 200 sparker. This brings the total number of acoustic sources tested on this line to ten. For more details on this campaign, we refer to report SBO120003\_WP1.2.3\_E.

#### 5) April 2015 (13 - 17)

During this campaign a total of 395 kilometres of 2D high resolution seismic reflection data were acquired in the central part of the Belgian Continental Shelf (so-called Middle and Offshore Platforms). The survey was conducted on board of the RV Simon Stevin. The water depth in the area ranges from 10 to 30m. Only one seismic source was used during the whole survey, the GSO 360 sparker. The main objective of this campaign was to survey areas of the BCP with low or poor seismic coverage where ancient river terraces from the Meuse and Rhine rivers are suspected to be present. For more details on this campaign, refer to report SBO120003\_WP1.2.3\_F

#### 6) May 2016 (09 - 13)

During this campaign a total of 408 kilometres of 2D high resolution seismic reflection data were acquired in the northern and north-western part of the Belgian Continental Shelf. The survey was conducted on board of the RV Simon Stevin. The water depth in the area ranges from 20 to 40m. Only the GSO 360 sparker and the SIG sparker were used during the survey. The main objective of this campaign was to survey areas of the BCP with scarce seismic coverage. This area is believed to be strongly influenced by fluvial processes by the Rhine and the Meuse during periods of lower sea-level. It is these depositional environments of specifically the last ice age that have been preserved. For more details on this campaign, refer to report SBO120003\_WP1.2.3\_G

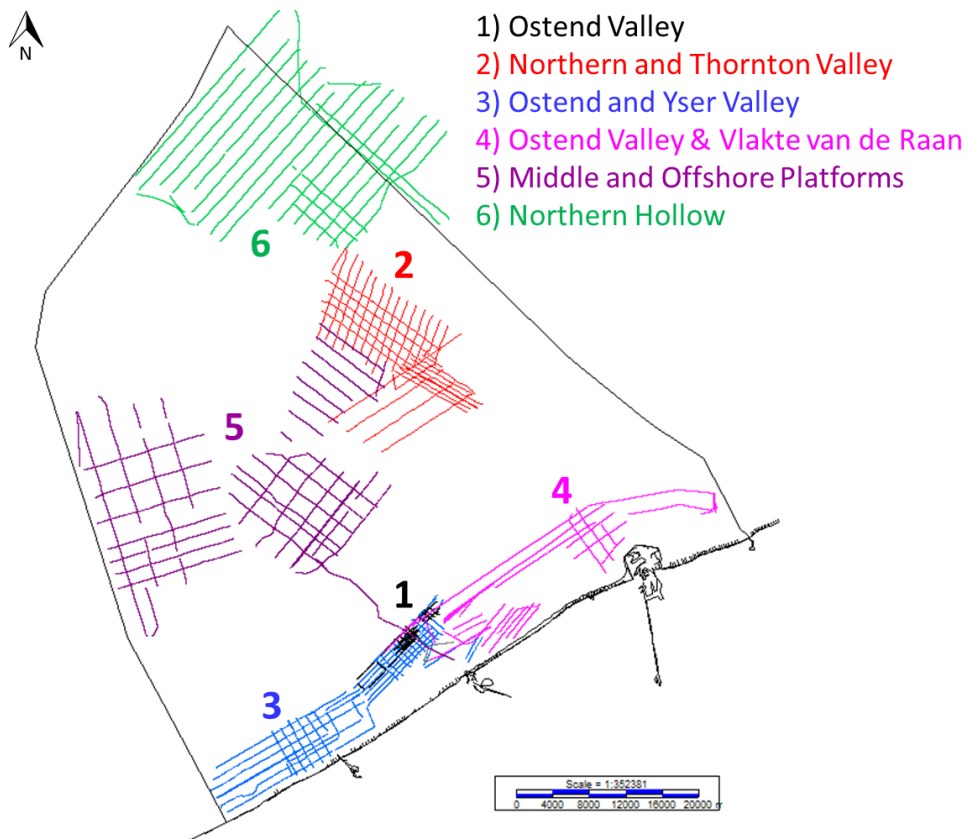


Figure 3 – Location of the different offshore seismic campaigns

## 4. Tests results

### 4.1. Comparative tests of different seismic sources at the Ostend Valley

One of the main focuses of the project was to investigate buried river valleys. It is well known that early humans often established their settlements next to rivers as the latter are fertile areas providing drinking water, food, and material for tools (stones, pebbles). One of the major buried river valleys of the Belgian Continental Shelf (BCS) is the Ostend Valley. It consists of a buried fluvio-tidal channel partially covered by a large sandbank (Figure 4). It started as a small river valley during the Saalian. When the sea level rose during the Eemian, the river valley evolved into an open estuary, where coastal and tidal forces reshaped it into the funnel-shaped valley we know today. During the Weichselian ice age, sea-level dropped, producing further fluvial incisions, wind activity increased and earlier fluvial sediments accumulated in the form of sand ridges that eventually damned the valley more inland, thereby redirecting the river to its current flow more to the north. During the subsequent Holocene sea-level rise the valley got buried beneath tidal and marine sediments, including several large sandbanks (Mathys, 2009).

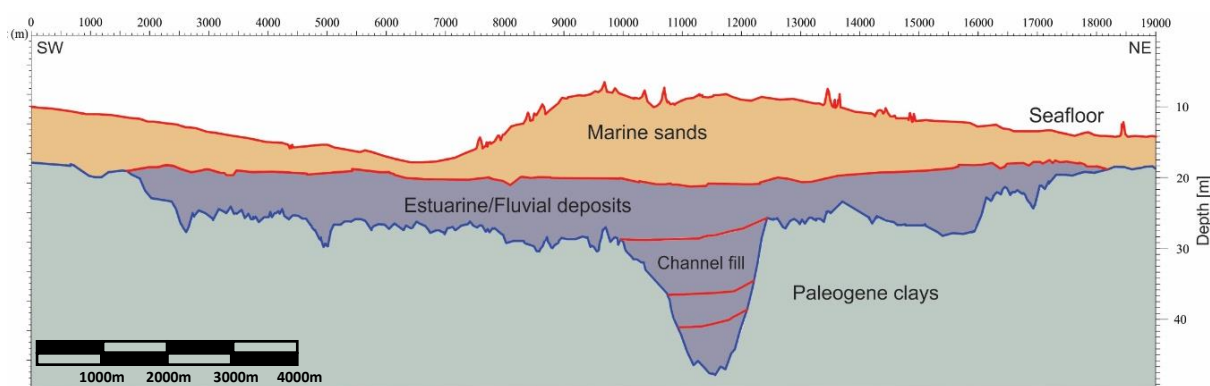


Figure 4 – Geological cross section of the Ostend Valley (adapted from Mathys, 2009).

We defined a 10km test line that crossed the entire width at the central part of the valley at one of its deepest locations. Here the valley is covered by a large tidal sandbank (Figure 5). Such sandbanks are a common feature on the BCS. From a geophysical point of view, this setting represents a big challenge because the short wavelength sound waves are quickly absorbed in the heterogeneous coarse sandy sediments of the sandbank. This results in a fast decrease in penetration depth impeding accurate imaging of the deposits below. Furthermore, the sandy seafloor often induces strong multiples that obscure the data, especially in shallow water depths (5-10m).

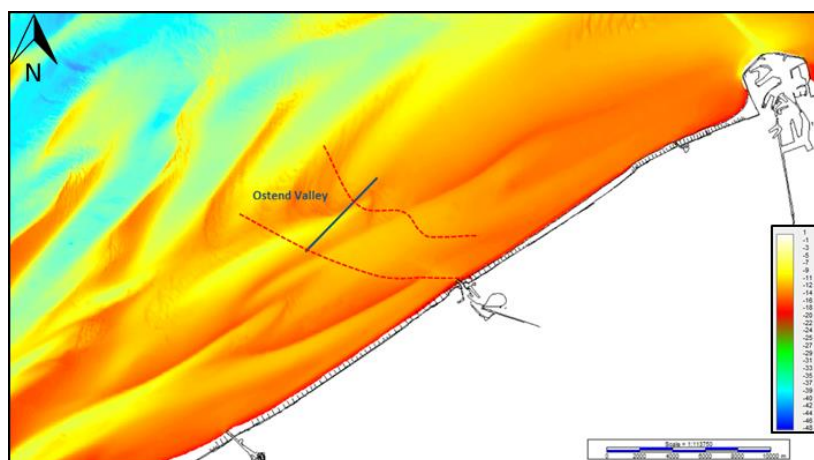


Figure 5 – Location of the test line (in black) across the Ostend Valley (De Clercq, 2015). The red dashed line marks the approximate valley boundaries. Background map is the current seafloor bathymetry (colour scale in metres).

The test line was surveyed using ten different seismic sources (Sleeve gun, SIG sparker, Geo-Source 200 sparker, Centipede sparker, Seistec boomer, 300J boomer, 500J boomer, Geopulse, X-Star chirp and parametric echosounder (PES)) and recorded with a single-channel (SC) and a multi-channel (MC) (24 channels) streamer. All recorded profiles followed the same track line in order to allow for optimal comparison between the different datasets. Maximum lateral deviation between different profiles was not bigger than 100m. Some profiles are slightly shorter due to systems failures during recording or the presence of navigational obstructions (e.g. passing vessels). More acquisition details are summarized in the table below.

| Source            | Date       | Shot interval (sec) | Sailing direction | Energy   | Wind (knt) | Wave height* |
|-------------------|------------|---------------------|-------------------|----------|------------|--------------|
| Sleeve gun        | 24/03/2015 | 2                   | NE-SW             | 10 cu.in | 3-4        | 50 cm        |
| SIG sparker       | 08/10/2013 | 0.5                 | NE-SW             | 300 J    | 3-4        | 30 cm        |
| Geo-Source 200    | 24/03/2015 | 1                   | SW-NE             | 1000 J   | 4-5        | 60 cm        |
| Centipede sparker | 07/10/2013 | 0.5                 | SW-NE             | 300 J    | 2-3        | 40 / 50 cm   |
| Seistec Boomer    | 07/10/2013 | 0.5                 | NE-SW             | 300 J    | 2-3        | 40 cm        |
| 300J boomer       | 07/10/2013 | 1                   | NE-SW             | 300 J    | 2-3        | 30 / 40 cm   |
| 500J boomer       | 13/05/2014 | 0.5                 | SW-NE             | 300 J    | 2-3        | 60 cm        |
| Geopulse          | 08/10/2013 | 0.5                 | SW-NE             | N.A.     | 3-4        | 40 cm        |
| X-Star chirp      | 07/10/2013 |                     | NE-SW             | N.A.     | 2-3        | 30 / 40 cm   |
| PES               | 07/10/2013 |                     | SW-NE             | N.A.     | 2-3        | 30 / 40 cm   |

*Table 3 – Acquisition parameters of the test lines across the Ostend Valley (1 knt =1.852 km/hour)  
\*wave height measurement obtained from pile Westhinder. Source: VLIZ <http://www.vliz.be/>.*

It can be observed that for all the test lines, despite having been acquired on different dates over a period of two years, weather conditions were fairly similar and relatively good (30 to 60cm wave height). The performance of the seismic systems is strongly dependent on the weather and sea state conditions (waves, wind) during the acquisition. In general, seismic surveys are planned to be acquired in calm weather in order to reduce the amount of noise recorded. When wave height exceeds 1m the data quality is considerably deteriorated. However, some sources perform better than others during relatively bad weather conditions (50 to 100cm wave height). For example, due to their strong directivity, boomer sources are more affected than sparkers by the sea state.

Streamers are also influenced by weather conditions. All seismic streamers are subject to significant mechanically-induced noise originating from wave and swell effects. Conventional fluid filled streamers are more sensitive to the weather and wave noise than modern solid filled streamers. Fluid filled streamers are filled with a fluid (often a hydrocarbon derivative) to provide positive buoyancy for the cable. In a solid streamer the buoyancy fluid is replaced by buoyant flexible polymer, usually either polyethylene or polyurethane based (Dowle, 2006). As a consequence, the hydrophones are isolated from the central strain member minimizing vibration noise from wave and swell effects and mechanical towing equipment. In typical fluid and gel streamers the hydrophone is coupled to the strain members and is therefore subject to vibration noise. During this project conventional fluid filled streamers were used.

#### 4.1.1. Single-channel data results

The resulting seismic profiles for single-channel data are displayed in figures 7 to 16. Data is ordered based on its frequency content, from low to high. Horizontal scale is in meters and vertical scale is in milliseconds (two-way traveltimes; 10ms equals roughly 7.5m). Given that in some cases the demultiple algorithm slightly attenuated primary reflectors that occur at roughly the same time as the seafloor multiple, we have chosen to display the data without any demultiple applied. Demultiple results are described in detail later in this section (Figure 17) and in Appendix B.

Figure 6 illustrates the geological complexity of the Ostend Valley. Apart from the seafloor (in blue), the most prominent reflectors are the Top-Palaeogene boundary (in red), the top of the valley (in yellow), the valley infillings (in green) and the internal layering of the sandbank (in orange). Other reflectors might be observable and have been identified as back-barrier deposits (in purple).

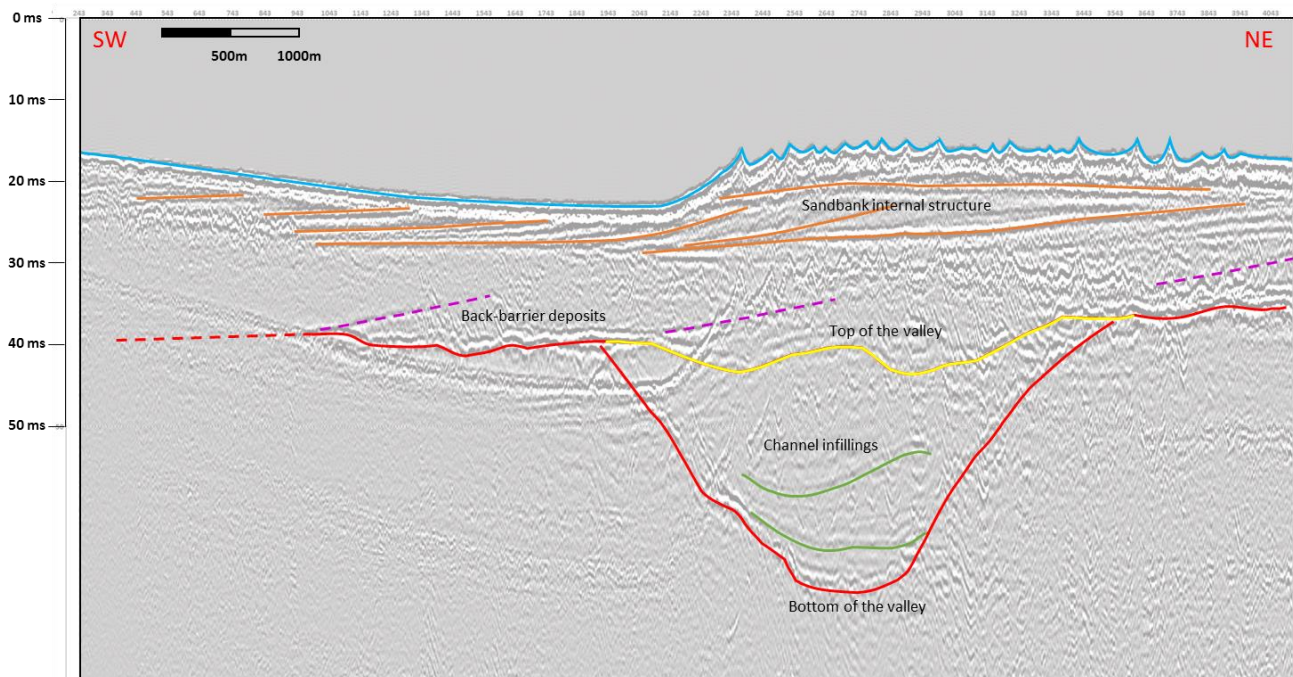


Figure 6 – Geological interpretation of the Ostend Valley at the test line location

Data displayed below was processed following the processing flow explained in Section 2.4.

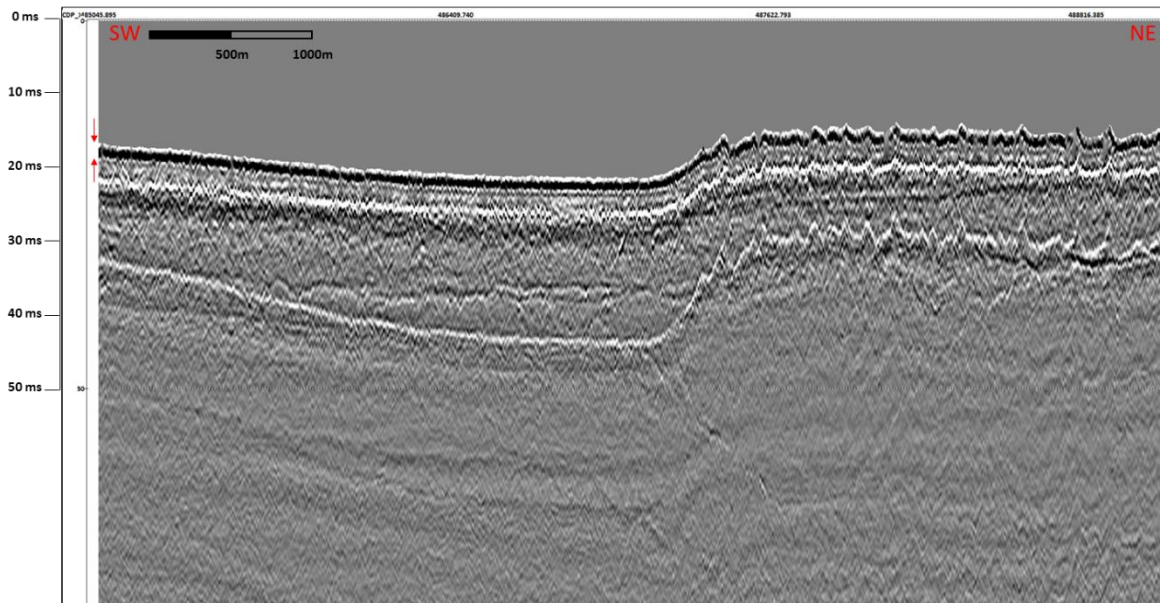


Figure 7 – Sleeve gun profile, test line across the Ostend Valley.

The sleeve gun (Figure 7) shows a relatively short wavelet (see red arrows on the top left) that produced fairly sharp images of the deeper buried reflectors. However, it failed at imaging very shallow reflectors, largely due to the strong and thick water bottom reflector. This effect is caused by the bubble pulses that come from the expansion-collapse cycle of the generated air bubble. This cycle occurs just after the initial air release and causes interferences with the primary pulse. Thus, air-guns do not provide ideal sound pulses (i.e. a single spike) as explosives can do. This unwanted effect can be minimized by firing several guns at the same time. The use of multiple guns cause destructive interference of bubble pulses and minimize the bubble effect.

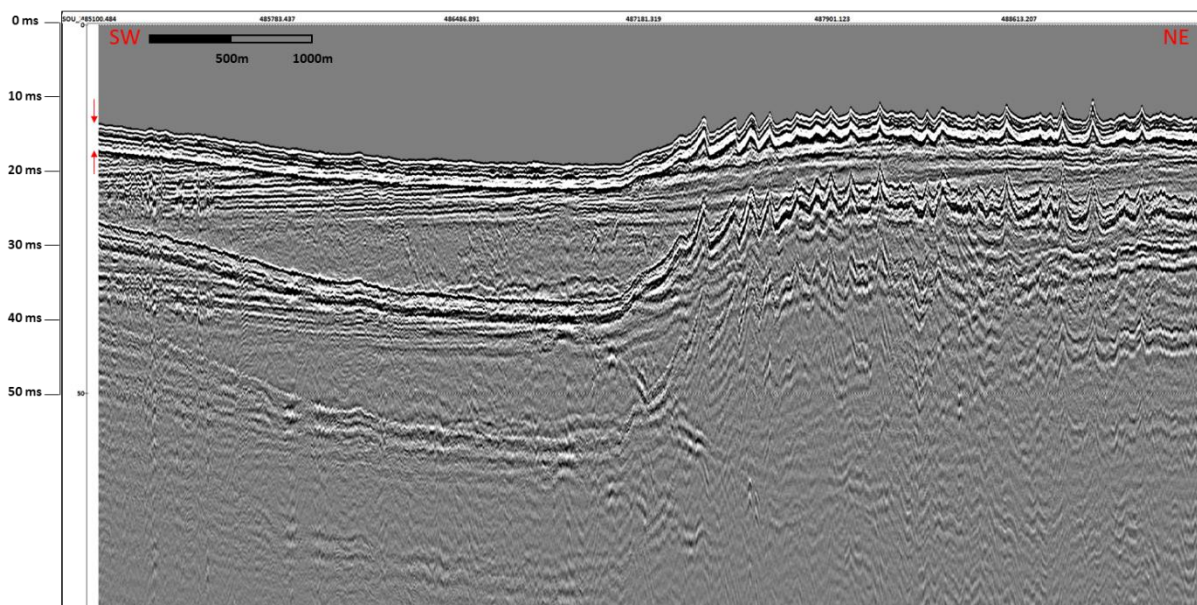


Figure 8 –SIG sparker profile, test line across the Ostend Valley.

The SIG sparker (Figure 8) shows a strong and coarse signal (see red arrows). As a consequence, very shallow events are obscured and/or indistinguishable and seafloor multiples are very thick. Internal layering within the channel is blurred and the bottom of the valley is difficult to interpret. Overall the SIG sparker shows acceptable penetration of investigation but poor resolution.

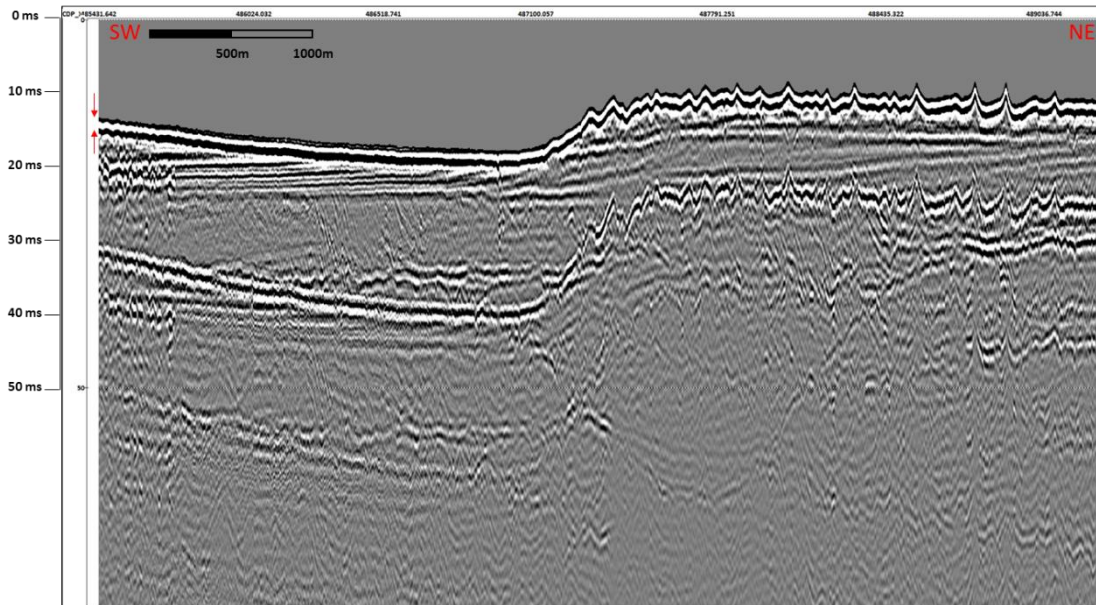


Figure 9 – Geo-Source 200 sparker profile, test line across the Ostend Valley.

The Geo-Source 200 sparker (Figure 9) presents a relatively short signal (see red arrows) producing sections with good resolution throughout the whole profile. Shallow reflectors are very clear and distinctive. It also shows good penetration depth. The bottom of the valley, as well as its flanks, is clearly recognisable. Internal reflectors within the channel are also well defined although they show rather weak energy.

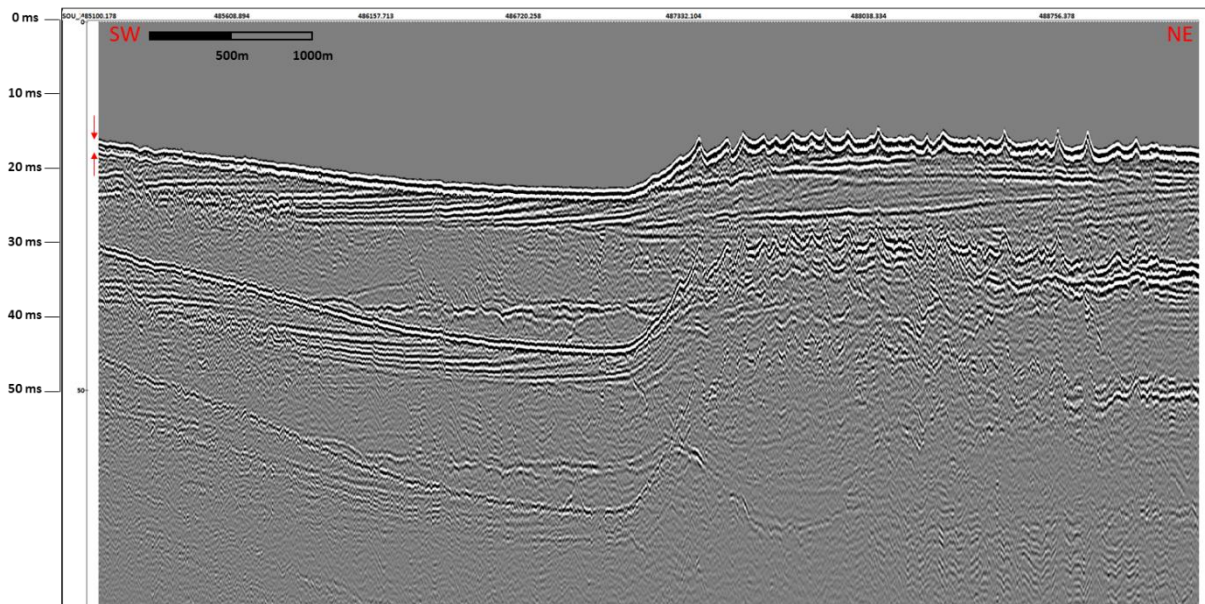


Figure 10 – Centipede sparker profile, test line across the Ostend Valley.

Overall, the Centipede sparker (Figure 10) shows the best resolution and penetration trade-off of all tested sources. Its short source signal (see red arrows) results in a high vertical resolution of the shallow reflectors in the range of 1-2 meters. The signal penetration is high and allows imaging the bottom of the valley as well as its internal reflectors. The only downside is the resolution of the flanks of the channel which is not as good as the resolution obtained with the Geo-Source 200 sparker.

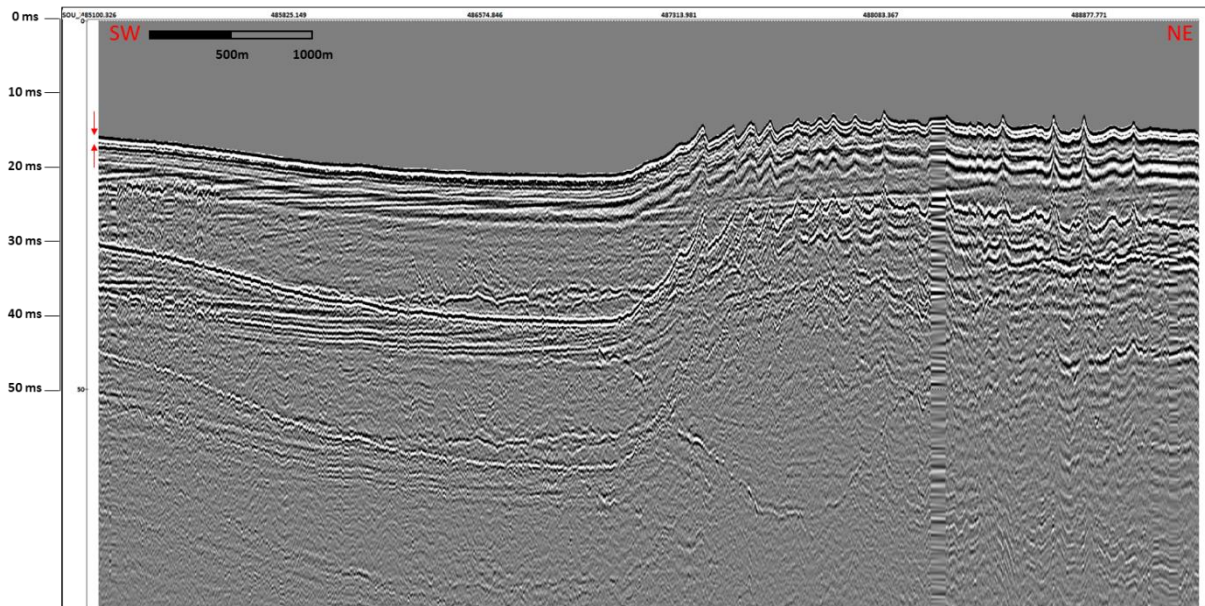


Figure 11 –Seistec boomer profile, test line across the Ostend Valley.

The Seistec boomer (Figure 11) shows a very short and sharp signal (see red arrows) as well as good penetration depth. Resolution of the deeper part of the profile is very good, but the resolution of the very shallow reflectors is very poor, mainly because they are obscured by ringing on the water bottom reflector. This ringing might be caused by the use of the streamer as recording system instead of the system’s internal line-in-cone hydrophone receiver array. However when the internal hydrophone was used, the resulting images were highly contaminated with low frequency ringing that was likely due to instrumental problems in the system.

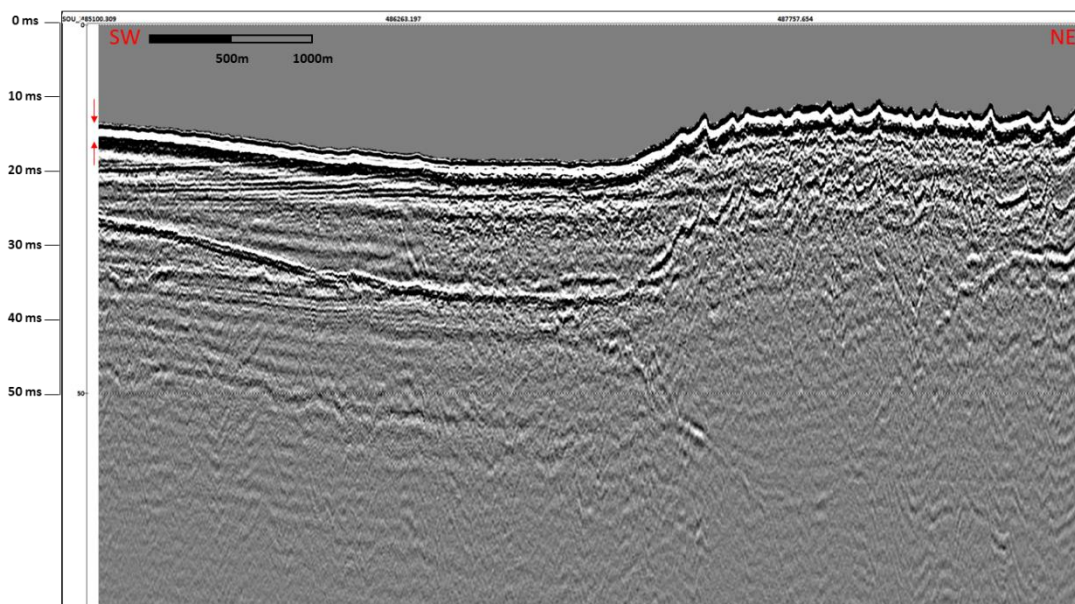


Figure 12 – 500J boomer profile, test line across the Ostend Valley.

Data acquired with the 500J boomer (Figure 12) presents a relatively wide source signal (see red arrows) producing a profile with low resolution. Additionally its signal fails at imaging the internal

structure of the sandbank. On the other hand, its penetration is fairly good. The bottom of the valley is visible but shows very low resolution and the internal layers of the channel are blurry.

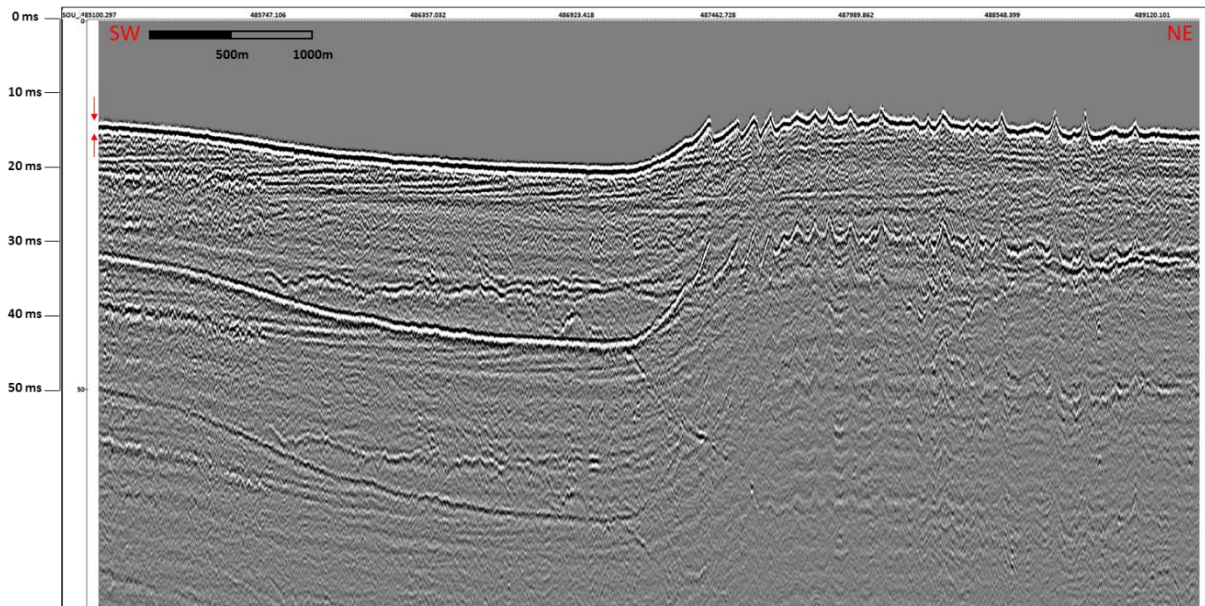


Figure 13 – 300J boomer profile, test line across the Ostend Valley.

The source signal observed on the profile acquired with the 300J boomer (Figure 13) is short but weak (see red arrows). Therefore, it shows relatively good resolution on the shallow reflectors but poor penetration depth, especially below the sandbank. There is no information about the bottom of the valley nor its flanks. In general, results are poor compared to those obtained with the sparker sources.

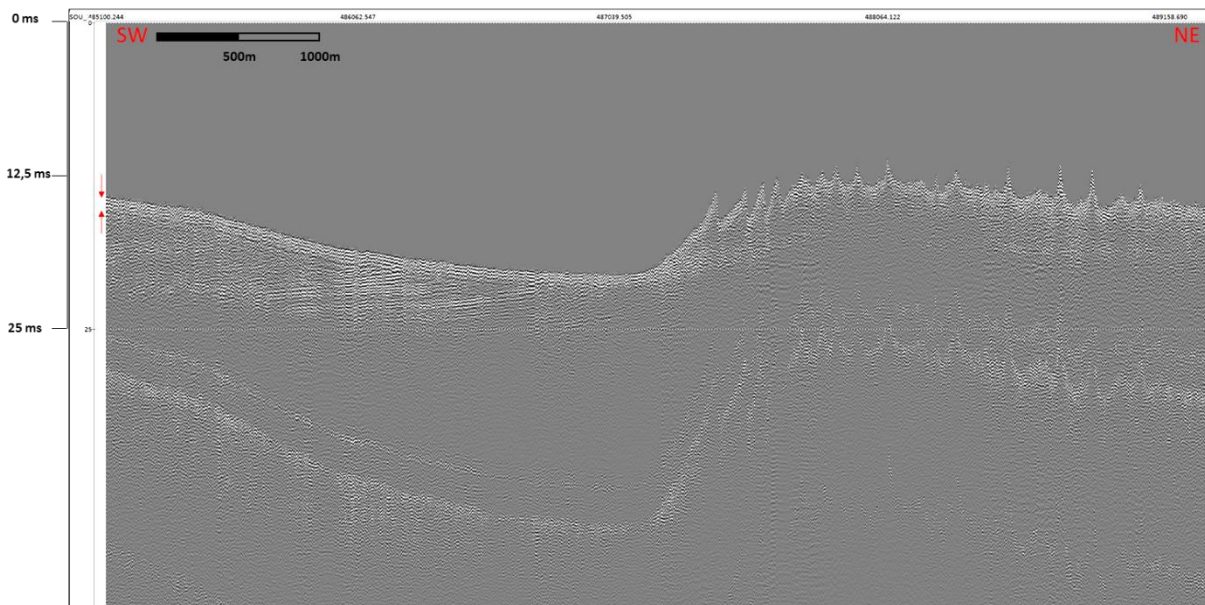


Figure 14 – Geopulse pinger profile, test line across the Ostend Valley.

The source signal of the Geopulse pinger (Figure 14) is short (see red arrows) but presents very low penetration of investigation. Only very shallow dipping events outside and/or on the flanks of the sandbank are visible. The acoustic signal was not able to penetrate the hard sandy bottom of the sandbank. Additionally, strong horizontal ringing was observed on the data. This ringing was

removed during processing but it is based on an algorithm that compares similar events observed on consecutive traces. If reflectors are horizontal, the algorithm will consider them as noise and will remove them so it can have detrimental effects on the quality of the data.

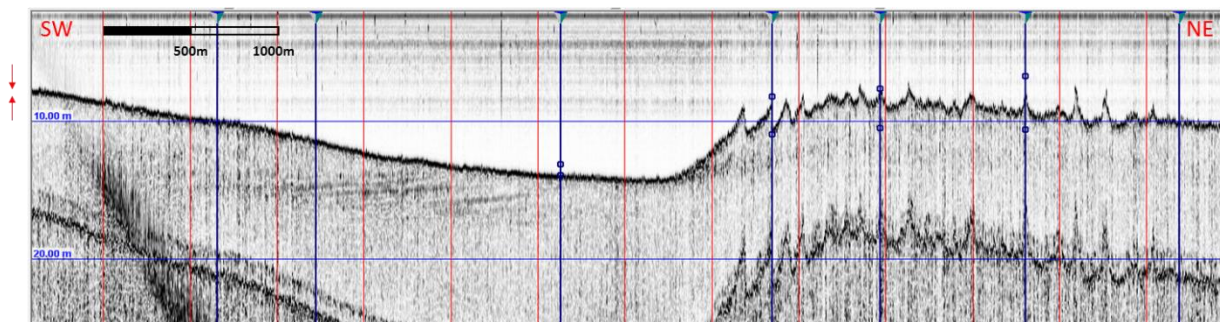


Figure 15 – X-star Chirp profile, test line across the Ostend Valley.

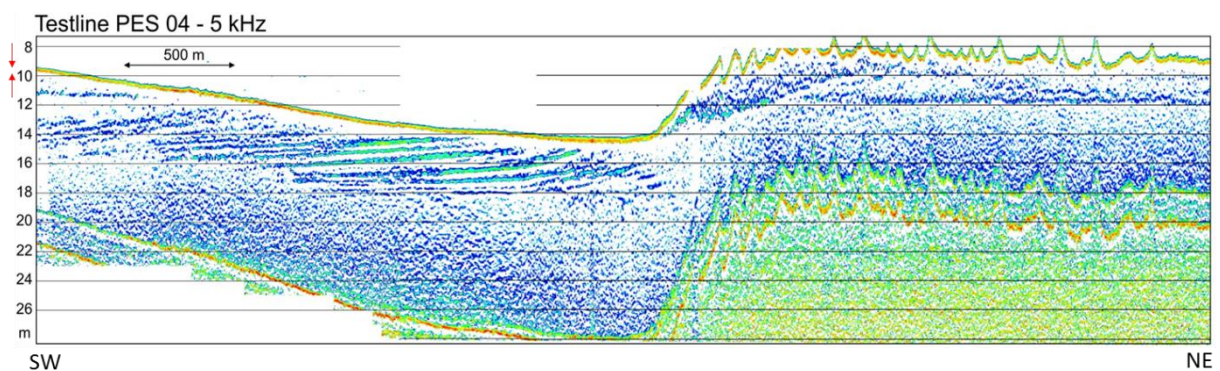


Figure 16 – Parametric echosounder (PES) profile, test line across the Ostend Valley.

Both X-Star chirp (Figure 15) and the parametric echosounder (Figure 16) show very short and sharp signals (see red arrows) producing seismic profiles with very high resolution in the shallowest sections. Due to their intrinsic frequency content they show very low penetration (no more than five metres). Compared to the chirp the PES signal gave a better image of the internal structure of the uppermost part of the sandbank and the shallow deposits in the swale towards the west; the chirp particularly failed at imaging the internal layers of the sandbank.

From this evaluation, the Centipede sparker and the Geo-Source 200 sparker produced the best compromise between resolution and depth of investigation. Both sources were capable of imaging reflectors inside and outside the sandbank. Their penetration depth was comparable although resolution of the Centipede sparker was superior. These sources were the only ones capable of clearly depicting the valley's upper boundary, but it must be mentioned that this reflector was often masked by seafloor multiple reflections so no final conclusion can be drawn with this respect. It is important to stress that the above discussed results are only valid to the records collected under the specific weather and sea-state conditions that prevailed during acquisition.

As mentioned before, no demultiple method was applied to produce the profiles displayed above. According to Verschuur (2006) the techniques for suppressing multiples can be classified into two main categories. The first group of techniques are based on difference in spatial behaviour between primaries and multiples (F-K and T-P filtering). The second group are based on periodicity (predictive deconvolution) and predictability (Surface Related Multiple Elimination (SRME)) of the multiple reflections.

Methods in the first category exploit the fact that multiples travel through different geological structures than their corresponding primary reflectors, therefore at non-zero offsets multiples separate out from the primaries due to the difference in their arrival times. These filters are by definition applicable only to multi-channel datasets.

In the second category, demultiple techniques exploit the fact that multiples are periodic in nature (i.e., they keep occurring at regular interval of time in the seismic trace) and have an inherent relationship with primary reflections which implies that multiples can be predicted from its generating primaries after which they can be subtracted from the data. These techniques are suited for near-offset single-channel or stacked seismic data but their performance is superior when applied before stack.

The demultiple algorithm used in RadExPro is based on adaptive subtraction of a model of multiples from the original wave field. The model is obtained from the data itself, either by static shift of the original traces or by auto convolution.

In figure 17 we display the profile obtained with the Geo-Source 200 sparker before (top) and after demultiple (bottom).

It can be observed that seafloor multiples have been attenuated and it becomes easier to interpret the data. The channel's upper boundary is clearly distinguishable.

In Appendix B the results before and after demultiple for all relevant sources are displayed.

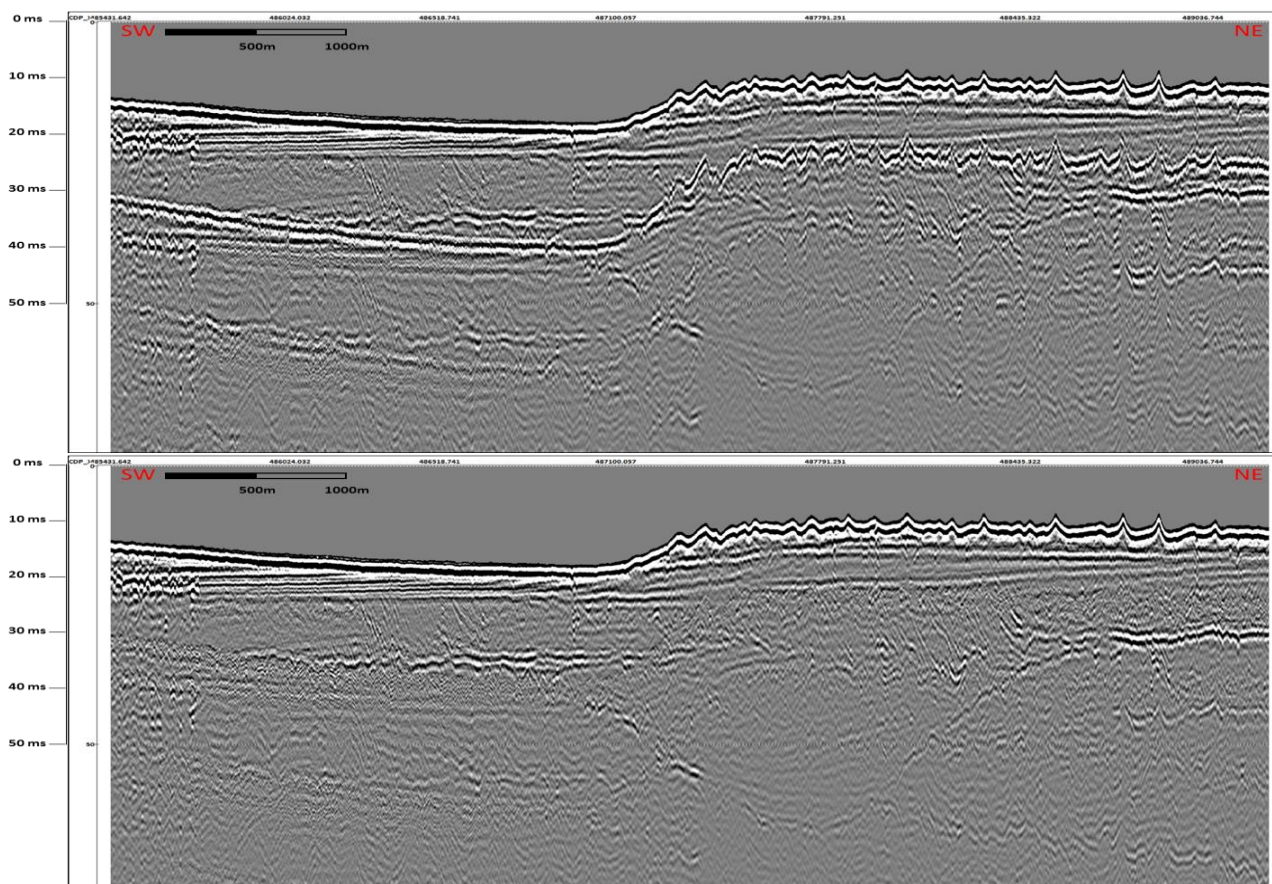


Figure 17 – Geo-Source 200 data before (above) and after (bottom) demultiple.

#### 4.1.2. Multi-channel data results

Data from sleeve gun, sparkers and boomers sources was recorded with a 24-channel multi-channel streamer (3,125m channel spacing) and were later processed according to the flow described in section 2.4. Below we display a comparison between Centipede sparker data recorded with a single-channel (SC) streamer and a multi-channel (MC) streamer. Results for other sources are similar and therefore are not included in the report.

The multi-channel stacked section (Figure 18, bottom) shows a better signal-to-noise ratio than the single-channel data (Figure 18, top). Seafloor multiples have been attenuated, mostly thanks to detailed velocity analysis. The bottom of the valley is much clearer in the stacked profile, and also the internal structure of the valley and its side flanks can now be clearly observed. On the other hand, the resolution of the image in the shallow part of the profile is slightly inferior.

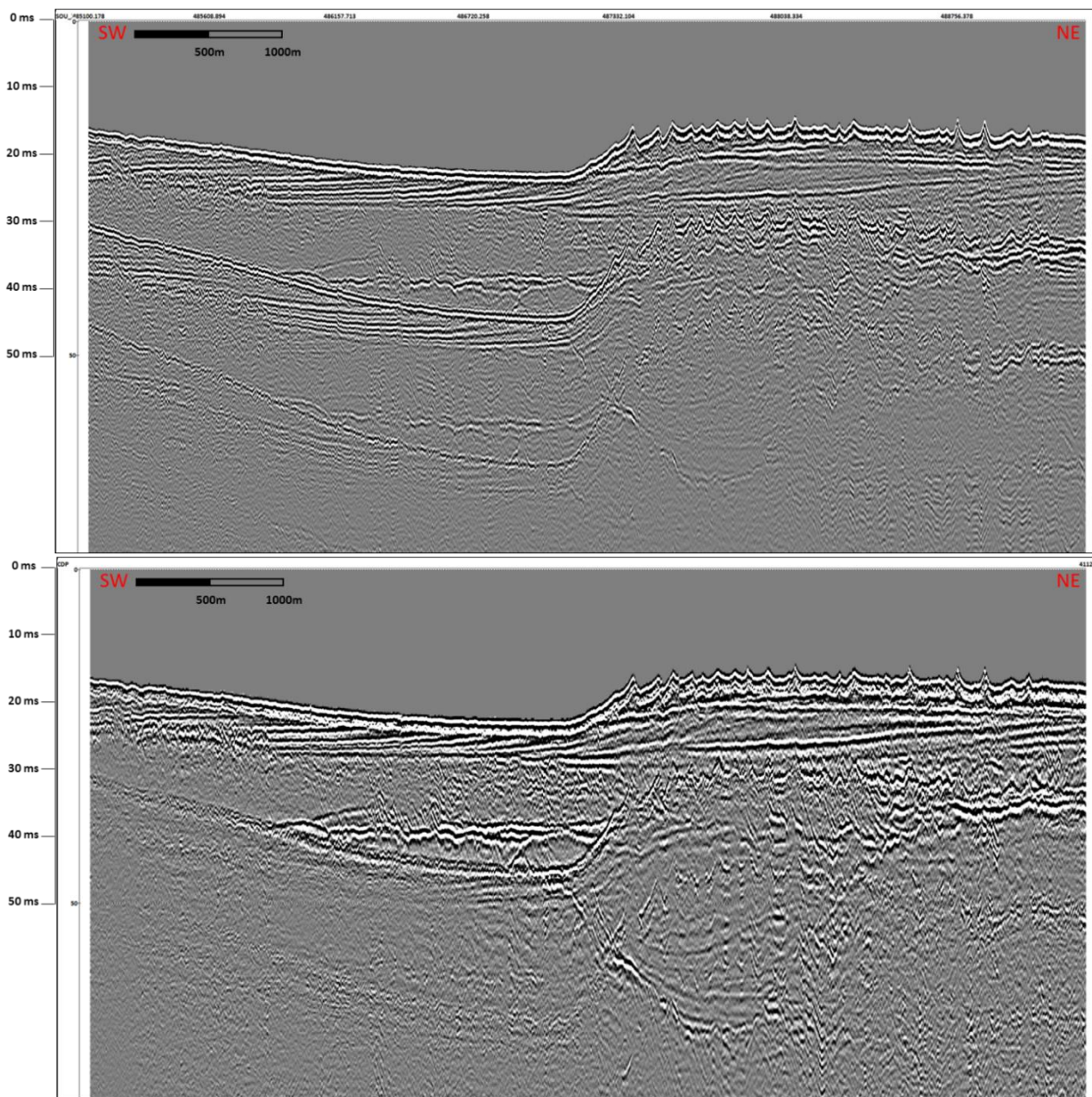


Figure 18 – Centipede Sparker data recorded with SCS (above) and MCS (bottom)

In order to show the importance of performing a detailed velocity analysis, we display data stacked with a velocity function based on geological information only (Figure 19, top) and with the velocity function obtained after detailed velocity analysis every 250 CDPs (Figure 19, bottom).

The improvement of the section obtained when stacking with the final velocity field is significant, especially for the deeper reflectors (below 30ms).

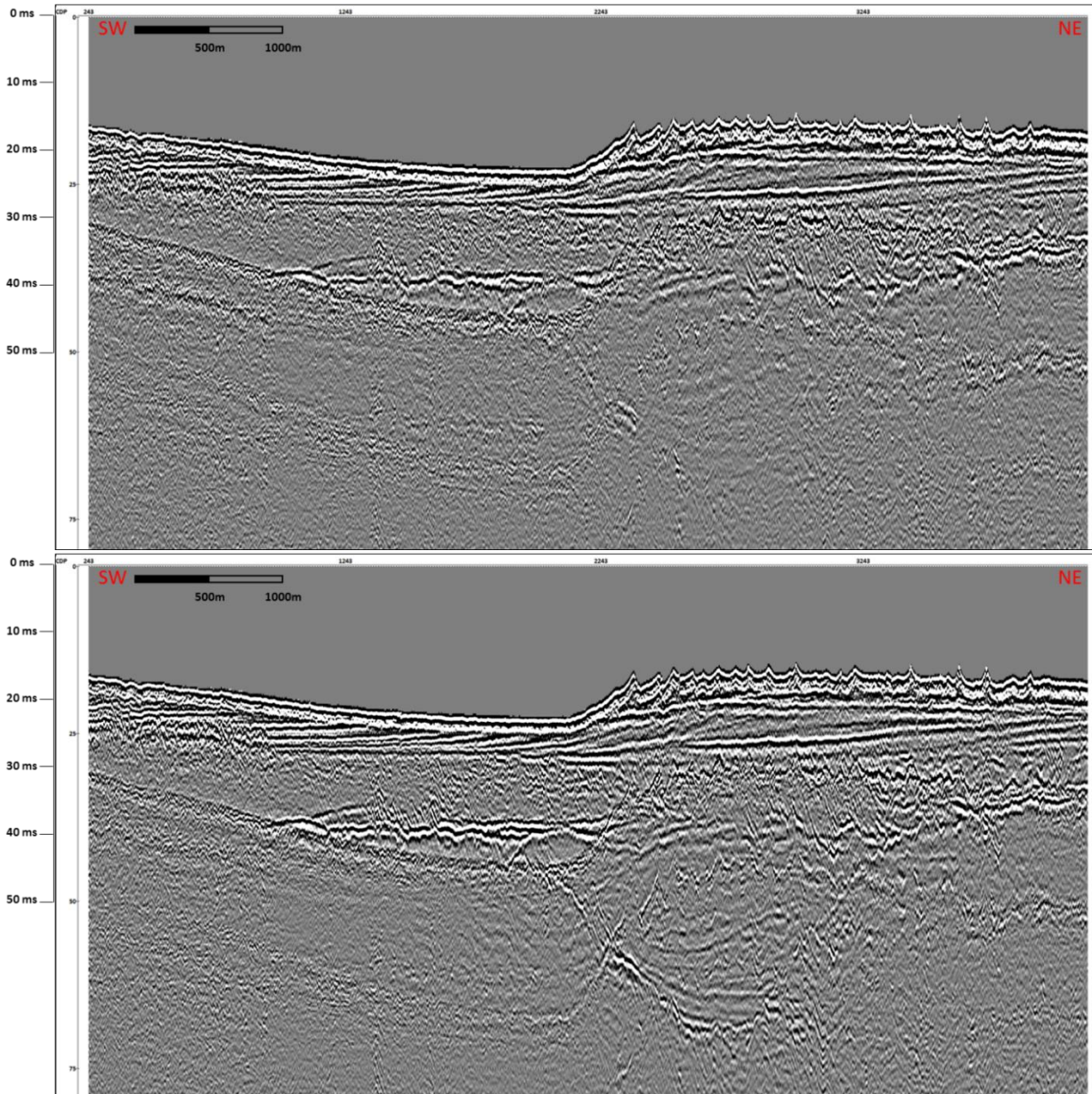


Figure 19 – Centipede Sparker data stacked with dummy velocity field (above) and obtained velocity function (bottom)

With the purpose of showing the response of the MC streamer we show a shot gather acquired with a 48 channels MC streamer (3,125m channel spacing) and a Geo-Source 200 sparker (Figure 20, left) with its corresponding FK spectrum (Figure 20, right). The F-K spectrum clearly shows the steepest events (direct waves and far offset arrivals) are heavily aliased. As explained in section 2.2. this is caused by the use of streamers with large channel intervals.

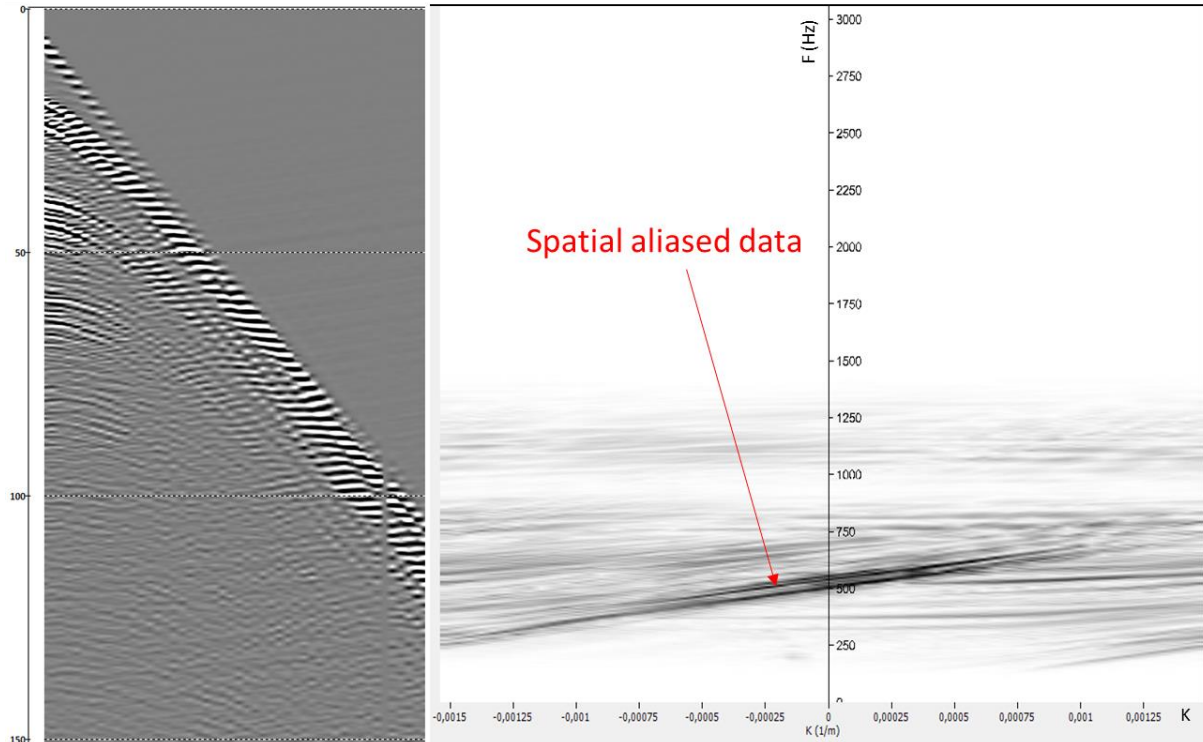


Figure 20 – Shot gather (left) and its frequency spectrum (right). Channel spacing 3,125m.

Finally, a test was performed reducing the number of channels of the streamer as input to the stacking process in order to verify the maximum offset required. Stacking with 18 channels (Figure 22) instead of the full 24 channels (Figure 21) had negligible effects on the final section. This is due to the fact that the outer mute applied before the stack removes all the far data, as explained in section 2.4. Reducing the number of channels to 12 (Figure 23) resulted in a slight decrease in the quality of the data, in particular in the attenuation of seafloor multiples and signal to noise ratio of the deeper events (below 50ms). Further reduction to 6 channels (Figure 24) made the stacked section similar to the results obtained with the single-channel streamer, i.e. lower signal-to-noise ratio, slight increase in the resolution of the very shallow part of the profile and increased amplitude of higher order multiples (see below for the corresponding images).

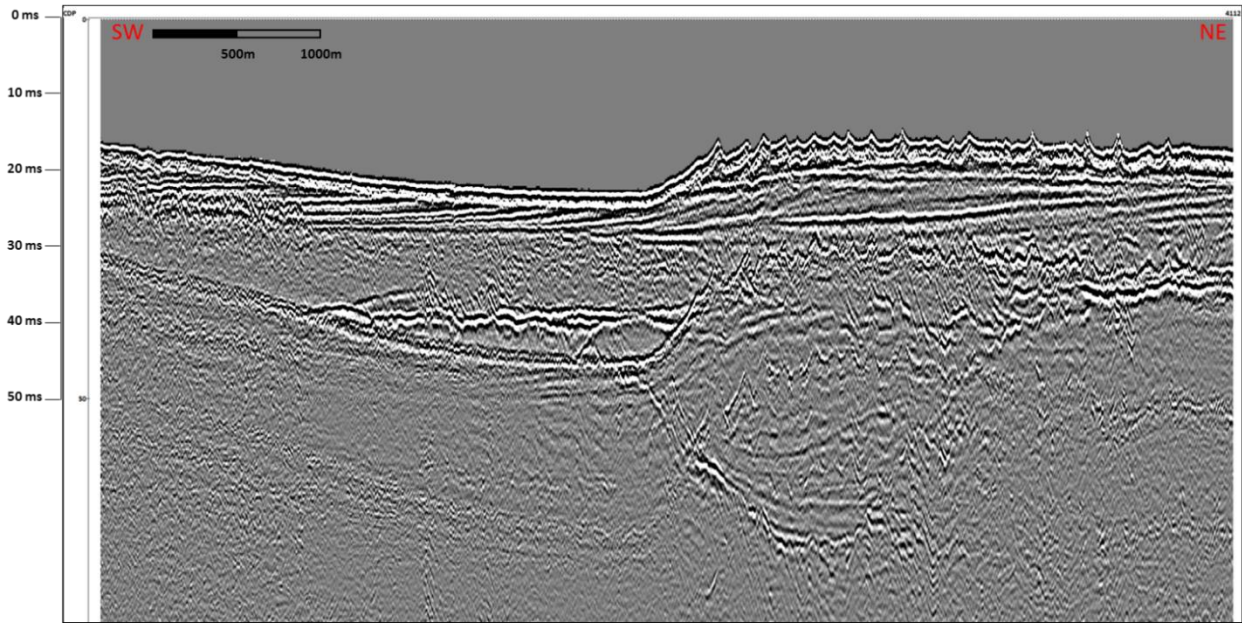


Figure 21 – Centipede Sparker MC data (24 channels)

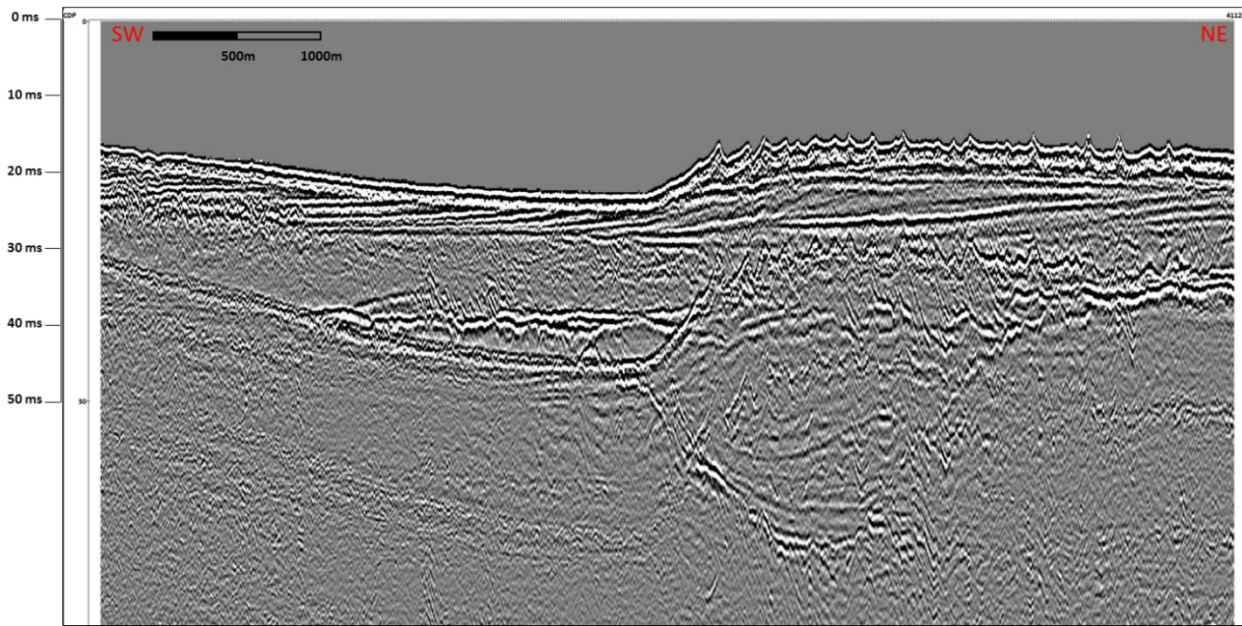


Figure 22 – Centipede Sparker MC data (18 channels)

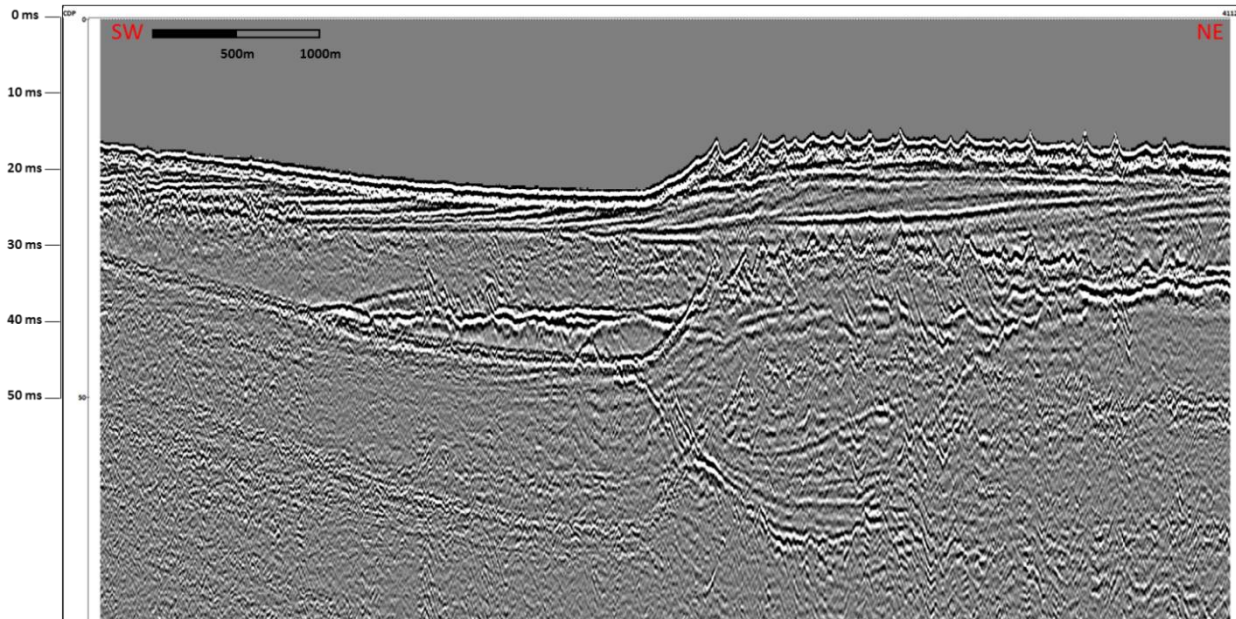


Figure 23 – Centipede Sparker MC data (12 channels)

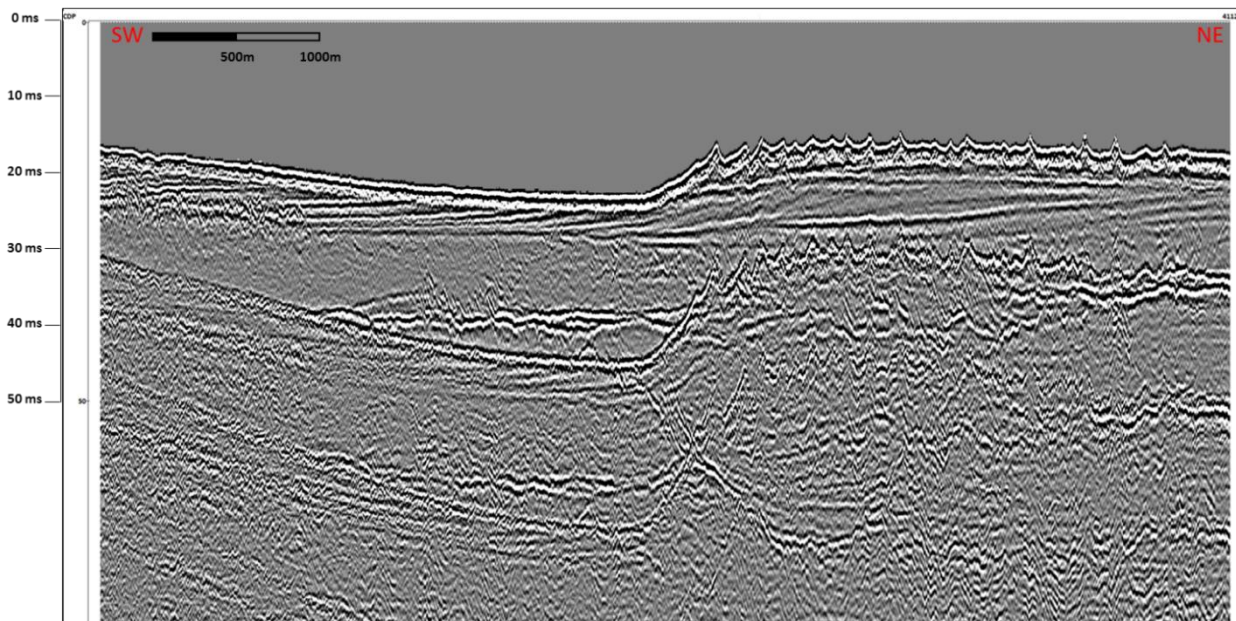


Figure 24 – Centipede Sparker MC data (6 channels)

Reducing the offset by simply reducing the number of channels and leaving the distance between channels unchanged doesn't bring any benefit, the ideal would be to decrease the channel spacing by half and keep the number of channels, this way we would use the relevant offsets and also increase the lateral resolution.

#### 4.2. Comparative tests of different seismic sources at the Thornton Bank

The Thornton Bank is a 20km long tidal sandbank located about 30km off the harbour of Zeebrugge and near the border with the Netherlands. This area is marked by a network of shallow, buried river valleys (e.g. Thornton valley, Northern valley) filled with fluvial (fine sands to gravel) and possibly shallow marine deposits. Large parts of the area are used for windmill farms and can no longer be accessed. The goals of the survey were to obtain more precise information on the connection between the Thornton Valley and the Northern Valley (see figure 25) and to assess the ability to characterize the sediments inside and below the sandbank through the comparison of various high-resolution seismic source/receiver configurations. Sandbanks on the BCS are mostly made-up of coarse sandy sediments and present strong sedimentological heterogeneity (Trentesaux, 1999). Additionally, their complex sea-floor morphology make them a challenging structure to study by means of high resolution seismic reflection methods.

We defined a 6 km long test line that crosses the entire width of the Thornton sandbank (Figure 25) and surveyed it using three different seismic sources (SIG sparker, Centipede sparker and Seistec Boomer) and recorded the data with a single-channel (SC) and a multi-channel (12 channels) streamer. Unfortunately, the MC streamer was defective and the data were only recorded with the SC streamer. The test line was located as close to the valley structure as possible, in view of the large no-go area of the windmill farms.

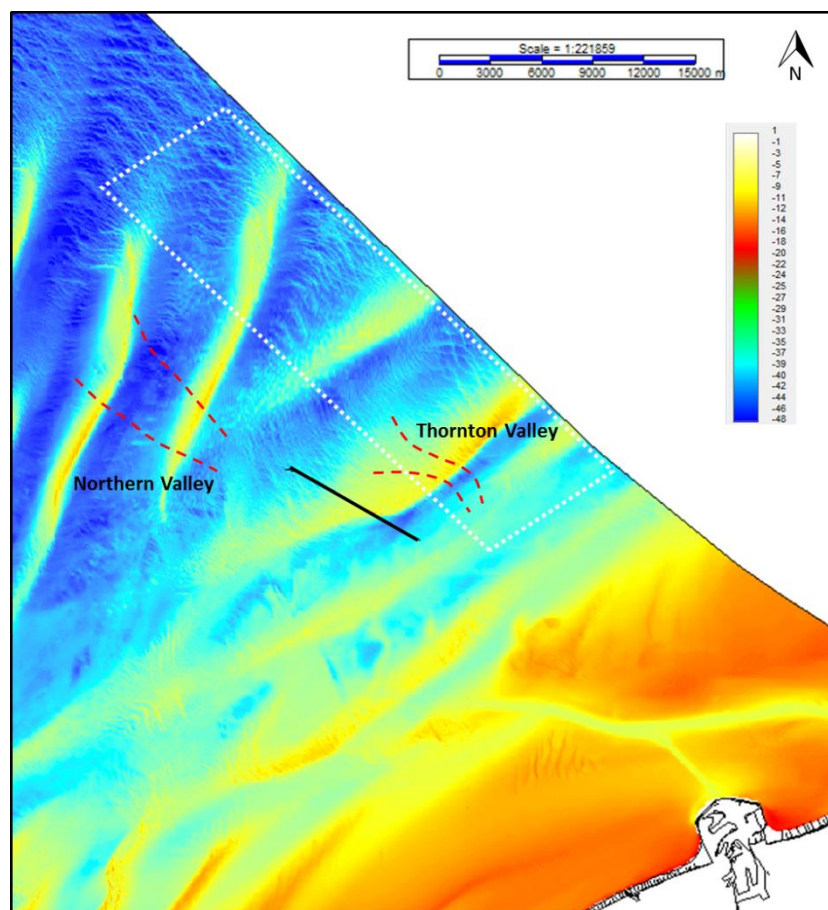


Figure 25 – Location of the test line (in black) at the Thornton Bank. The red dashed lines mark the approximate locations of the Thornton and Northern Valleys (De Clercq, 2015). White dashed area indicates the extent of the windfarm concessions. Background map is the current seafloor bathymetry (colour scale in metres).

A geological interpretation of the cross-section of the test line is presented in figure 26, showing the different geological features referred to in the text below.

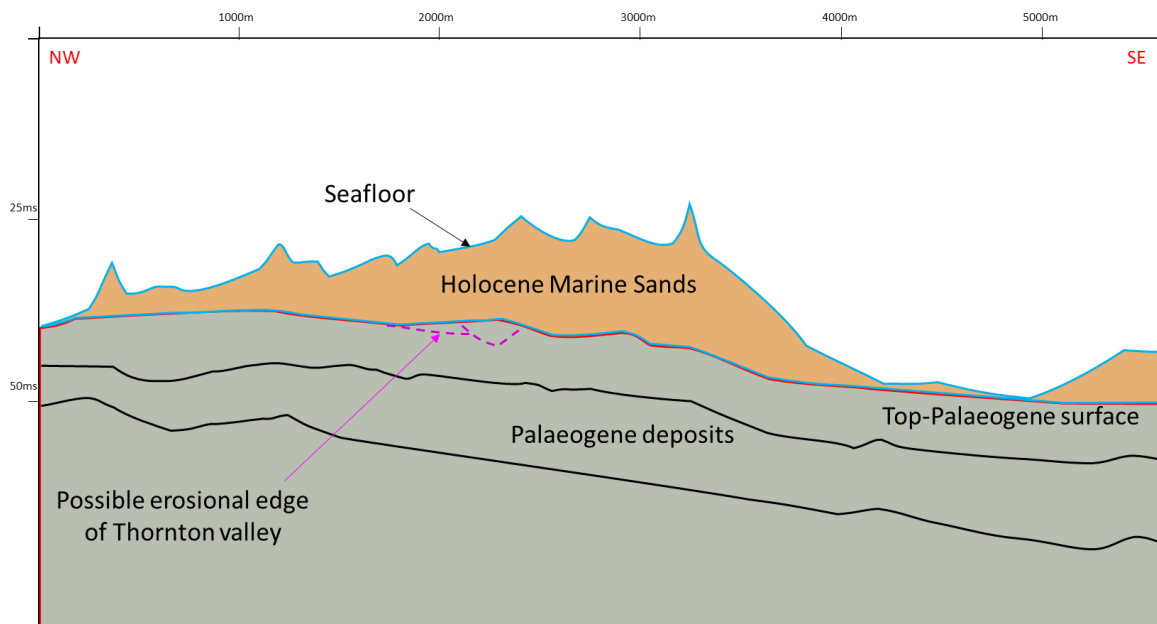


Figure 26 – Geological cross section of the Thornton Bank at the test line location

All the recorded profiles followed the same track line in order to allow for better comparison between the different datasets. Maximum lateral deviation between lines was not bigger than 100m. Acquisition details are summarized in table 4.

| Source            | Date       | Shot interval (sec) | Sailing direction | Energy | Wind (knt) | Wave height* |
|-------------------|------------|---------------------|-------------------|--------|------------|--------------|
| SIG sparker       | 24/04/2014 | 1                   | SE-NW             | 300 J  | 2-3        | 40 cm        |
| Centipede sparker | 22/04/2014 | 1                   | SE-NW             | 300 J  | 2-3        | 50-60 cm     |
| Seistec Boomer    | 23/04/2014 | 0.5                 | NW-SE             | 300 J  | 2-3        | 40 cm        |

Table 4 – Acquisition parameters of the test lines across the Thornton Bank

\*wave height measurement obtained from pile Westhinder. Source: VLIZ <http://www.vliz.be/>.

Weather conditions were fairly good for all lines and wave height during acquisition was always in the range of 40 to 60cm.

### Single-channel data results

The resulting seismic profiles, for single-channel data, are displayed in figures 27 to 29. For comparison reasons, no demultiple was applied to the displayed data. Horizontal scale is in meters; vertical scale is in milliseconds (two-way travelttime, 10ms equals roughly 7.5m).

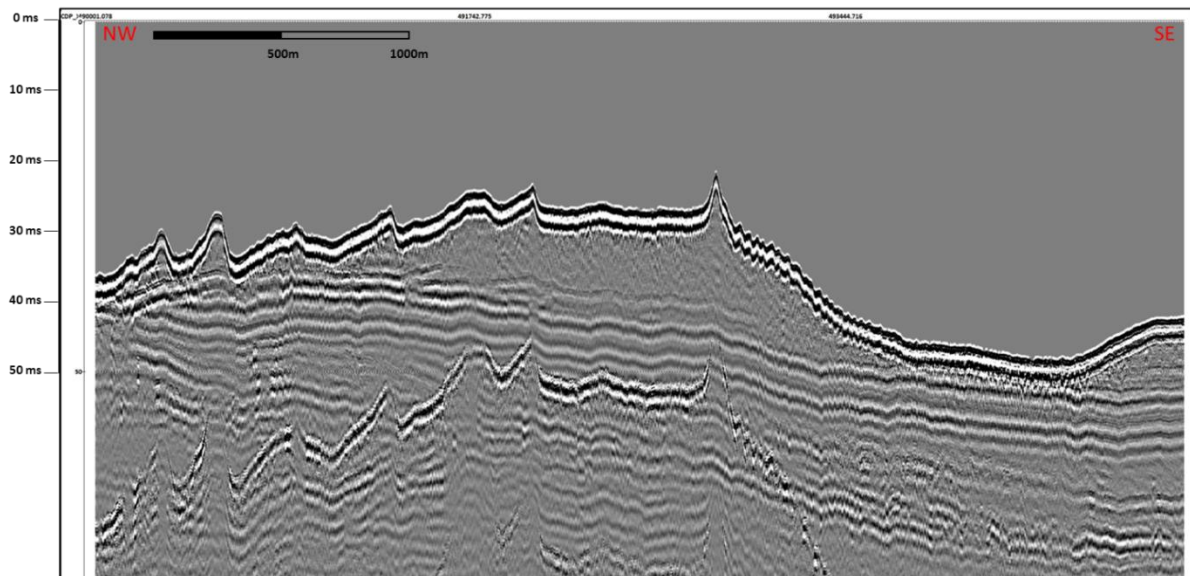


Figure 27 – SIG sparker profile, test line across the Thornton Bank

The source signal of the SIG sparker (Figure 27) is very strong and relatively coarse. Due to the length of the signal it produces profiles with limited vertical resolution. The SIG signal allows to image the base of the sandbank and the dipping clay layers underneath. However, it is hard to discern small erosional features related to the edge of the Thornton Valley and there is no information on the internal structure of the sandbank.

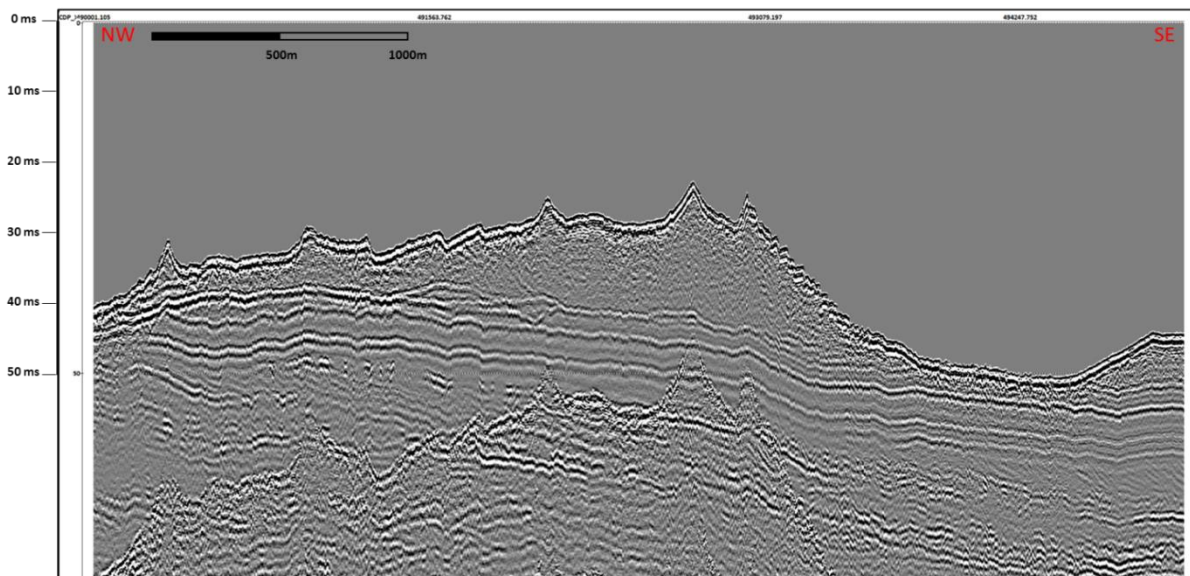
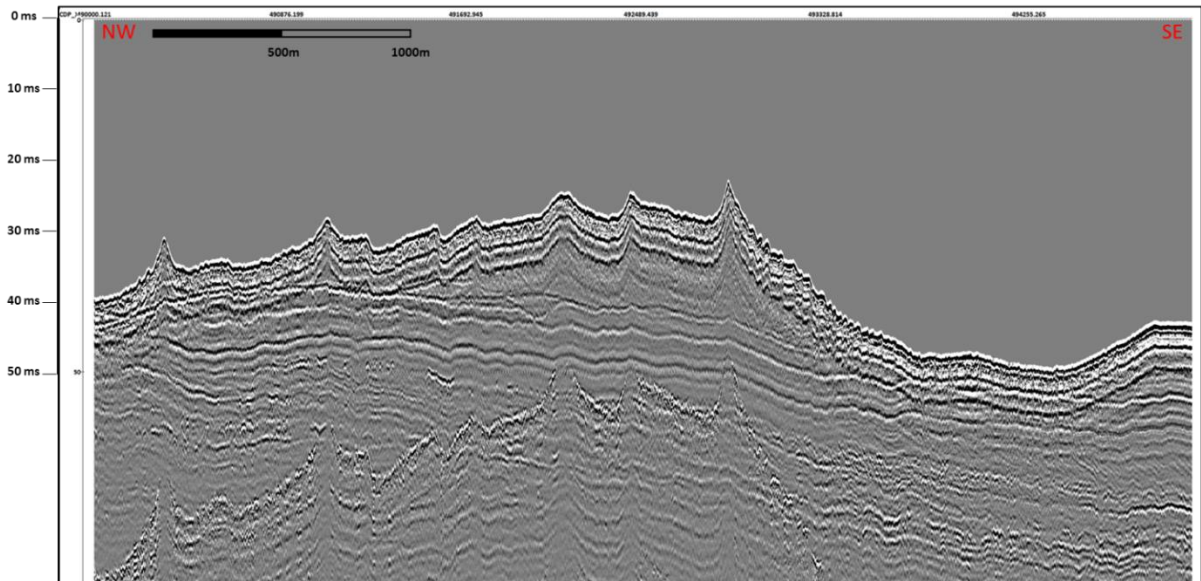


Figure 28 – Centipede sparker profile, test line across the Thornton Bank

The source signal of the Centipede sparker (Figure 28) is sharper than the SIG sparker and produces a sub-seafloor image with very high resolution. The top-Palaeogene surface is well defined and some (weak) internal layering of the sandbank can be observed. The signal penetration is very good and the internal structure of the deeper Palaeogene sequence is clearly visible (though still partly obscured by the seafloor multiple). The erosional structure at the edge of the Thornton Valley is clearly visible.



*Figure 29 – IKB Seistec Boomer profile, test line across the Thornton Bank*

The source signal of the Seistec boomer (Figure 29) is sharp and strong but highly contaminated by strong ringing on the water bottom reflector, hindering the resolution of the shallow most reflectors. The signal easily penetrates into the sandbank and allows a good image of the base of the Quaternary and the small erosional channel. However, its penetration of investigation is inferior to both sparker sources and the deeper clay reflectors are not well defined.

As a summary we can conclude that the Centipede sparker produced the best results, confirming results from the Ostend Valley test site. The Centipede sparker shows the best compromise between resolution and penetration depth and allows detailed characterisation of the sandbank and underlying geological layers.

### **4.3 Gas research - Zeebrugge Valley**

Seismic records from the nearshore area of the BCS are often marked by zones lacking seismic penetration. The most frequently observed features on these seismic profiles include acoustic blanking, acoustic turbidity, enhanced reflections, reversed polarity, bright spots, reverberations and velocity pull-down. Quite frequently these features may be seen in association with each other (Schroot et al., 2003). These anomalies have been attributed to the presence of shallow biogenic gas in the sediments. The origin of the gas is often difficult to determine but it is suspected it could be linked to the presence of a shallow, peat-rich layer of Late Pleistocene/Early Holocene age (i.e. Basal Peat). Local high sedimentation rates furthermore most likely favoured gas formation in the shallow fine-grained mud-rich Holocene sediments (Missiaen et al., 2002).

The presence of biogenic gas in shallow marine environments severely affects the propagation of acoustic energy. When gas bubbles in the sediment are submitted to the small strains caused by acoustic perturbations they oscillate or resonate at a fundamental frequency related to the bubble size, bubble resonance frequency, and the frequency of the acoustic disturbance. The greatest reverberation occurs when the acoustic frequency matches the resonance frequency of the bubbles (Wilkens, 1998).

According to Anderson & Hampton (1980), the relationship between the size of the gas bubbles and the frequency of the propagating acoustic energy plays an important role. For acoustic low frequencies or wavelengths considerably greater than the bubble size, the acoustic response is that of the bulk medium. In this case the compressional wave velocity is significantly reduced (even by small amounts of free gas). For acoustic waves with wavelengths of the same order of magnitude as the bubble size, the gassy sediments becomes highly dispersive because they strongly scatter the acoustic energy and further prevent transmission through the gas-charged sediment layer. For high frequencies or wavelengths below the size of the gas bubble, the bubbles simply scatter the sound, but the acoustic response is essentially that of the surrounding medium and as a consequence the velocity remains constant at a value comparable to the velocity of the gas-free sediment.

Studies performed by the University of Bremen in the southern Baltic Sea (Toth et al., 2014) proved that low-frequency sources like mini air guns (200Hz) produce wavelengths (7.5m at 1500m/s) considerably larger than the size of gas bubbles in the sediment (0.5 to 5 mm average size gas bubbles for muddy sediments). Since these waves with long wavelengths do not backscatter from the small bubbles they suffer less attenuation and therefore achieve greater penetration depths. At these frequencies, the gassy layer is represented as a single reflector with reversed polarity, since the gas-charged layer is simply a part of the medium with lower velocity and/or density. On the other hand, when very high frequency sources like echosounders (> 20 kHz) were used, the attenuation slightly decreases and acoustic waves are transmitted and reflections can be observed beneath the gassy sediment layer. Finally, when sources with frequencies in the resonance frequency range (1.5 to 20 kHz), the gas bubbles strongly scattered the acoustic waves of these sources preventing transmission through the gas-charged sediment layer.

The goal of our test was to try different types of sources and configurations for their efficiency to penetrate the gassy sediments and image the shallow subsurface and the underlying Tertiary deposits. Good knowledge of the subsurface structure is crucial in order to plan the geotechnical investigations (deep cores and CPTs) that are scheduled in this area in the framework of future construction works.

#### 4.3.1. Test results

One of the locations along the Belgian coast showing a particularly high concentration of gas-rich sediments is the area around the port of Zeebrugge. Two different test zones (TA1 and TA2), located respectively west and east of the harbour, were defined (Figure 30). The original plan to define one long test line around the entire harbour had to be abandoned due to the heavy ship traffic on the main access lane to the port, and instead two smaller test zones were defined.



Figure 30 – Test areas around the harbour of Zeebrugge (Google Earth background map). The yellow dashed line marks the approximate valley boundary.

Both test zones are located near or on top of the buried Zeebrugge Valley, believed to be a smaller outflow of the ancient Scheldt river. Zone TA1 is presumably located above the western, more gentle flank of the valley whereas zone TA2 is supposed to be located above a steep clay cuesta that marks the eastern flank of the valley (Figure 31). The deepest point of the Zeebrugge Valley can reach up to 34m below LAT (De Clercq, 2015). Due to a lack of reliable data outside the harbour area the exact shape and location of the Zeebrugge valley are not well known.

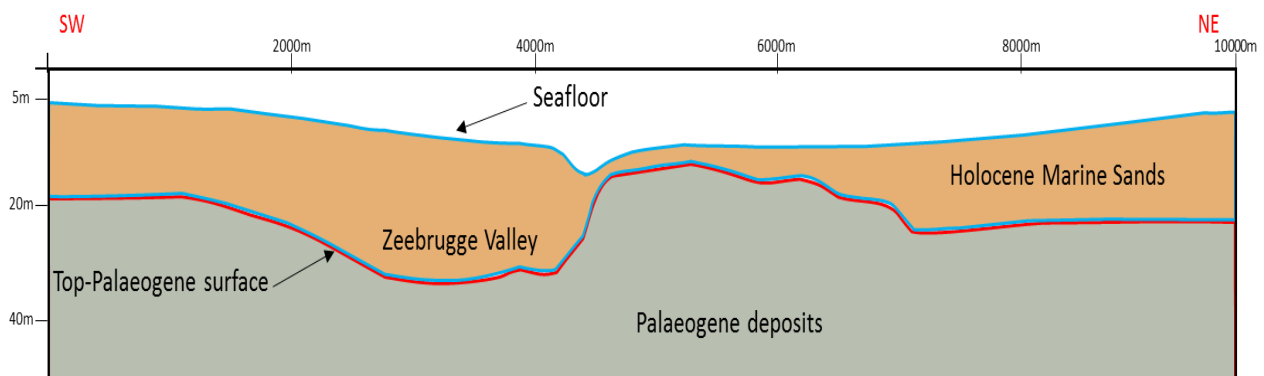


Figure 31 – Geological cross section of the Zeebrugge Valley. Vertical scale in TAW (De Clercq, 2015)

The two test zones were surveyed with four different seismic sources, ranging from low to very high frequencies (Sleeve gun, Centipede sparker, GSO 360 sparker and parametric echosounder) and recorded with a single-channel and a multi-channel (48 channels) streamer simultaneously when relevant. The parametric echosounder was used simultaneously with the other sources.

### Test area 1 (TA1)

The acquisition details for test area 1 are summarized in Table 5 below.

| Source            | Date       | Shot interval (sec) | Sailing direction | Energy   | Wind (knt) | Wave height* |
|-------------------|------------|---------------------|-------------------|----------|------------|--------------|
| Sleeve gun        | 25/03/2015 | 2                   | E-W               | 10 cu.in | 4          | 80 cm        |
| Centipede sparker | 25/03/2015 | 0.5                 | W-E               | 300 J    | 5          | 100 cm       |
| GSO 360 sparker   | 25/03/2015 | 1                   | W-E               | 1000 J   | 4          | 80 cm        |
| PES               | 25/03/2015 |                     | E-W               |          | 4          | 80 cm        |

Table 5 – Acquisition parameters for Test Area 1 west of Zeebrugge.

\*wave height measurement obtained from measuring pile A2. Source: VLIZ <http://www.vliz.be/>.

Weather conditions were poor for all lines with wave height exceeding 80cm.

The results of the single-channel profiles obtained in the western test area (TA1 in figure 30) are displayed in figures 33 to 35 (horizontal scale in meters; vertical scale in milliseconds). The location of each of the recorded profiles is shown below (Figure 32). Due to strong currents and tidal restrictions it was not possible to sail exactly along the same line. This resulted in a relatively large maximal lateral deviation between the profiles in the order of 500m.

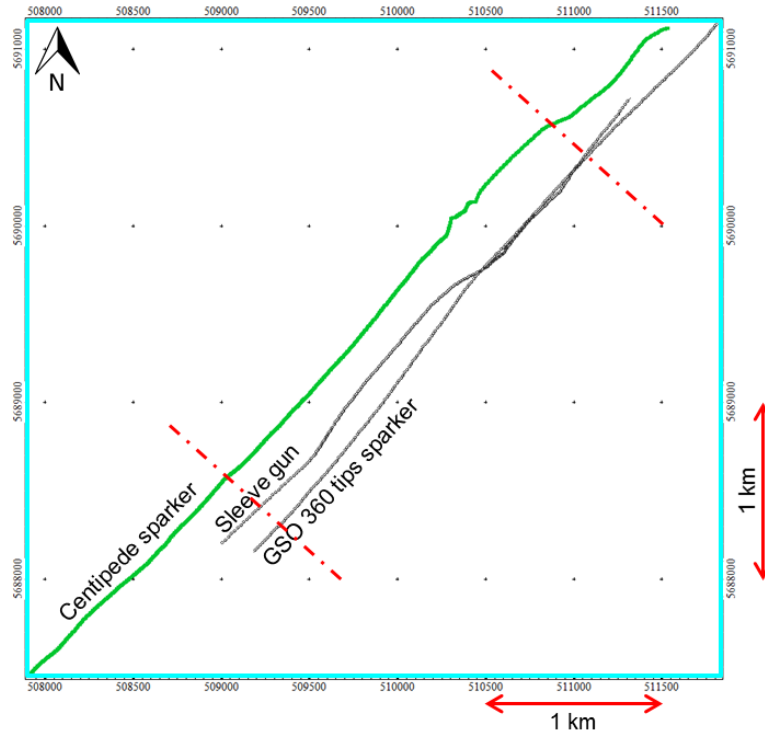


Figure 32 – Relative line location of the recorded profiles in Test Area 1. Red dashed lines indicate the limits of the displayed profiles.

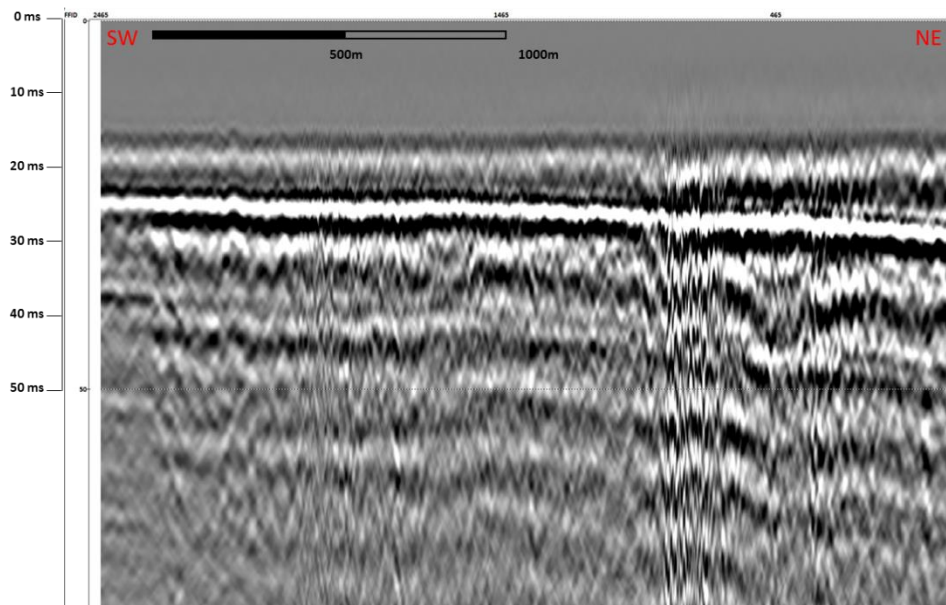


Figure 33 –Sleeve gun profile acquired west of Zeebrugge harbour

The low-frequency Sleeve gun data (Figure 33) is severely affected by the presence of gas and shows no information of the expected sub seafloor reflectors.

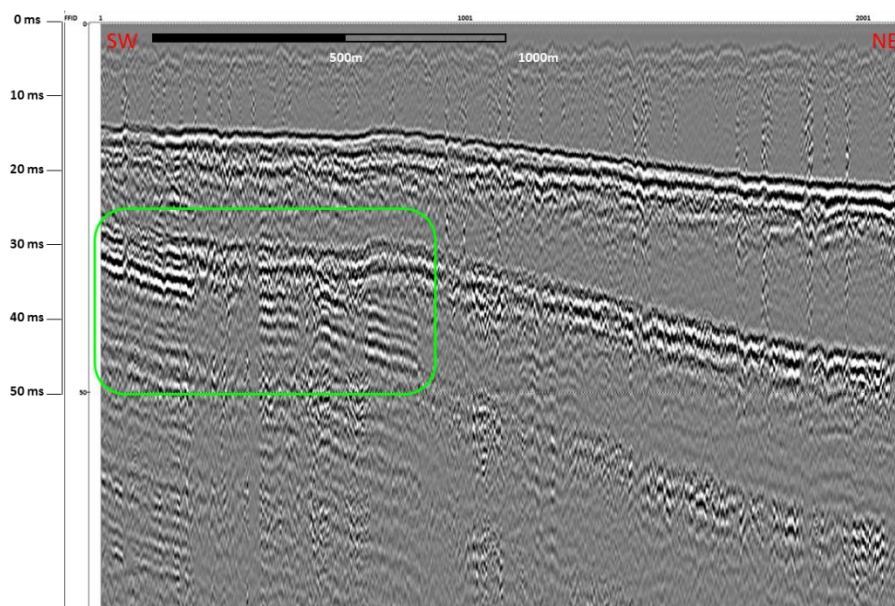


Figure 34 – GSO 360 sparker profile acquired west of Zeebrugge harbour

The GSO 360 sparker profile (Figure 34) shows some dipping events on its westernmost part (see green highlighted area). These reflectors are believed to correspond to the dipping layers of the Palaeogene. A number of very shallow reflectors seem to be present but the resolution is very poor, probably due to bad weather conditions at the moment of the acquisition. The Top Palaeogene surface cannot be observed.

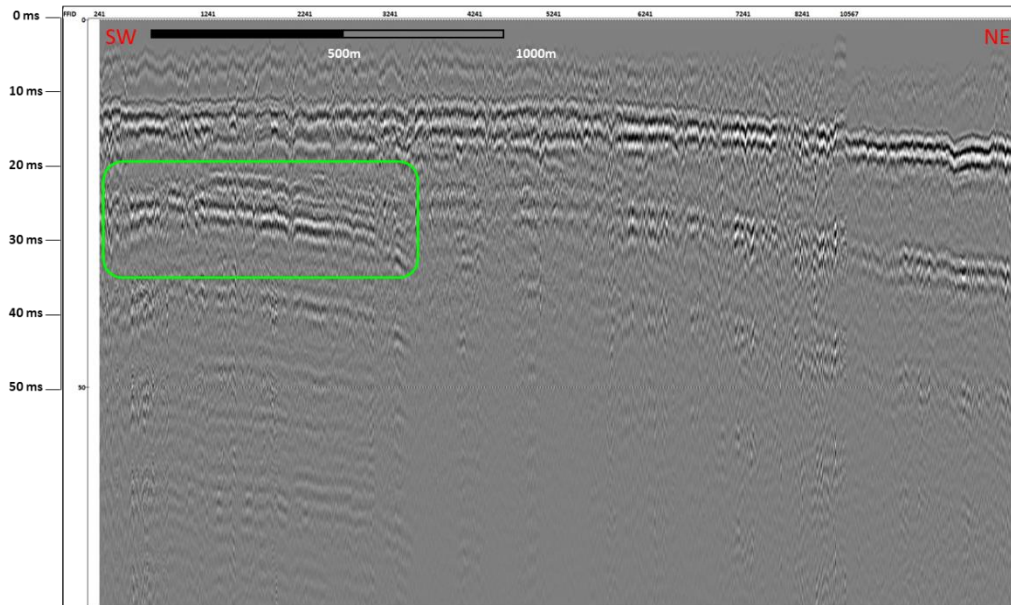


Figure 35 – Centipede sparker profile acquired west of Zeebrugge harbour

The Centipede sparker data (Figure 35) shows some weak reflectors on its westernmost part of the section (see green highlighted area) that probably correspond to the same dipping events observed with the GSO 360 sparker (Figure 34). Some very shallow (around 20ms) events are noticeable at the centre of the profile but these show low amplitude and no lateral coherency so they might be attributed to noise. Resolution and amplitude strength are generally poor.

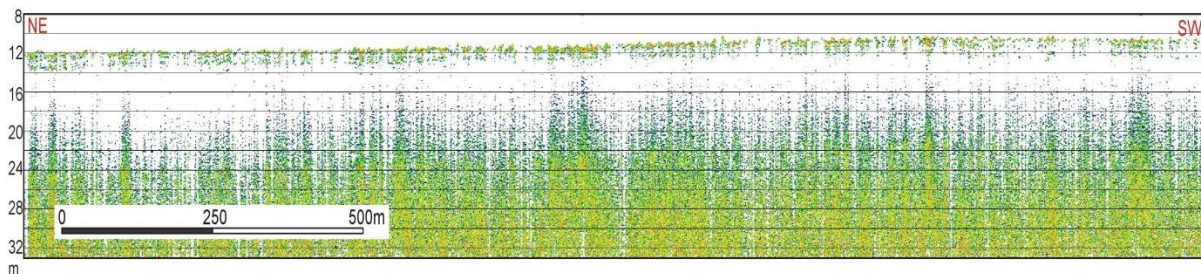


Figure 36 – Parametric echosounder profile acquired west of Zeebrugge harbour

The parametric echosounder (Figure 36) failed at imaging any reflector below the seafloor.

Results from Test Area 1 show that none of the tested sources was capable of imaging inside nor below the gassy sediments. Gas seems to be very shallow meaning that even very shallow reflectors were not observed. Additionally, weather conditions were inadequate for acquisition of high resolution seismic data in very shallow environments.

### Test area 2

The results of the single-channel profiles obtained in the eastern test area (TA2 in figure 30) are displayed in figures 38 to 40. The location of each of the lines is shown below (Figure 37). Due to strong currents and presence of other vessels it was not possible to sail exactly along the same line. As a result the maximal lateral deviation between the lines was very large, in the order of 1000m.

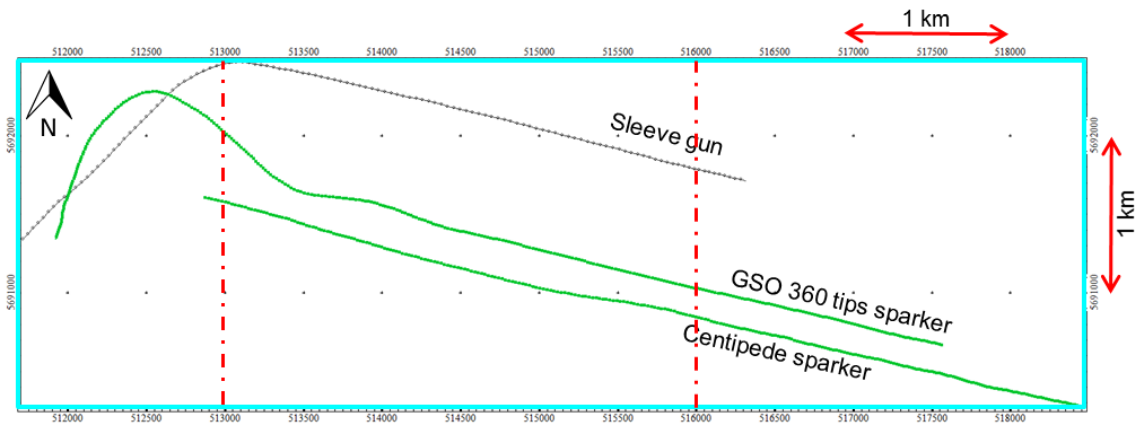


Figure 37 – Relative line location corresponding to Test Area 2.  
Red dashed lines indicate the limits of the displayed profiles.

The acquisition details for test area 2 are summarized in Table 6 below.

| Source            | Date       | Shot interval (sec) | Sailing direction | Energy   | Wind (knt) | Wave height* |
|-------------------|------------|---------------------|-------------------|----------|------------|--------------|
| Sleeve gun        | 25/03/2015 | 2                   | W-E               | 10 cu.in | 4          | 100 cm       |
| Centipede sparker | 25/03/2015 | 0.5                 | E-W               | 300 J    | 3          | 100 cm       |
| GSO 360 sparker   | 25/03/2015 | 1                   | W-E               | 1000 J   | 3          | 100 cm       |

Table 6 – Acquisition parameters for Test Area 2 east of Zeebrugge  
\*wave height measurement obtained from measuring pile A2. Source: VLIZ <http://www.vliz.be/>.

Weather conditions were poor for all lines with wave height averaging 100cm.

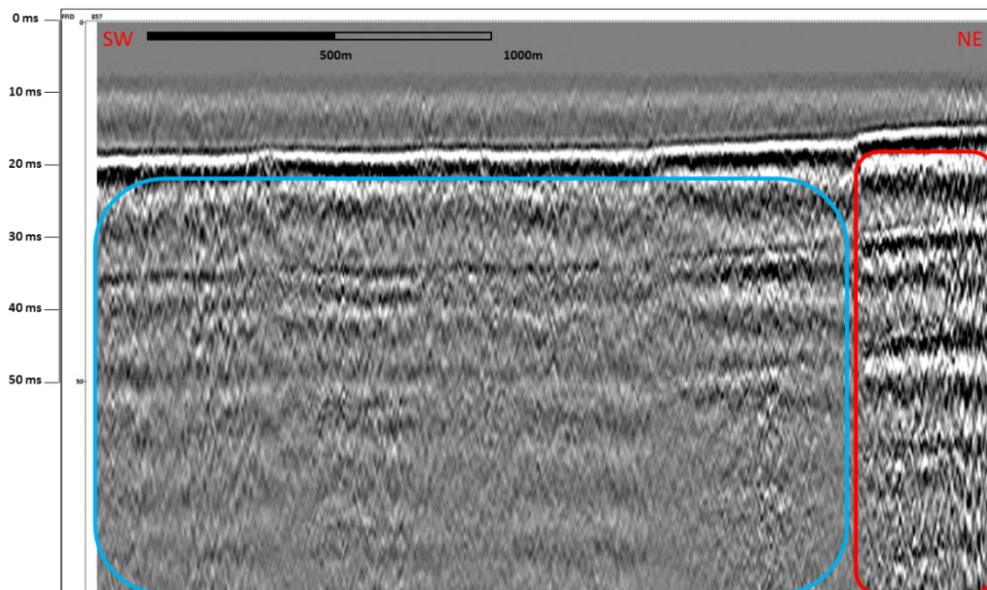


Figure 38 – Sleeve gun profile acquired east of Zeebrugge harbour.  
Red box = acoustic turbidity; blue box = acoustic blanking.

Data corresponding to the Sleeve gun (Figure 38) is severely affected by acoustic turbidity (east, in red) and blanking (west, in blue) and shows no information of the sub seafloor reflectors.

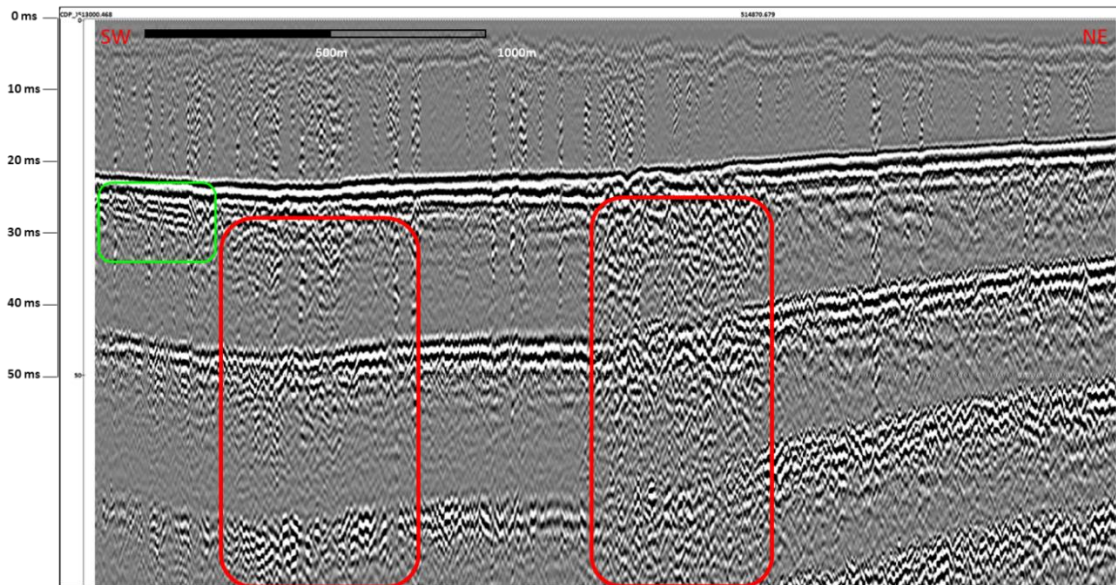


Figure 39 – GSO 360 sparker profile acquired east of Zeebrugge harbour. Red box = acoustic turbidity.

On the data acquired with the GSO sparker (Figure 39) some shallow events are noticeable in the west part of the section (see green area) but no deeper reflectors are noticeable. Two sections with acoustic turbidity are clearly noticeable at the centre of the profile (in red). Strong seafloor multiple reflections (another effect of the presence of gas) are observable throughout the whole section.

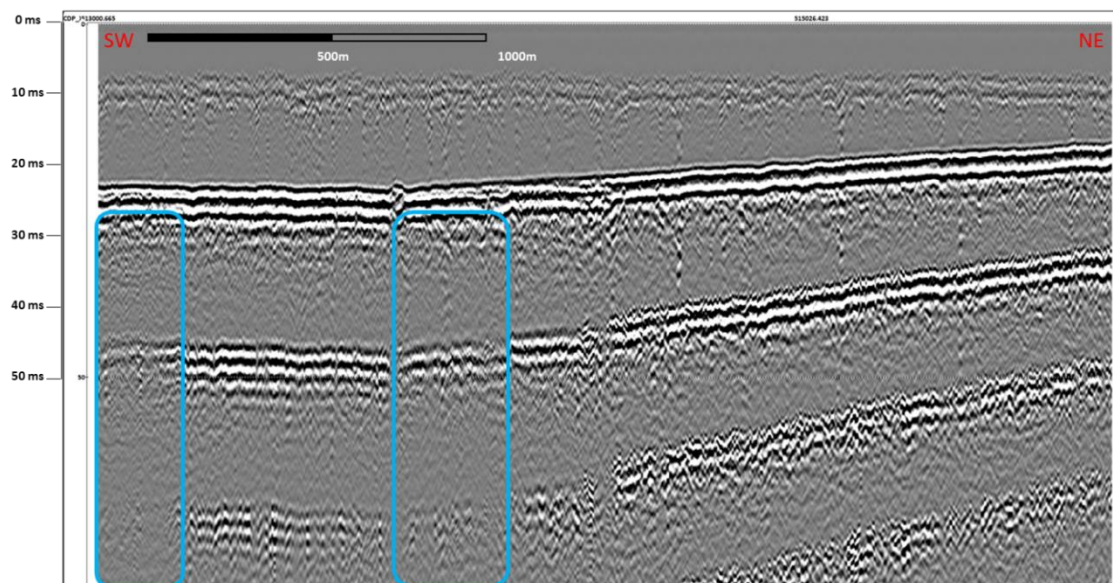


Figure 40 – Centipede sparker profile acquired east of the harbour. Blue box = acoustic blanking

On the centipede sparker data (Figure 40) no information from the sub seafloor reflectors can be observed, most of the energy has been absorbed and the only clear events are the strong seafloor multiples that are only interrupted by small areas showing acoustic blanking (in blue).

We can conclude that no source was capable of imaging through the gassy sediments. Weather conditions were not optimal during acquisition but their influence is not to blame for the inability to penetrate the gassy sediments. Further tests, e.g. measurements of bubble size, shape, distribution, relationship between sediment and pore fluid matrix, must be performed in order to find out the resonance frequency of the gas bubbles before considering acquiring new seismic data in the area.

#### 4.4. Gas research – Ostend Valley long offset tests

##### 4.4.1. Long offset principle and problems

In order to find ways to image underneath gas-rich sediments it was decided to test increasing the distance between the source and the receiver (offset). Long offset data ‘illuminate’ the subsurface differently from conventional short offset configurations and therefore may contain additional information about the subsurface that could eventually help in imaging the sediments below the gassy area (Figure 41).

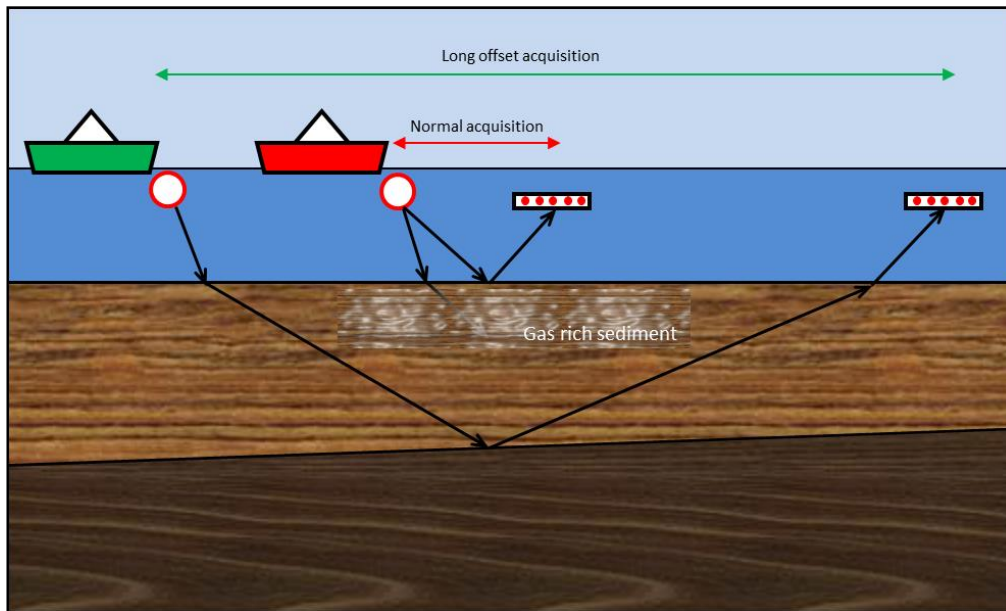


Figure 41 – Comparison between conventional acquisition and long offset acquisition

In order to achieve very long offsets we used two vessels simultaneously, the RV Belgica acting as source vessel and the RV Simon Stevin as receiver vessel (Figure 42). To perform such test a powerful source was needed, therefore a sleeve gun was used as seismic source and a multi-channel streamer (24 channels, 3.125m spacing) was used as receiver.



Figure 42 – RV Belgica and RV Simon Stevin during joint operations

While long-offset data can provide extra information about the subsurface, it also implies additional challenges for the processing and imaging. Four main problems are encountered when dealing with this kind of data (Lin, 2003):

a) Excessive normal moveout stretch

The “moveout” is the difference between the traveltimes of a receiver located at a certain distance from the source (offset) and the traveltimes of a receiver placed at zero-offset distance. The moveout correction is therefore the process of removing the moveout effects on traveltimes. As a result of moveout correction, traces are stretched in a time-varying manner, causing their frequency content to shift towards the low end of the spectrum (Figure 43). This distortion is more pronounced for shallow events and larger offsets (Yilmaz, 2001).

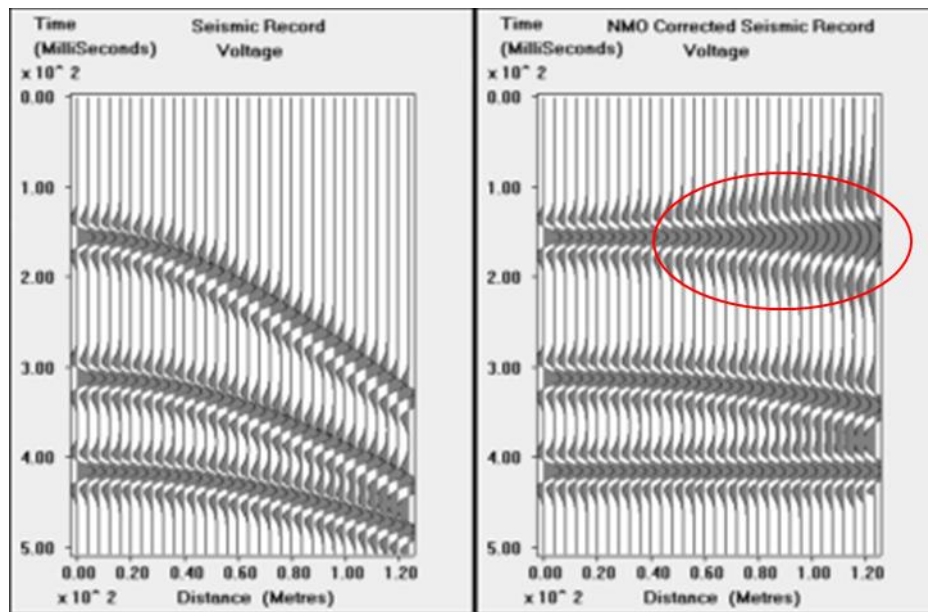


Figure 43 – Normal moveout stretch (<http://www.ucl.ac.uk/>)

b) Non-hyperbolic moveout

The observed moveout at a certain distance from the source can be calculated with the following equation

$$t^2(x) = c_0 + c_1x^2 + c_2x^4 + \dots (1)$$

where  $t(x)$  is traveltime at offset  $x$ ,  $c_0$  is the zero-offset traveltime ( $t_0^2$ ),  $c_1 = 1/v_{rms}^2$  (RMS velocity),  $c_2$  and  $c_3$  are complicated functions that depend on layers thickness and interval velocity.

When offsets are small compared to the depth of investigation the equation can be simplified to

$$t^2(x) = t_0^2 + \frac{x^2}{v_{rms}^2} (2)$$

However, when offsets are larger than previously stated, the higher order terms in equation (1) become significant and need to be included in the velocity analysis in order to accurately correct the observed moveout (Figure 44). While additional terms do increase the accuracy of the equation, they also cause the equation to become unstable. Small errors in the estimation of  $v$  and  $x$  can cause large errors in the calculated traveltime  $t(x)$ .

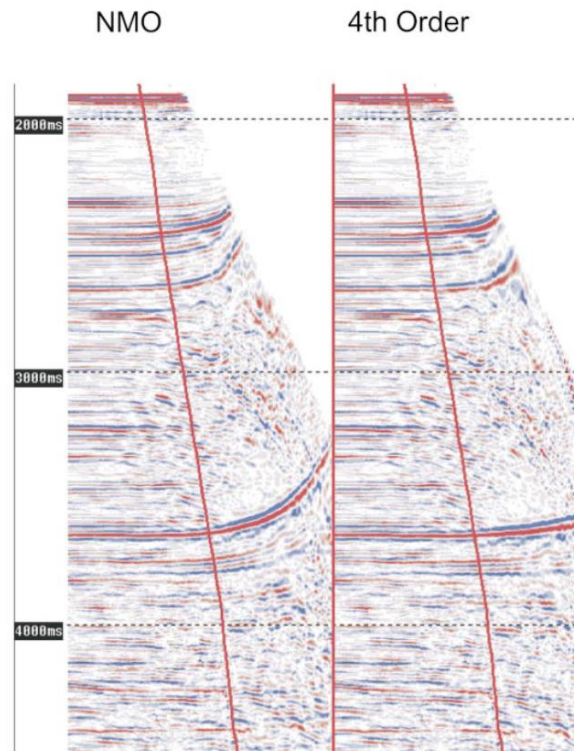


Figure 44 – Non-hyperbolic moveout correction (Dutta, 2002)

c) Waveform distortion around and beyond the critical angle

According to energy partition predicted by the Zoeppritz equation, around and beyond the critical angle, the percentage of energy reflected from a seismic interface increases compared to the energy transmitted through the interface. As a consequence the amplitude versus offset relation becomes much more complicated and it is more difficult to apply conventional semblance velocity analysis.

d) Inversed arrival times

Long offsets contain reflections from deeper layers which generally present higher velocities than the shallower (gas-free or gas-rich) sediments. As a consequence, deep reflections arrive earlier than the overlying reflections. If near offset data is not recorded then it becomes very difficult to identify observed events on the recorded data gather because reflections cannot be mapped to normal incident along a continuous offset range.

To illustrate this phenomenon we defined a simple layered model (Figure 45) and generated synthetic gathers with offsets up to 450m. Figure 46 shows the obtained (synthetic) seismic gather, including information from direct, refracted, reflected and seafloor multiple arrivals. We can observe that for offsets longer than 200m, arrival times inversion occurs and it becomes more important when the offset increases. If only far offset data are recorded it becomes almost impossible to identify the observed events (Figure 47).

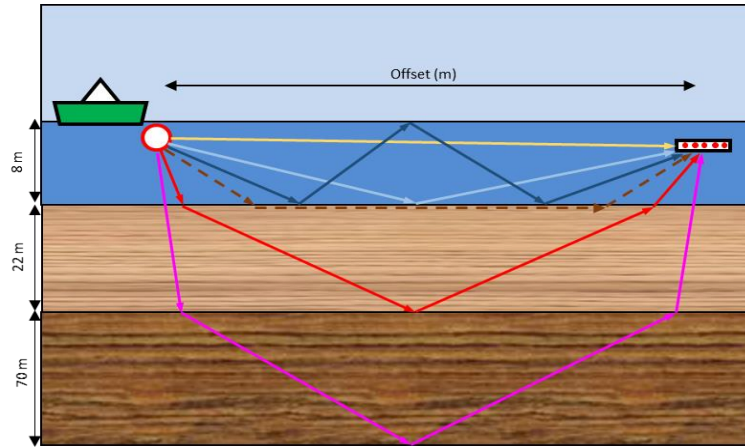


Figure 45 – Travel paths of seismic events. Yellow = direct wave, Light blue = seafloor reflection, Dark blue = seafloor multiple, Brown dashed = refracted wave, Red and green = reflected waves

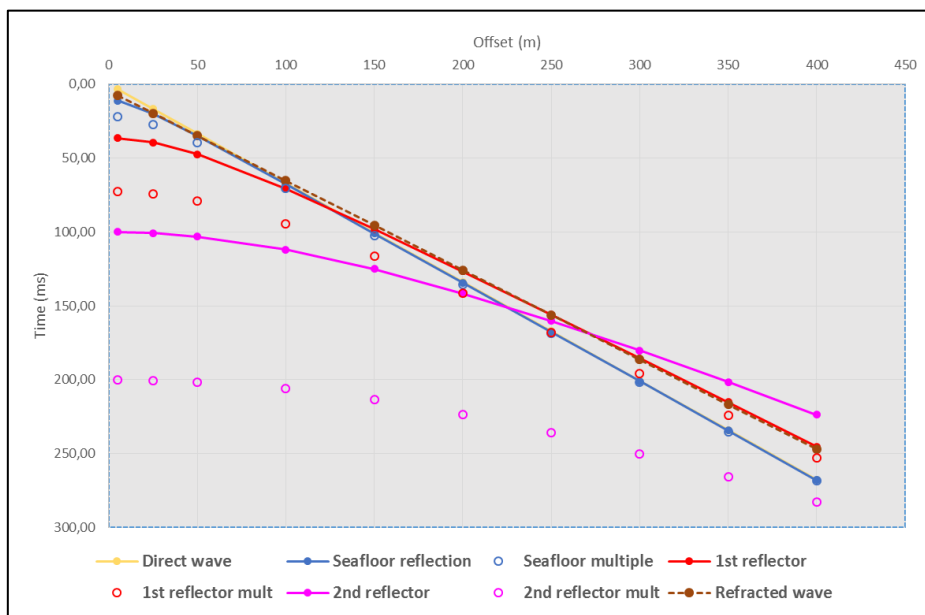


Figure 46 – Travel paths of seismic events (full record)

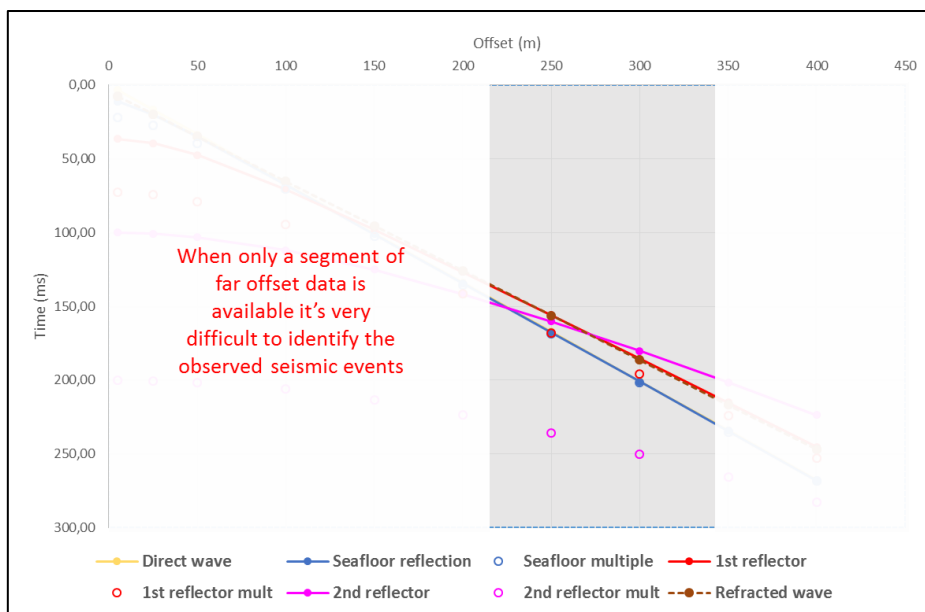


Figure 47 – Travel paths of seismic events (far offset record only)

#### 4.4.2 Long offset test results

The test line for the long offset tests was located a couple of kilometres offshore Ostend (Figure 48). This location is marked by the presence of alternating gas-rich and gas-free areas, as opposed to the test area near Zeebrugge where the gas-rich area is more extended and free-gas zones are rare. Furthermore the heavy ship traffic near Zeebrugge would severely hinder the already difficult navigation involving two ships sailing simultaneously.

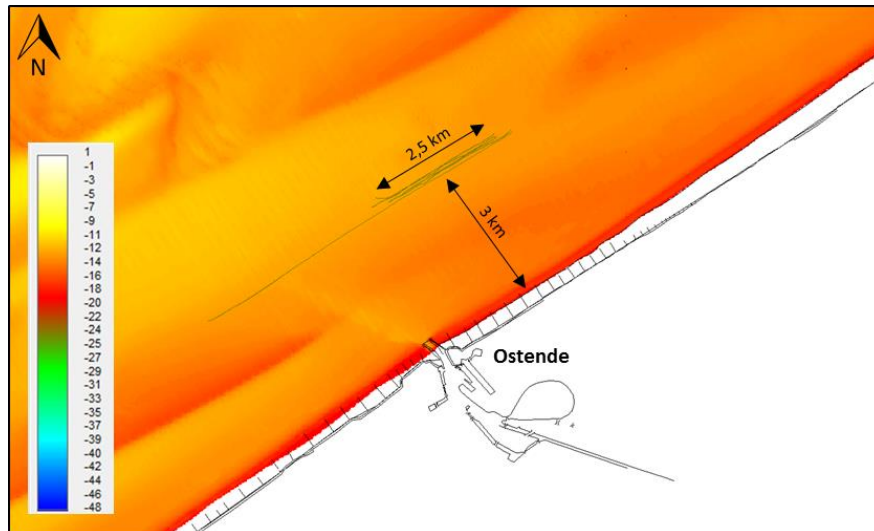


Figure 48 – Long offset lines location offshore Ostend.  
Background map is the current seafloor bathymetry (colour scale in metres).

The test line was located on top of the so-called Sepia Pits, three deeply incised scour hollows within the Ostend Valley reaching depths of up to 50m and mainly filled in with sandy deposits (De Clercq, 2015). The underlying deposits consist of Palaeogene clays that can reach up to 200 m deep where Cretaceous chinks are found underneath (Figure 49).

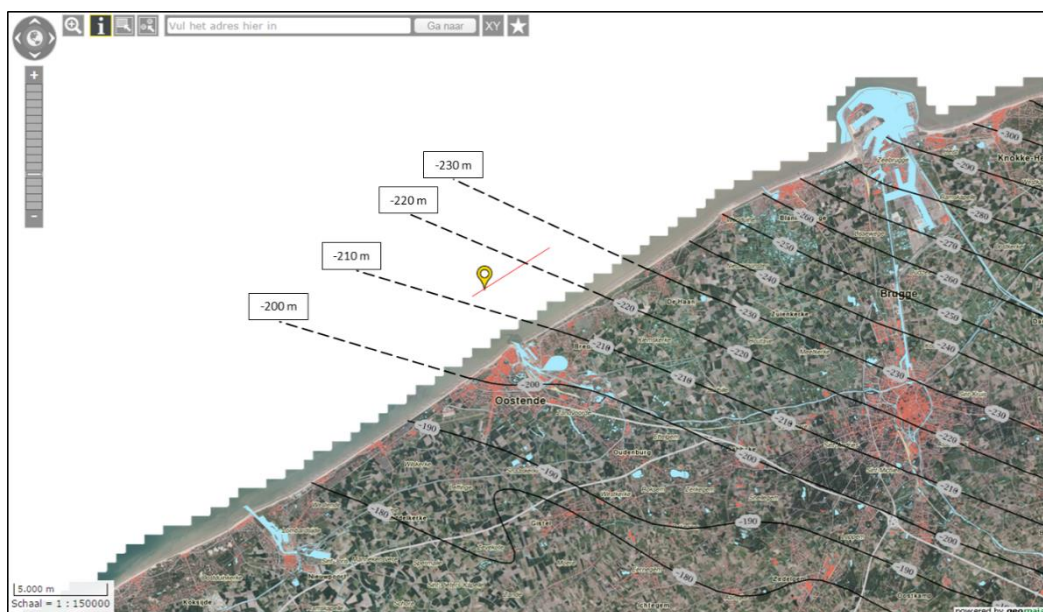


Figure 49 – Map showing the depth of the top of the Cretaceous chinks in the inland vicinity of the test line  
(DOV.vlaanderen.be)

Figure 50 shows a 2D seismic section from the same location showing the above mentioned structures.

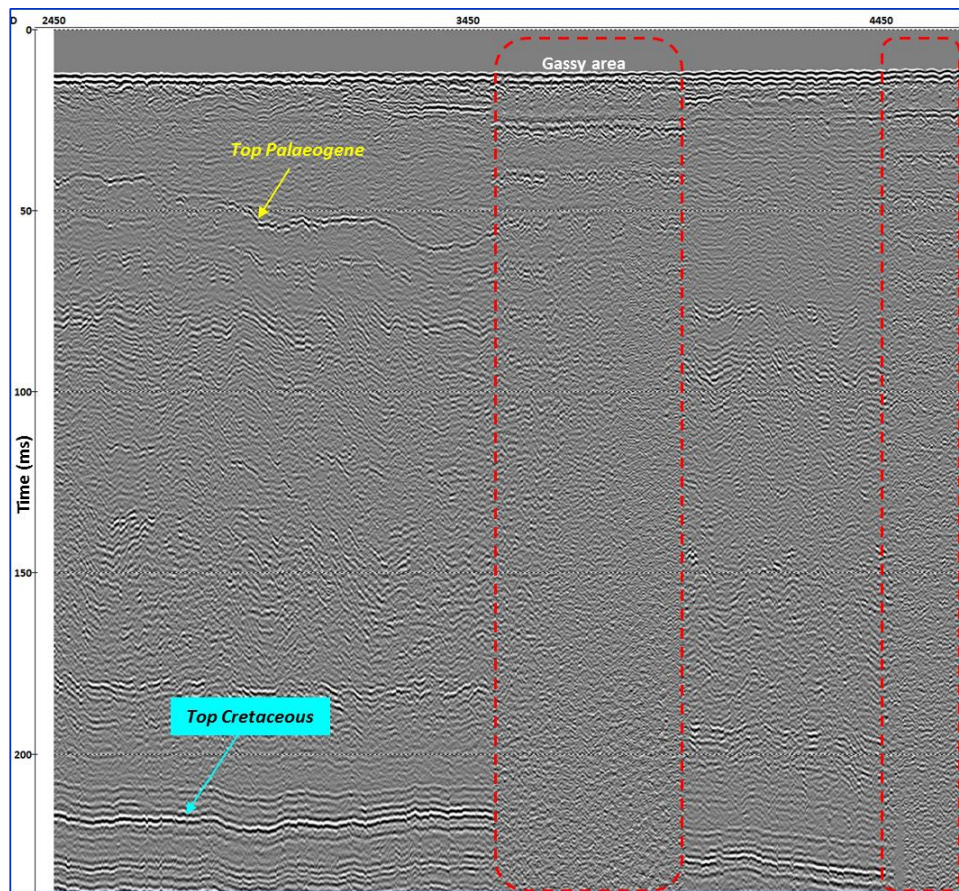


Figure 50 – Single-channel seismic reflection section showing the different geological strata at the Sepia Pits test site

Figure 51 shows a simplified geological section of the sediments encountered at the test line.

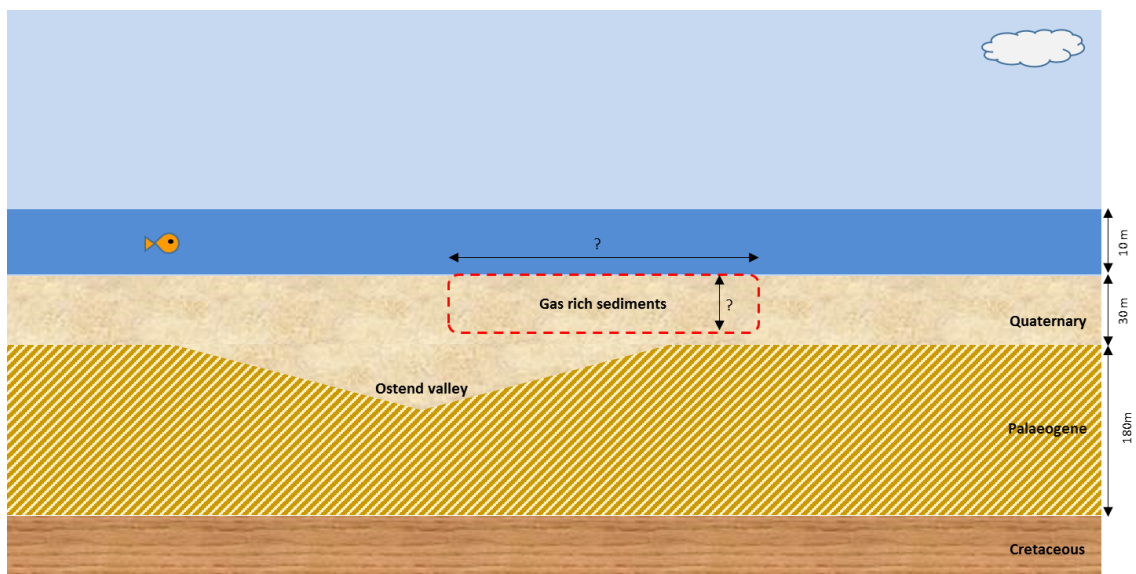


Figure 51 – Simplified geological model of the Sepia Pits test site for long offset tests

For the long offset tests three different acquisition configurations were used.

1. Acquisition configuration 1 (Figure 52)

This configuration consisted of the two vessels sailing in line separated by a constant distance. The test was intended to be performed twice using two different offsets of 200m (Test 1.1) and 300m (Test 1.2) respectively.

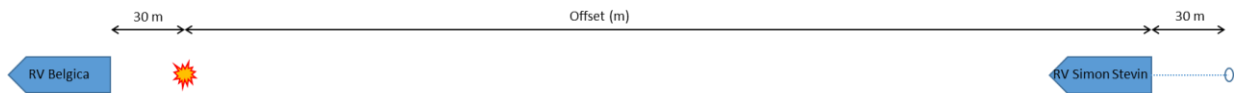


Figure 52 – Long offset acquisition configuration 1 (vessels sailing in line)

However, it proved to be very difficult to maintain a constant distance between the vessels during the whole acquisition. The actual distance between the vessels ranged from 140 to 240m during Test 1.1. (Figure 53) and from 200 to 380m during Test 1.2. (Figure 54).

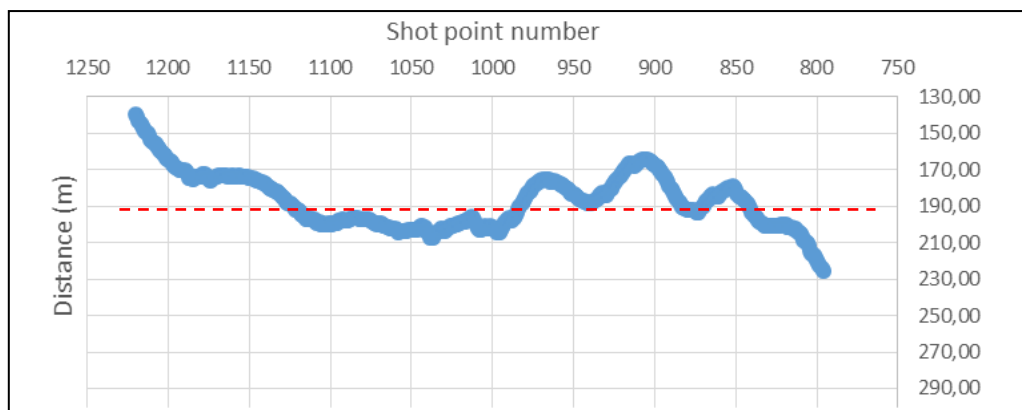


Figure 53 – Distance between source and receiver channel 1 (Test 1.1). The red line indicates the nominal offset (200m).

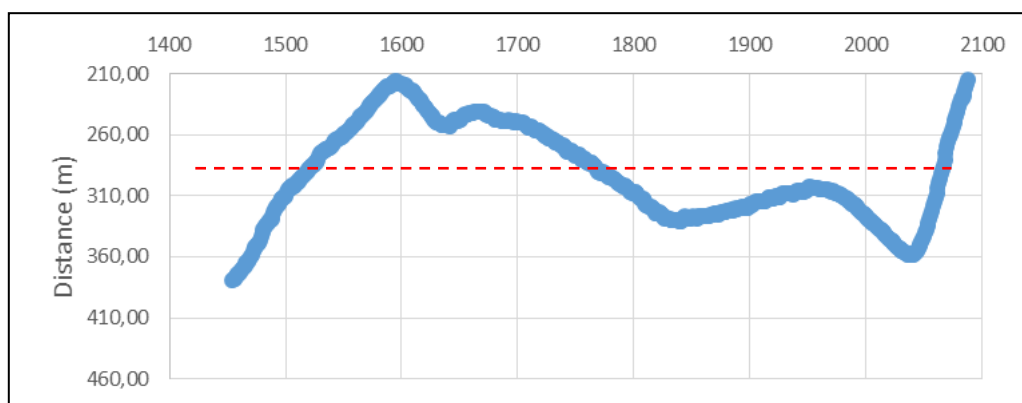
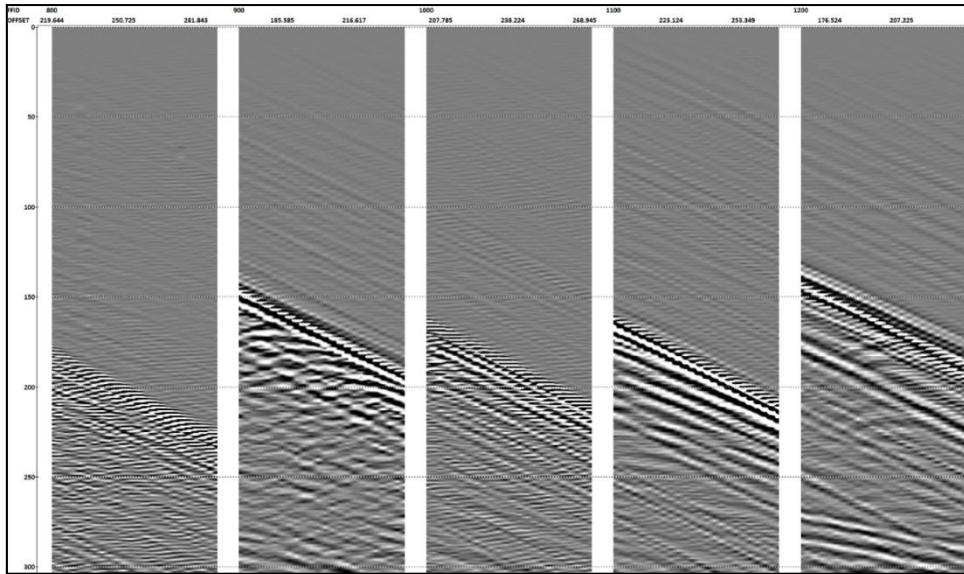


Figure 54 – Distance between source and receiver channel 1 (Test 1.2). The red line indicates the nominal offset (300m).



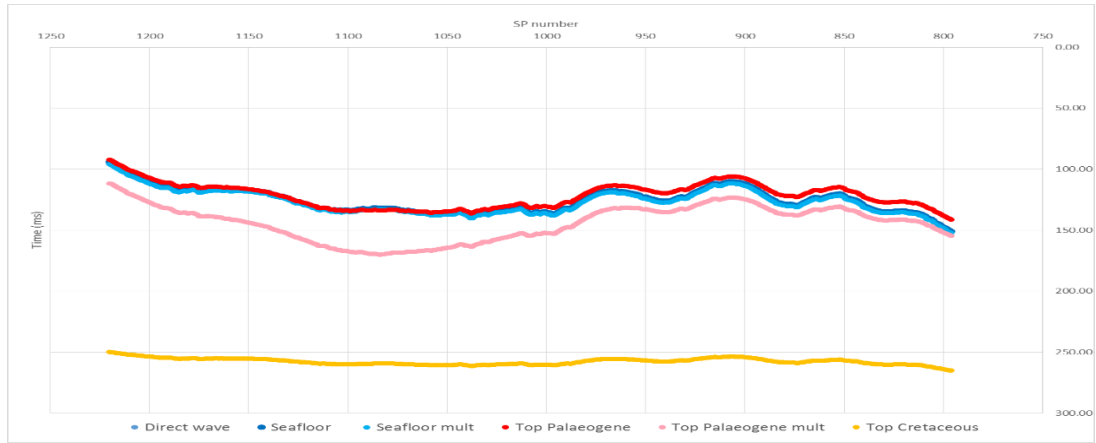


Figure 57 – 200m offset (Test 1.1) - Synthetic response of the model (Channel 1)

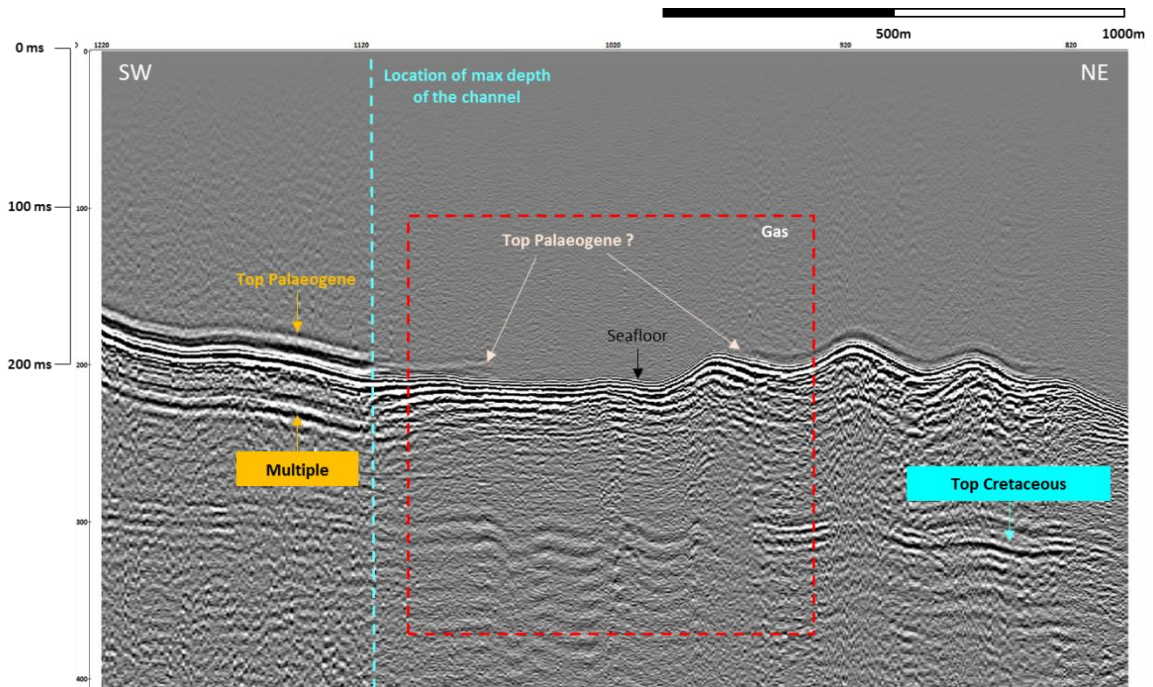


Figure 58 – 200m offset seismic profile (Test 1.1) (Channel 24)

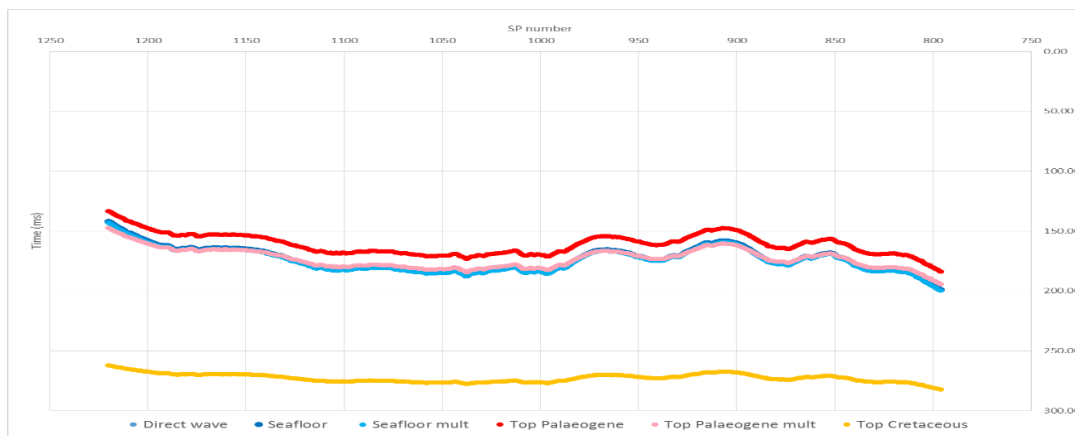


Figure 59 – 200m offset (Test 1.1) - Synthetic response of the model (Channel 24)

Results for Test 1.2 are shown below. Again, the corresponding theoretical channel displays (Figures 61 and 63) are shown underneath the actual seismic profiles (Figures 60 and 62).

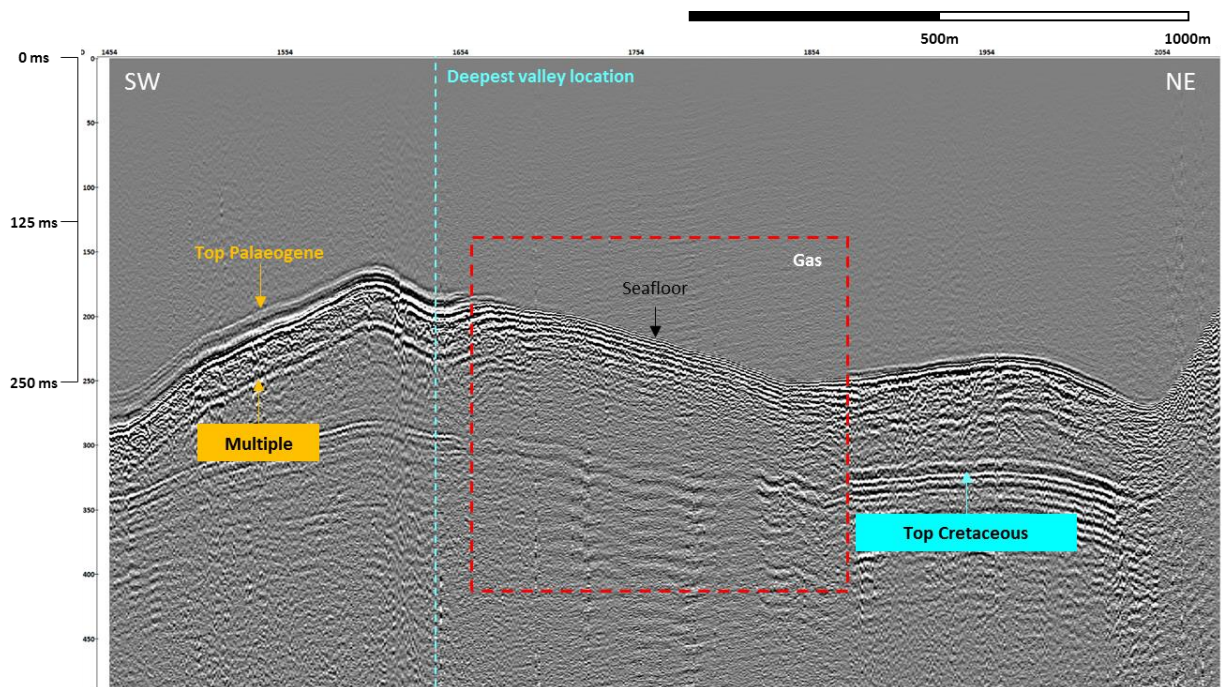


Figure 60 – 300m offset seismic profile (Test 1.2) (Channel 1)

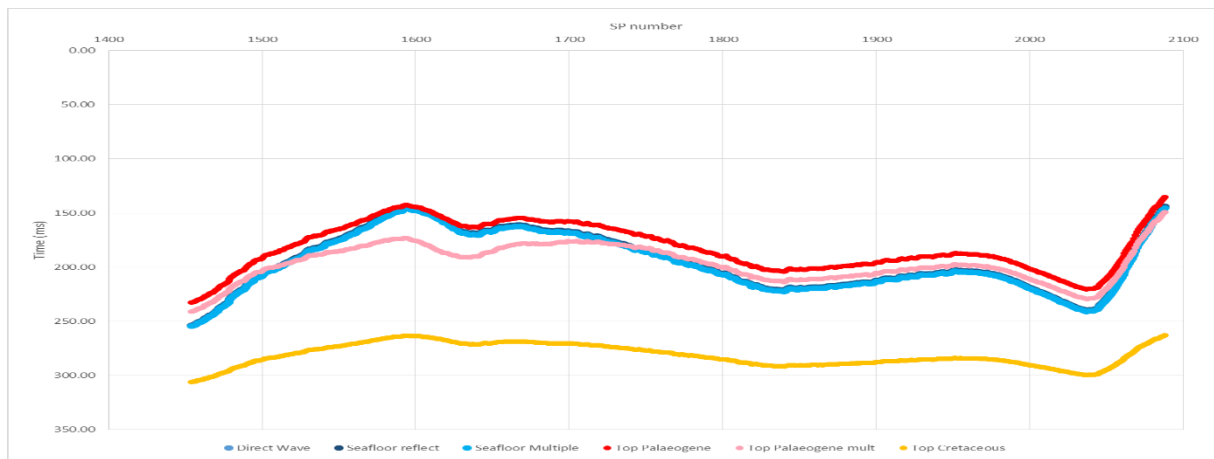


Figure 61 – 300m offset (Test 1.2) - Synthetic response of the model (Channel 1)

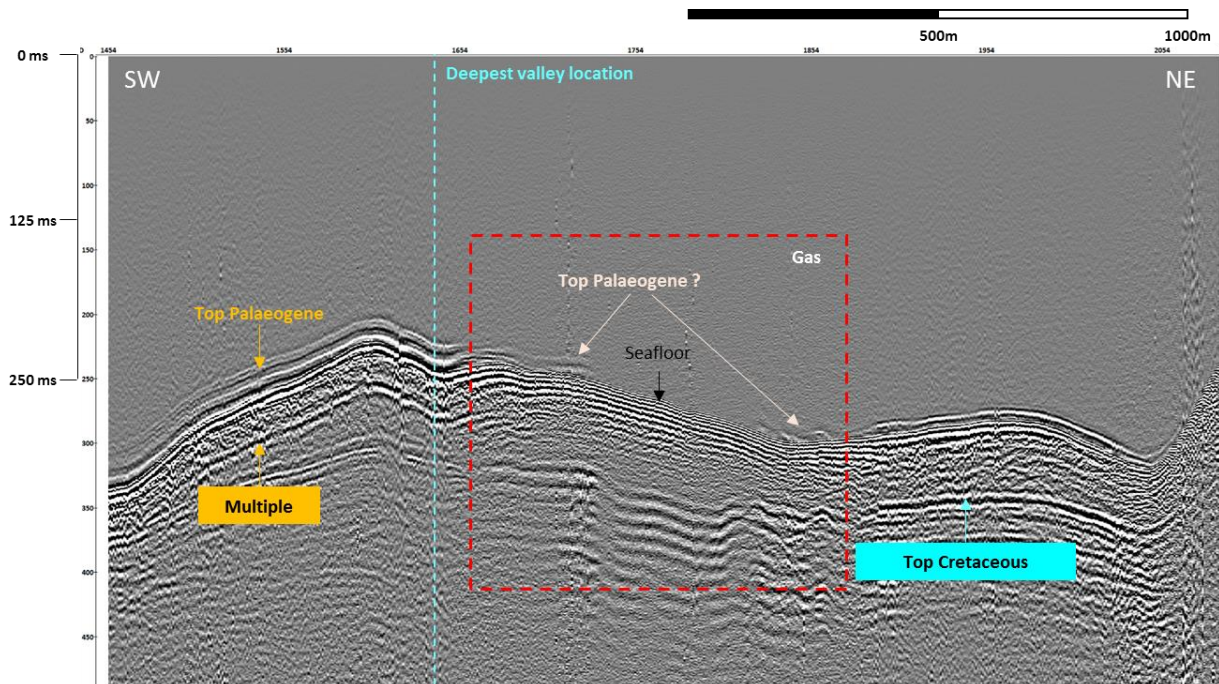


Figure 62 – 300m offset seismic profile (Test 1.2) (Channel 24)

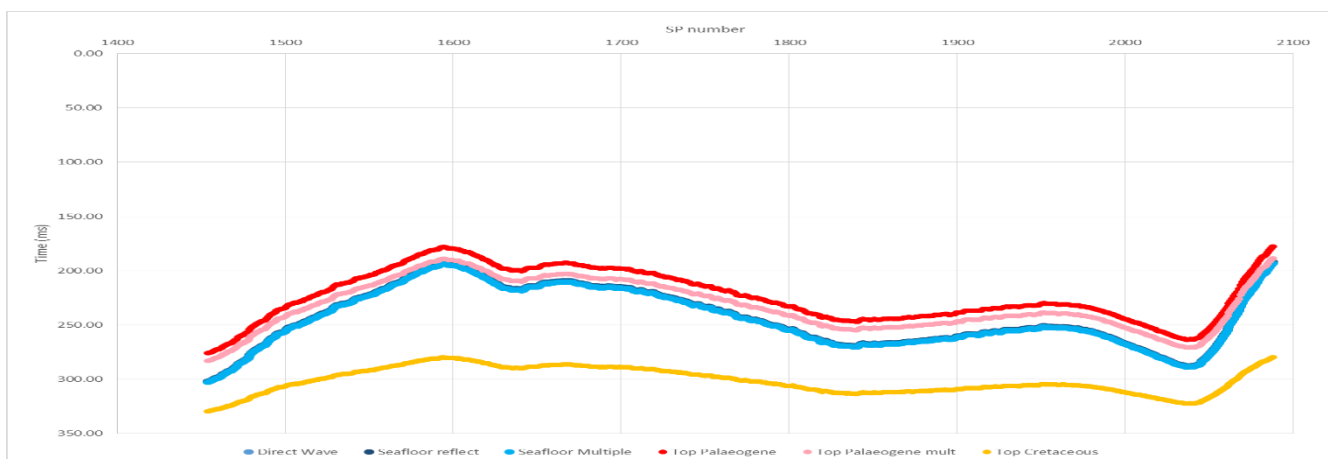


Figure 63 – 300m offset (Test 1.2) - Synthetic response of the model (two horizontal layers + valley) (Channel 24)

It can be observed that the synthetic responses (i.e. calculated arrival times) correspond relatively well with the arrival times observed on the recorded seismic profiles. The field data shows that the gassy sediments obscure or affects all the reflections from underlying sediments. Since the exact dimensions of the gassy area (both laterally and vertically) are largely unknown, it might be possible that the gassy area is larger and/or thicker than previously believed and we were not able to actually “undershoot” below the entire gas area.

When using a longer offsets (channel 24 instead of channel 1) some shallow events are partly visible on the edges of the gassy area. Based on their arrival times, these events have been interpreted to correspond to the Top Palaeogene surface (Figure 58 and 62) but the degree of uncertainty is too important to confirm it. Additionally, admitting these events were related to the Top Palaeogene it is impossible to say whether they are reflected or refracted waves from the Top Palaeogene surface. On the other hand, deeper reflectors, believed to correspond to the top Cretaceous horizon (over 200m deep), can be followed over the whole length of the profile, although the amplitude and

continuity of this reflector are clearly affected under the gassy areas. Further studies need to be carried out in order to confirm or invalidate the above mentioned observations.

## 2. Acquisition configuration 2 (Figure 64)

This configuration consisted of the source and receiver vessels sailing in parallel separated by a constant distance.

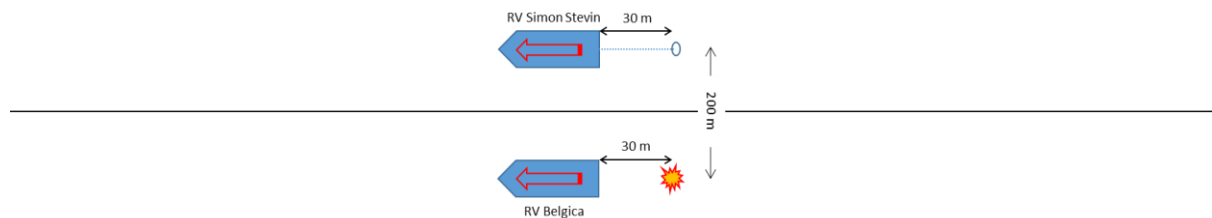


Figure 64 – Long offset acquisition configuration 2 (vessels sailing in in parallel)

The test was performed twice using two different offsets of 200m (test 2.1) and 300m (test 2.2) respectively. However, as with the previous configuration, the actual distance between the vessels was not kept constant and fluctuated from 200 to 340m during test 2.1 (Figure 65) and from 240 to 340m during test 2.2 (Figure 66).

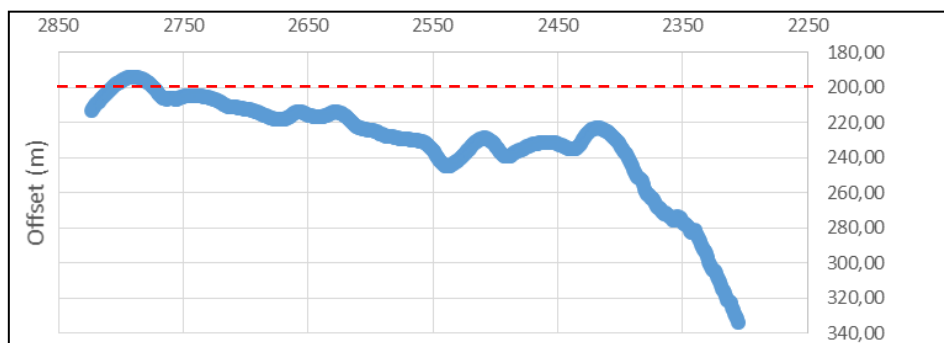


Figure 65 – Distance between source and channel 1 (Test 2.1). The red line indicates the nominal offset (200m)

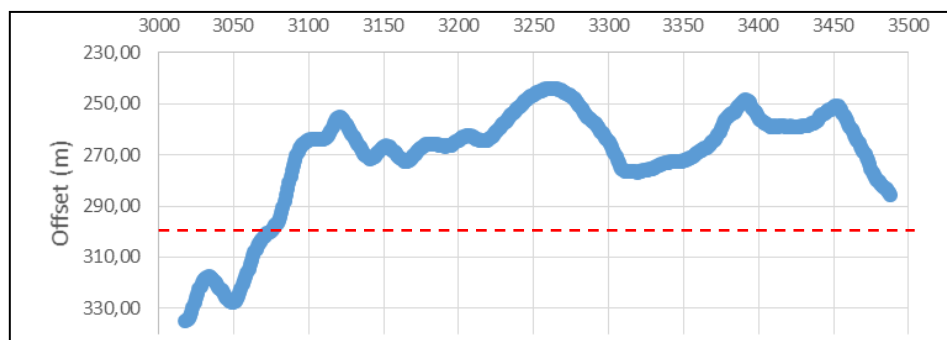


Figure 66 – Distance between source and channel 1 (Test 2.2). The red line indicates the nominal offset (300m)

Apart from the fact that the distance between the vessels was not kept constant, the relative position of the vessels also changed many times during the acquisition. In theory, both vessels should have sailed at the same relative position but very often the RV Belgica was ahead of the RV Simon Stevin and inversely. As a consequence, using channel 1 or channel 24 doesn't produce any difference on the results. We therefore display only channel gathers corresponding to Channel 1.

Similarly to the previous acquisition configuration, below we display the common channel gathers (Figures 68 and 70) and compare them to the synthetic data (Figures 67 and 69) from the simplified model in Figure 51.

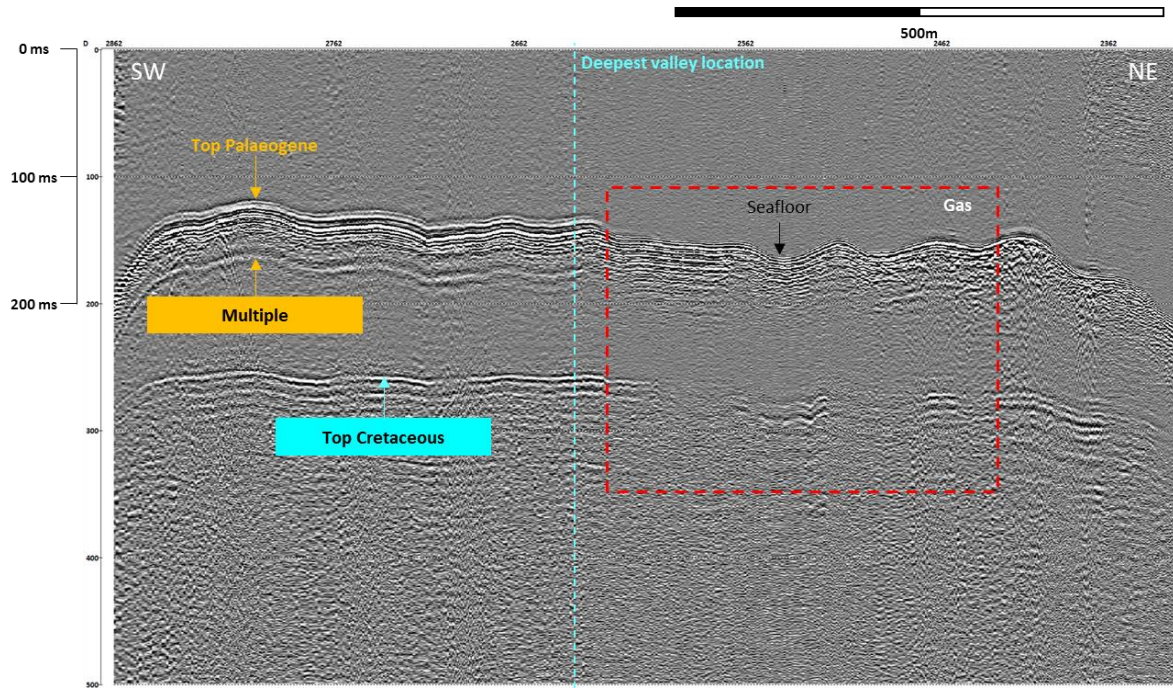


Figure 67 – 200m offset seismic profile (Test 2.1) (Channel 1)

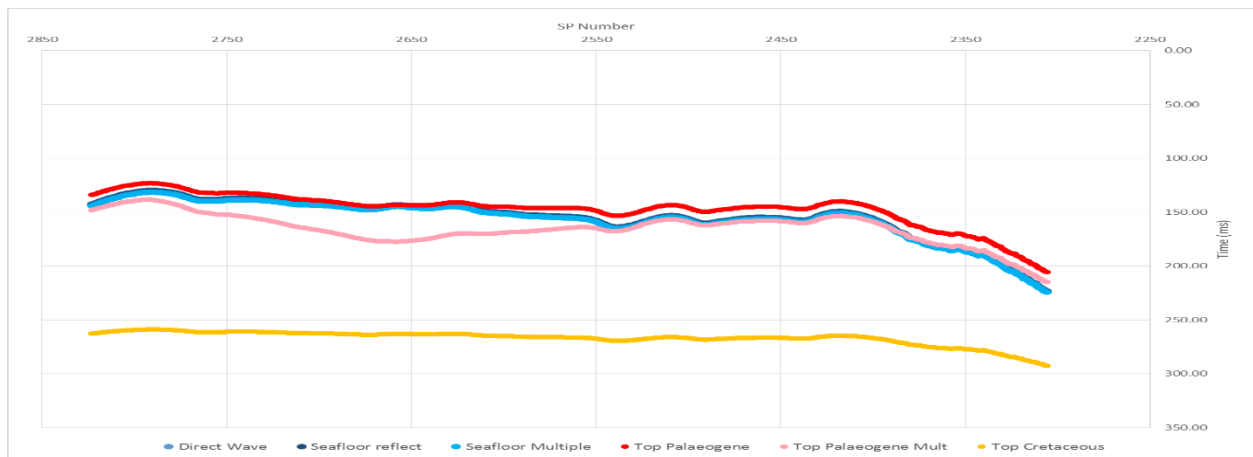


Figure 68 – 200m offset (Test 2.1) - Synthetic response of the model (two horizontal layers + valley) (Channel 1)

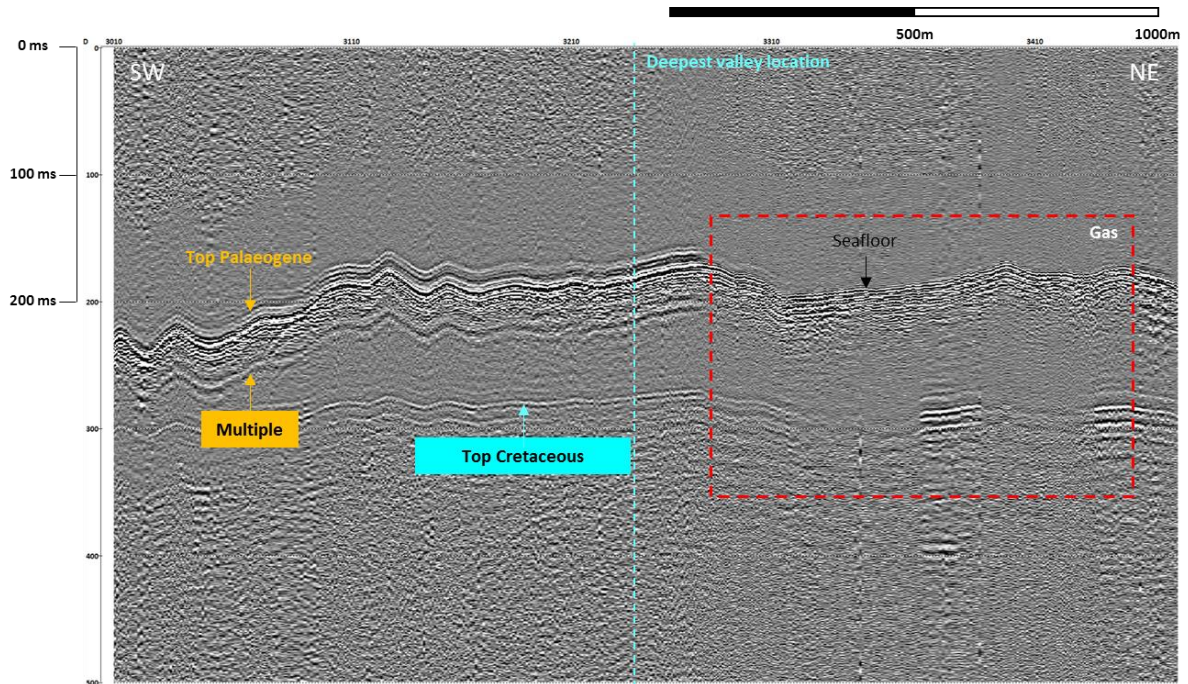


Figure 69 – 300m offset seismic profile - Test 2.2 (Channel 1)

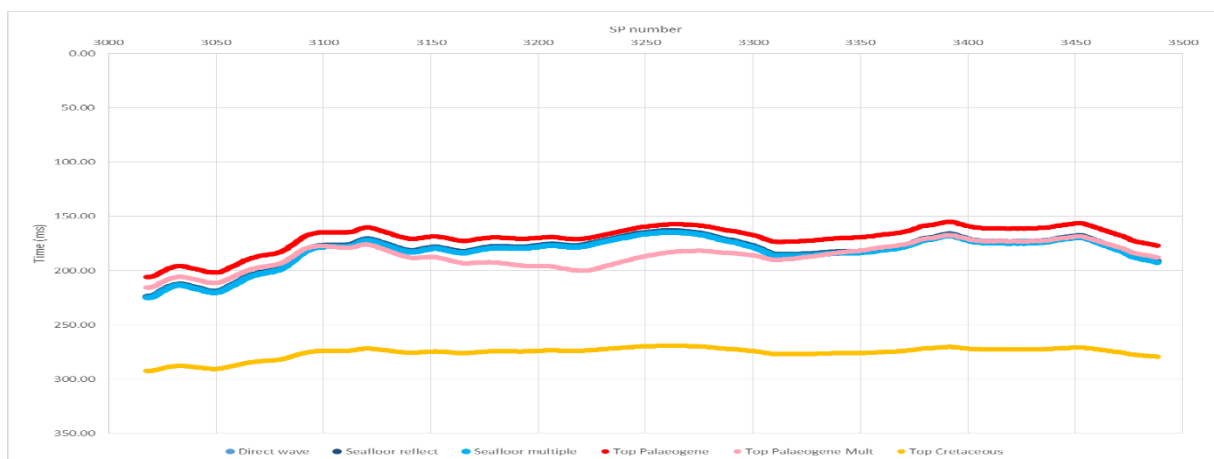


Figure 70 – 300m offset (Test 2.2) - Synthetic response of the model (two horizontal layers + valley) (Channel 1)

The results of Tests 2.1 and 2.2 are very similar and this is not surprising given that the actual offsets during the acquisition were relatively similar for both tests (240m average offset for Test 2.1 and 270m average for Test 2.2). Results confirm that reflectors below the gassy area are not distinguishable and only deep horizons (believed to correspond to the Top Cretaceous boundary) can be observed at 250ms (~190m) or deeper. As opposed to results from Test 1.1. and 1.2. the reflectors believed to correspond to the Top Palaeogene boundary are not visible. This may be caused by the fact that maximum offset was not as long as the maximum offsets obtained in tests 1.1. and 1.2.

### 3. Acquisition configuration 3 (Figure 71)

In this test a seismic refraction layout was used, keeping the source vessel (RV Belgica) stationary, while the receiver vessel (RV Simon Stevin) was moving alternately closer and away from the source. This test was aimed at obtaining velocity profiles rather than actually imaging the sediments below the seafloor. Four different test lines were acquired with this configuration (3.1 to 3.4).

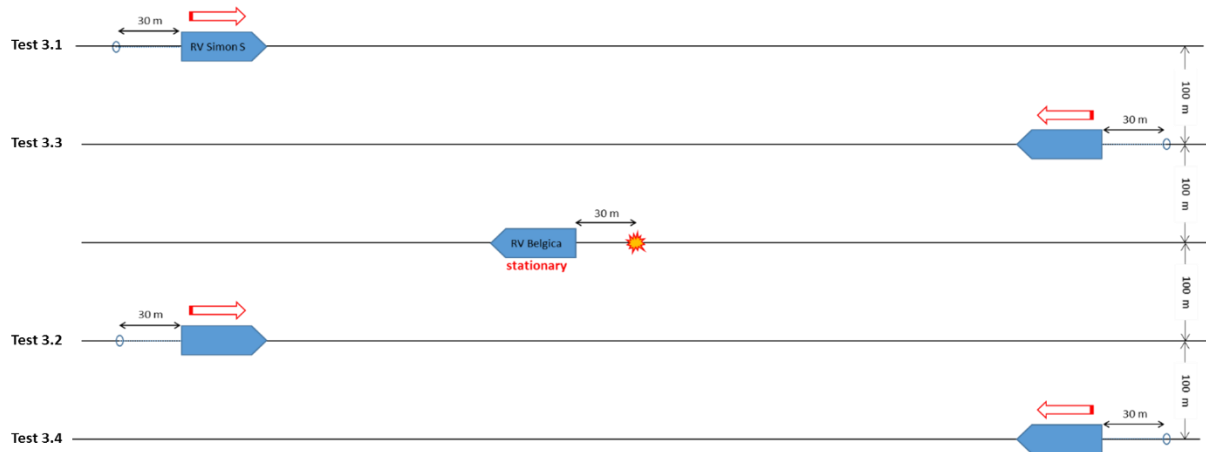


Figure 71 – Long offset acquisition configuration 3 (source vessel stationary and receiver vessel in motion)

The seismic refraction method involves the analysis of the arrivals times of acoustic waves that travel at the interface between a low and a high velocity geological layer. It is based on the principle that when a seismic wave impinges upon a boundary across which there is a contrast in velocity, then the direction of travel of that wave changes on entry into the new medium. The amount of change of direction is governed by the contrast in seismic velocity across the interface according to Snell's law (Reynolds, 1997).

Once data have been collected, arrival times are computed from the seismographs. Arrival times can be represented on a travel-time graph or T-X plot (Figure 72), that arrival times (usually in milliseconds) versus offset (distance between source and receiver). The obtained travel time plot is interpreted assuming the subsurface is made of a series of discrete layers of different seismic velocity. Based on the travel times of the arrivals, the velocities of the layers above and below the interface can be determined from the slopes of the arrivals. Also, using the depth to the interface can be obtained from the intercept time at zero offset (Figure 72).

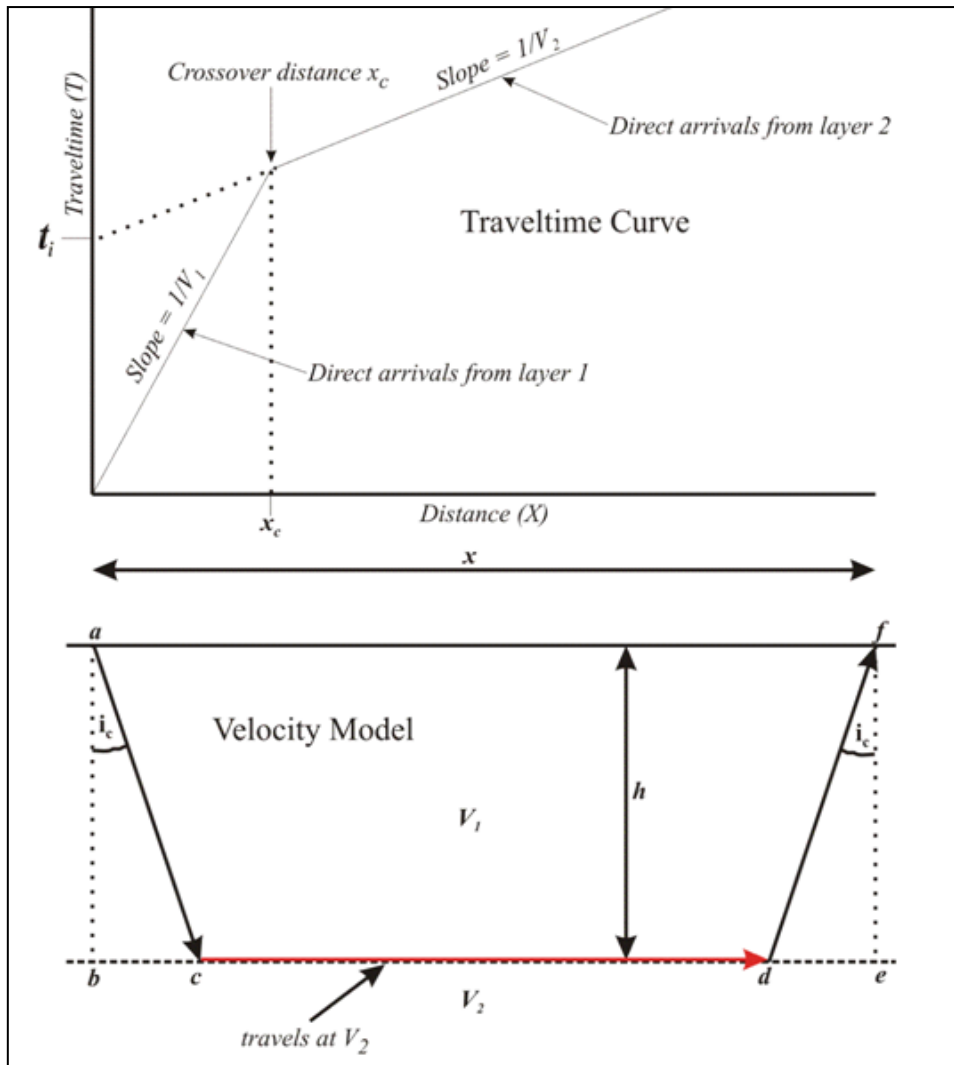


Figure 72 – Seismic refraction principles

If  $V_2 < V_1$ , the energy refracts toward the normal. None of the refracted energy makes it back to the surface. A slower layer beneath a faster layer will not be detected by seismic refraction. The presence of a velocity inversion can lead to errors in depth calculations.

Figures 73 to 76 show shot gathers from tests 3.1 to 3.4. The slope of the observed first arrivals is dependent on the velocity of the propagation media. By fitting a line to the observed arrival we can deduce its propagation velocity. Due to the absence of zero offset data, no information about the thickness of the layers can be obtained.

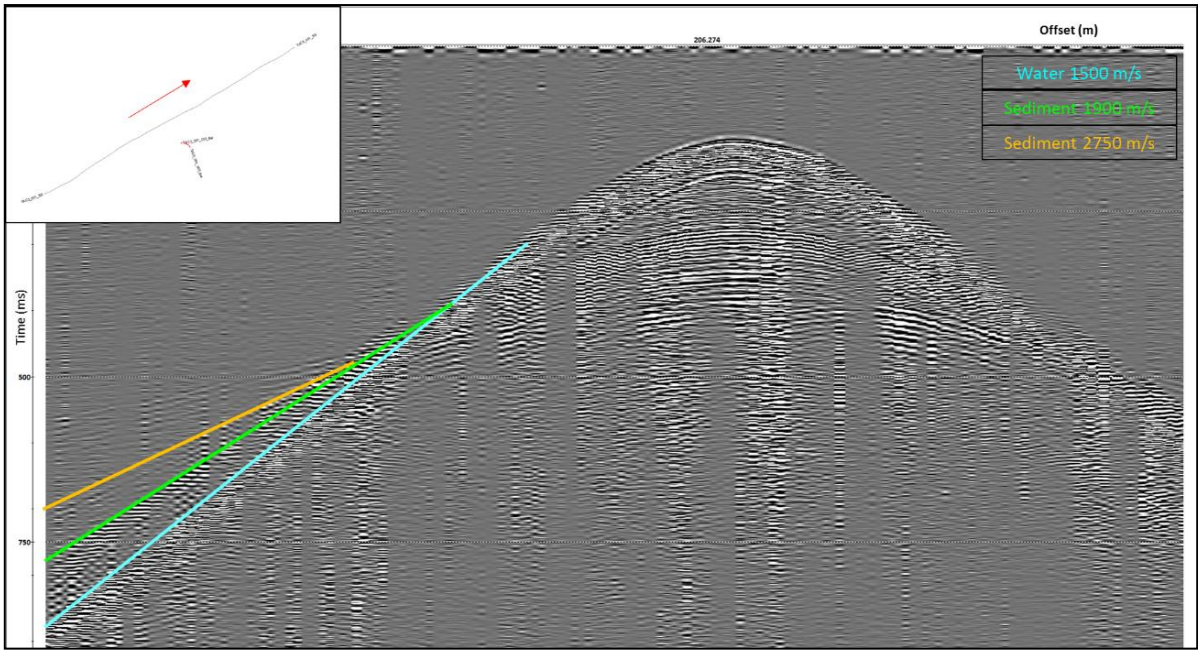


Figure 73 – Shot gather (Test 3.1)

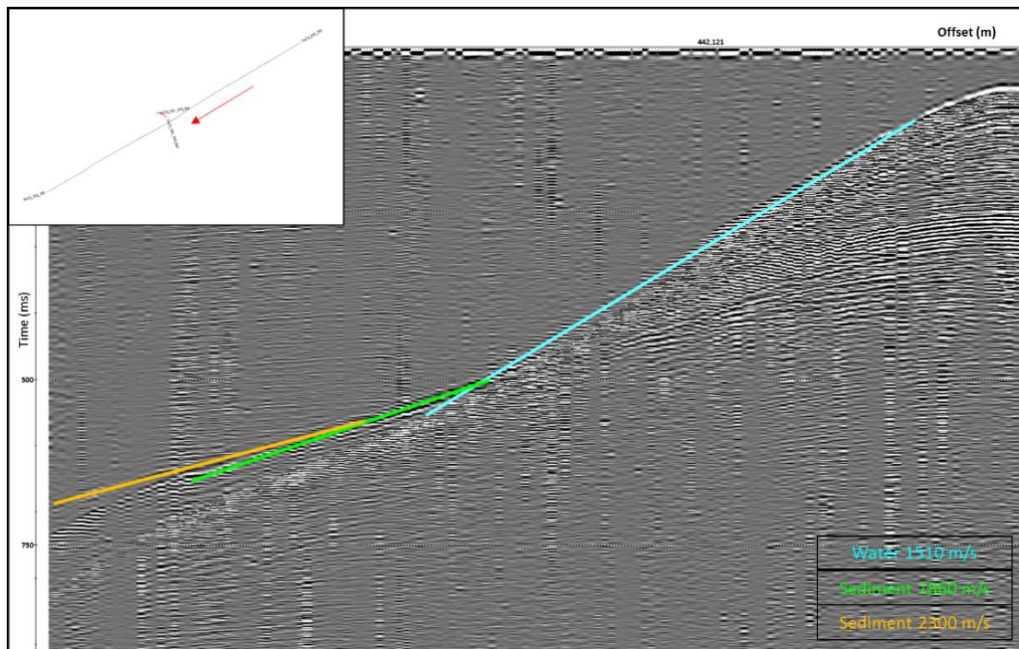


Figure 74 – Shot gather (Test 3.2)

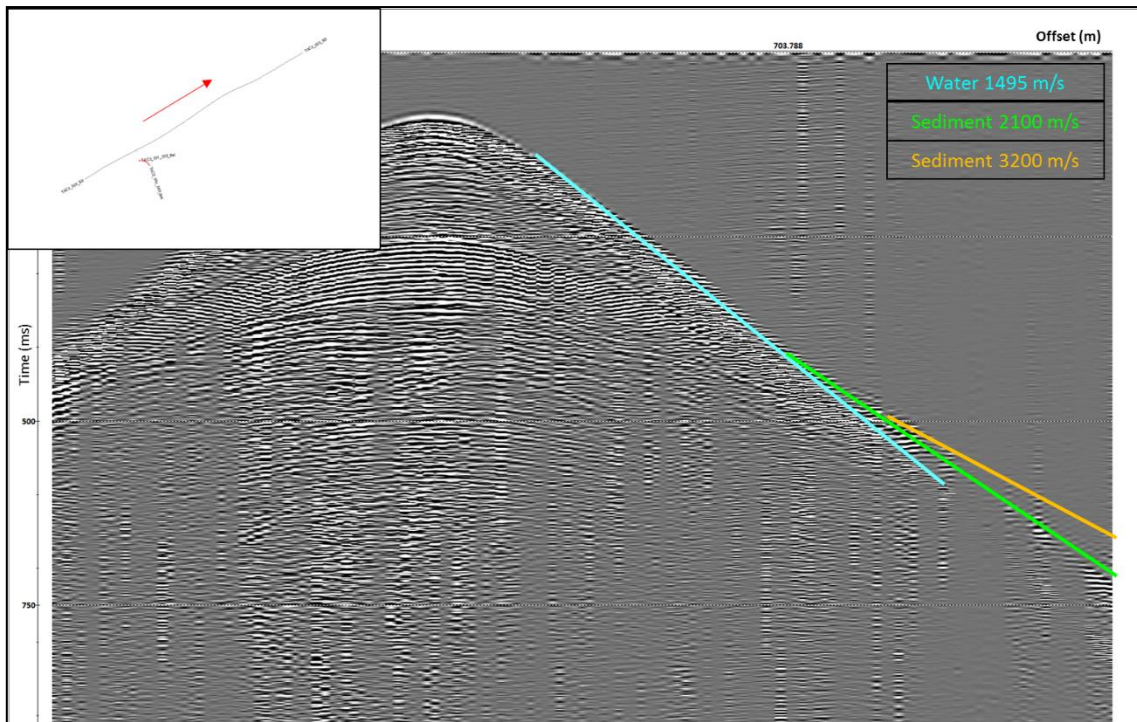


Figure 75 – Shot gather (Test 3.3)

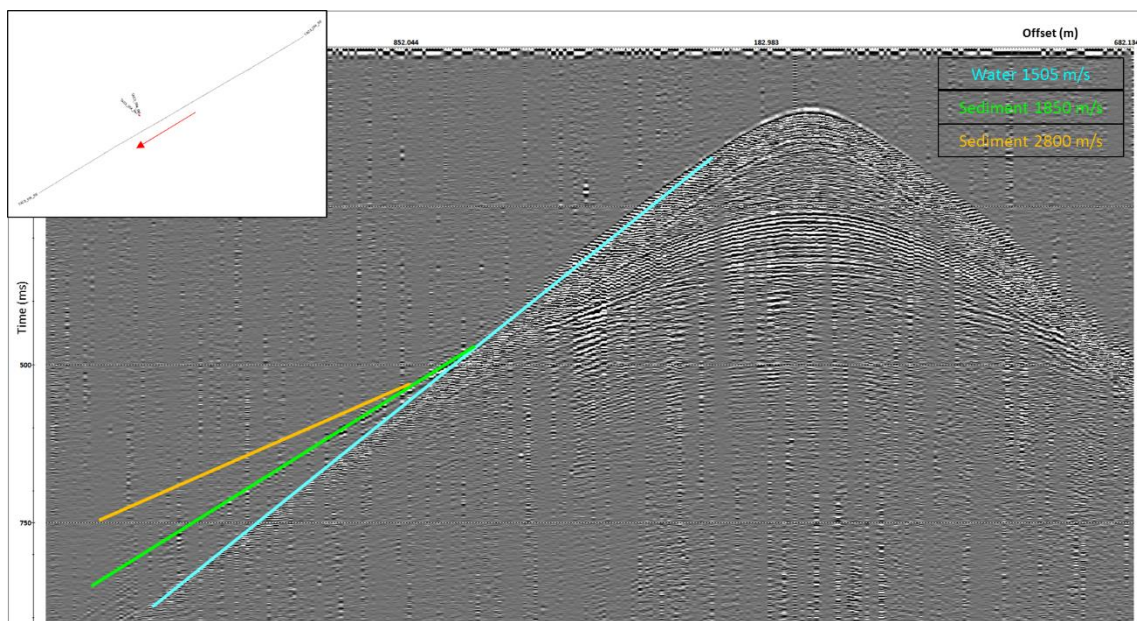


Figure 76 – Shot gather (Test 3.4)

The results for each test are summarized in Table 7 below

|                        | Test 3.1 | Test 3.2 | Test 3.3 | Test 3.4 | Average |
|------------------------|----------|----------|----------|----------|---------|
| Water velocity (m/s)   | 1500     | 1510     | 1495     | 1505     | 1500    |
| Layer 1 velocity (m/s) | 1900     | 1860     | 2100     | 1850     | 1925    |
| Layer 2 velocity (m/s) | 2750     | 2300     | 3200     | 2800     | 2775    |

Table 7 – Obtained velocity summary

Values in red are most likely not reliable. Variations in the speed of the source vessel can produce changes in the slope of the arrivals which will introduce errors in the velocity.

## 5. Summary

This study has demonstrated that high-resolution seismic imaging is an ideal tool to study buried landscapes, such as prehistoric river valleys, as they provide fast, cost-effective and non-destructive high-resolution information of the sub-seafloor.

Sparker sources provided the best compromise between resolution and penetration of investigation. They were the only sources capable of imaging shallow and deep reflector in detail at the same time. Among the tested sparker sources, the RCMG Centipede and the Geo-Source 200 produced the best results. However, the Centipede was more susceptible to weather and sea-state conditions than the Geo-Source 200 sparker. The SIG sparker produced a stronger and broader signal than the other sparkers and as a consequence produced seismic data of lower resolution.

The sleeve gun was not suited for this kind of investigation, data is too low frequency to accurately image shallow reflectors with the required levels of high resolution.

Boomer sources produced data of lower quality than the sparkers. Their resolution was relatively poor and their depth of investigation too. Only the IKB Seistec produced data of high resolution but its ringing damaged the very shallow reflections.

High frequency sources, like the pinger, chirp and echosounder, showed good resolution of the shallowest targets but their penetration depth was in the order of 5m. Among these sources, the pinger (Geopulse) produced the images with the lower quality, its signal was very weak and highly contaminated with ringing. For very shallow targets the PES proved the best solution.

Single-channel streamer produced relatively better images of the shallow reflectors than MC data. For deeper reflectors, multi-channel streamer gave much better results than SC data. It was demonstrated that smaller distances between channels in the MC streamer are necessary for increasing the resolution of the final image. Reducing the channel spacing and keeping the number of channels would reduce the unnecessary long offsets and distortions related to it. Using a MC streamer with such configuration will improve the resolution of the very shallow reflectors to such extend that they will be comparable or even better than the obtained with the SC streamer and therefore making the use of the later unnecessary.

Finally, imaging beneath or inside the gassy sediments was not possible with any of the tested techniques. The use of longer offsets may represent an opportunity but further studies and analysis need to be performed. Also, new long offset acquisition configurations need to be considered to avoid changes in the distance between the source and the receiver.

## 6. References

Anderson, A. L., Hampton, L. D., (1980). Acoustics of gas-bearing sediments I-II. *J. Acoust. Soc. Am.* 67, 1865-1903.

Reynolds, J.M., (1997). *An Introduction to Applied and Environmental Geophysics*. Wiley: 796 p.

Wilkins, R.H., Richardson, M.D., (1998). The influence of gas bubbles on sediment acoustic properties: in situ, laboratory, and theoretical results from Eckernförde Bay, Baltic sea. *Continental Shelf Research* 18, 1859-1892.

Trentesaux, A., Stolk, A. Berne, S., (1999). Sedimentology and stratigraphy of a tidal sand bank in the southern North Sea. *Mar Geol* 159: 253-272

Yilmaz, O., (2001). *Seismic Data Analysis: Processing, Inversion, and Interpretation of Seismic Data*. Society of Exploration Geophysicist, Tulsa. USA.

Dutta, N. C., (2002). Geopressure prediction using seismic data: Current status and the road ahead: *Geophysics*, 67, 2012–2041.

Missiaen, T., Murphy, S., Loncke, L., Henriët, J. P., (2002). Very high-resolution seismic mapping of shallow gas in the Belgian coastal zone. *T. Continental Shelf Research* 22 (2002) 2291–2301

Lin, Q., (2003). *A Study of long-offset seismic imaging with an upgraded physical modelling system (master's thesis)*. Retrieved from the Earth and atmospheric sciences department of the University of Houston website.

Schroot, B.M., Schüttenhelm, R.T.E., (2003). Expressions of shallow gas in the Netherlands North Sea. *Netherlands Journal of Geosciences / Geologie en Mijnbouw* 82 (1): 91-105

Dowle, R., (2006). Solid streamer noise reduction principles: *SEG Expanded Abstracts* 25, 85-89

Verschuur, D.J., (2006). *Seismic multiple removal techniques: past, present and future*. EAGE publications b.v., Houten, the Netherlands.

Mathys, M., (2009). *The Quaternary geological evolution of the Belgian Continental Shelf, southern North Sea*. PhD Thesis, Ghent University.

Tóth, Z., (2013). *Seismo-acoustic investigations of shallow free gas in the sediments of the Baltic Sea*. PhD Thesis, University of Bremen.

Tóth, Z., Spiess, V., Mogollón, J. M., Jensen, J. B., (2014). Estimating the free gas content in Baltic Sea sediments using compressional wave velocity from marine seismic data, *J. Geophys. Res. Solid Earth*, 119

De Clercq, M., Chademenos, V., Van Lancker, V., Missiaen, T., (2015). A high-resolution DEM for the Top-Palaeogene surface of the Belgian Continental Shelf, *Journal of Maps*.  
[doi.org/10.1080/17445647.2015.1117992](https://doi.org/10.1080/17445647.2015.1117992)

**Appendix A (Technical specifications on the seismic sources used)**

|  |  |
|--|--|
| <p>I/O Sleeve gun-IB (Deltares)<br/>         Chamber: 10 in<sup>3</sup><br/>         Dimensions: 50 x 26 x 10 cm<br/>         Weight: 31kg<br/>         Freq range: 0-256 Hz</p>   |  <p>The image shows a complex piece of seismic source equipment, the I/O Sleeve gun-IB, mounted on a boat deck. It consists of several white cylindrical chambers connected by a network of black and yellow cables. A large black hose is also visible, leading to a control unit on the deck. The background shows a body of water and a distant shoreline with buildings.</p> |
| <p>SIG sparker (UGent – RCMG)<br/>         Energy: 250 to 750 Joules<br/>         Dimensions: 100 x 40 x 5 cm<br/>         Weight: 1,25kg<br/>         Central freq: 800-900Hz<br/>         HV-power supply: 220V AC</p> |  <p>The image shows a SIG sparker electrode array lying on a grassy surface. It features a long, white, cylindrical central electrode with numerous thin, curved metal wires extending from its length, forming a fan-like shape. The wires are arranged in a regular pattern, likely for precise positioning in the water.</p>   |
| <p>Geo-Source 200 sparker (GSO)<br/>         Energy: 100 to 1000 Joules<br/>         Dimensions: 100 x 75 x 40 cm<br/>         Weight: 50 kg<br/>         Freq range: 250-2250Hz</p>                                     |  <p>The image shows a Geo-Source 200 sparker mounted on the deck of a boat. The equipment is primarily orange and white, with a large yellow coiled cable. The boat's name 'EUGRO NGADIE' and 'HYC' are visible on the side panel. The boat is on a body of water.</p>   |

GSO 360 sparker (GSO)  
Energy: 50 to 2400 Joules  
Dimensions: 109 x 75 x 43 cm  
Weight: 46.5 kg  
Freq range: 500-2000 Hz



RCMG Centipede sparker (RCMG)  
Energy: 300 - 600 Joules  
Dimensions: 195 x 20 x 20 cm  
Weight: 25 kg  
Central freq: 1100 – 1200 Hz  
HV-power supply: 220V AC



IKB-Seistec boomer (RCMG)  
Energy: 100 - 300 Joules  
Dimensions: 257 x 76 x 65 cm  
Weight: 100 kg  
Freq range: 1000 – 5000 Hz  
HV-power supply: 220V AC



Design Projects 500J boomer plate  
(Deltares)  
Energy: 500 Joules  
Freq range: 400 – 10000 Hz



Design Projects 300J boomer plate  
(Deltares)  
Energy: 300 Joules  
Freq range: 400 – 10000 Hz



Kongsberg Geopulse pinger (RCMG)  
Dimensions: 70 x 52 x 46 cm  
Weight: 120 kg  
Freq range: 2000 – 12000 Hz  
HV-power supply: 115/230 V AC



Edgetech X-Star chirp (Deltares)  
Dimensions: 160 x 124 x 47 cm  
Weight: 200 kg  
Freq range: 500 – 12000 Hz  
HV-power supply: 120/220 V AC



Innomar Parametric EchoSounder  
(TUDelft)  
Dimensions: 34 x 26 x 8 cm  
Weight: 22 kg  
Freq range: 6000 – 12000 Hz  
HV-power supply: 100/240 V AC



## Appendix B (Single channel data demultiple results)

Data without demultiple is shown on the left hand side of the comparison panel. Improvements or successful seafloor multiple attenuation are highlighted with a blue ellipse and deterioration of the data after the demultiple process are indicated with a red ellipse.

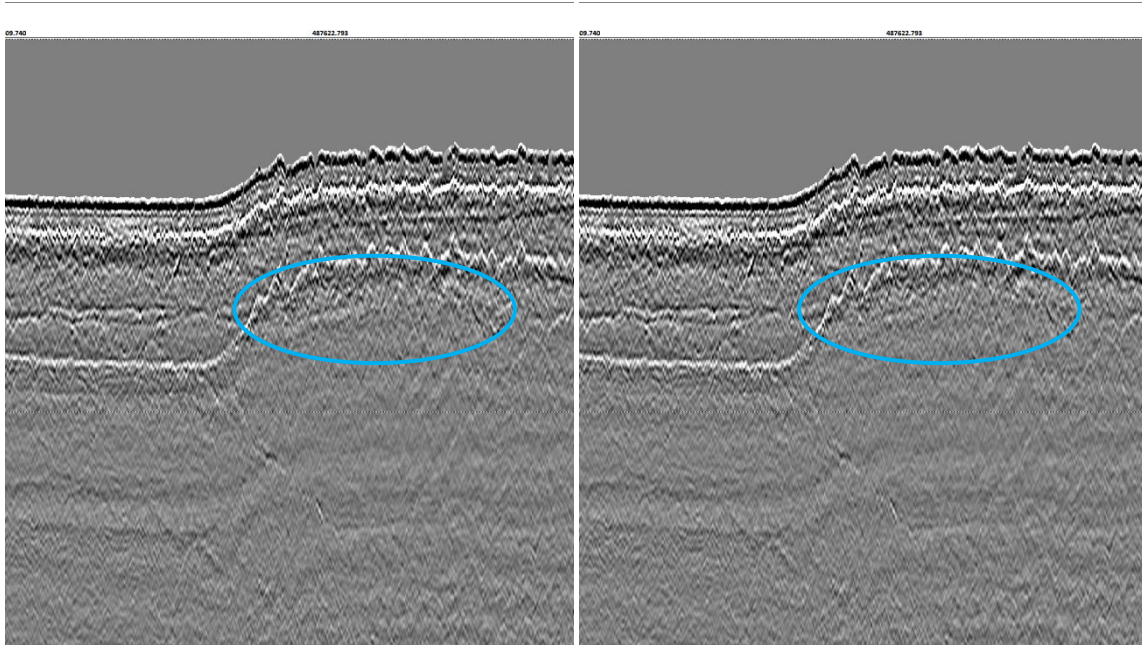


Figure B.1 – Sleeve gun profile, test line across the Ostend Valley. Before (left) and after (right) demultiple

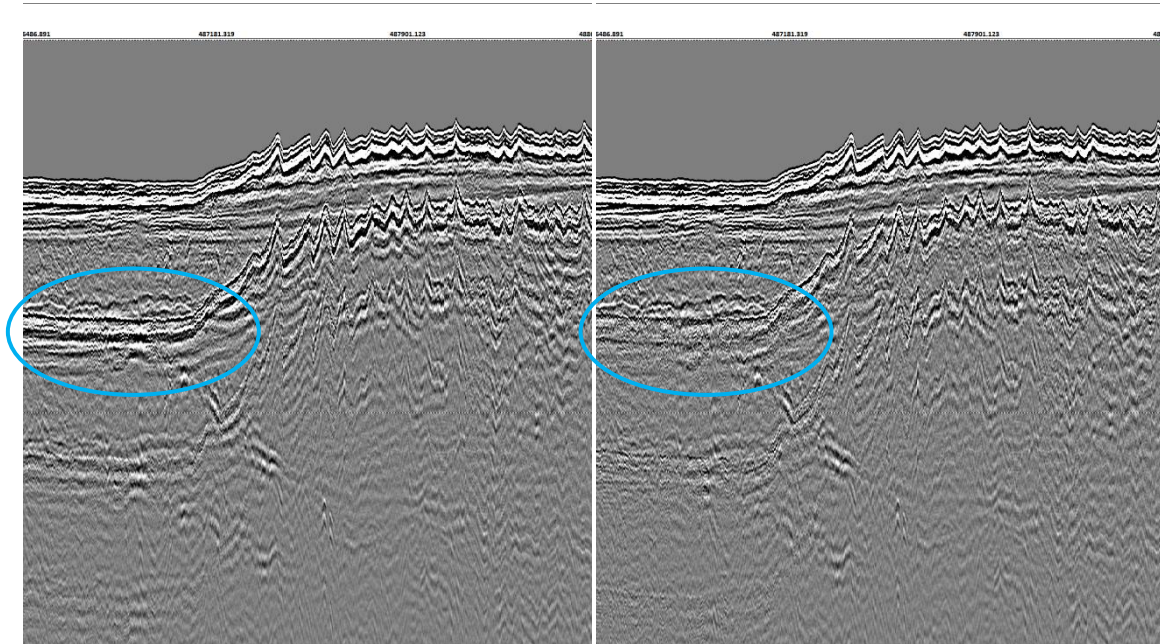


Figure B.2 – SIG sparker profile, test line across the Ostend Valley. Before (left) and after (right) demultiple

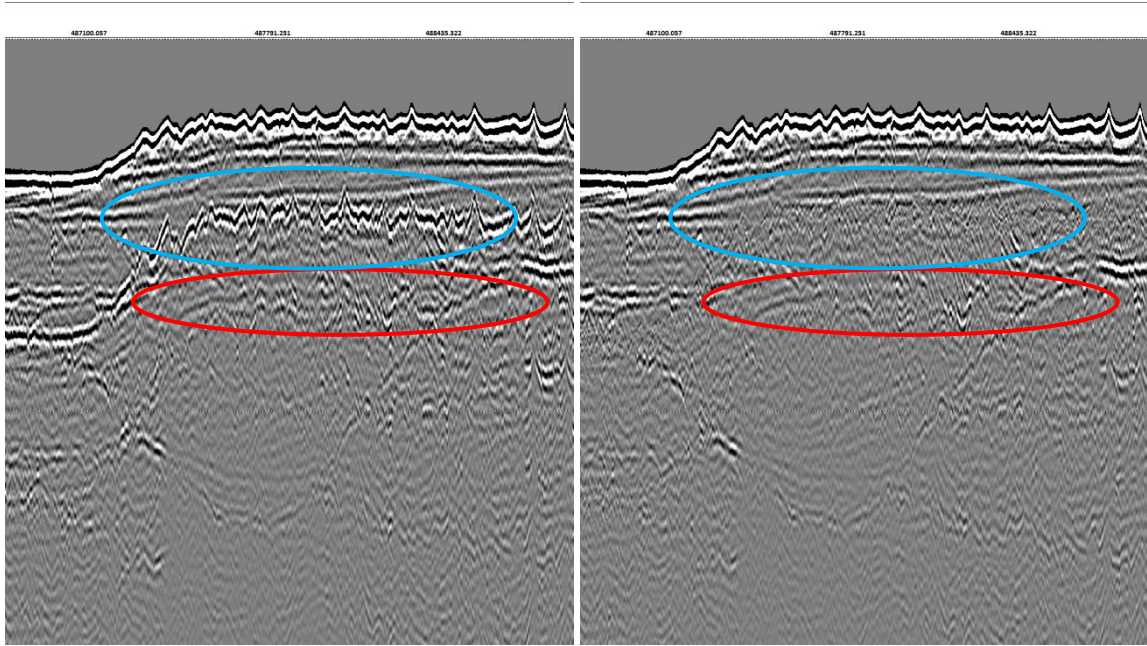


Figure B.3 – GeoSource 200 sparker profile, test line across the Ostend Valley. Before (left) and after (right) demultiple

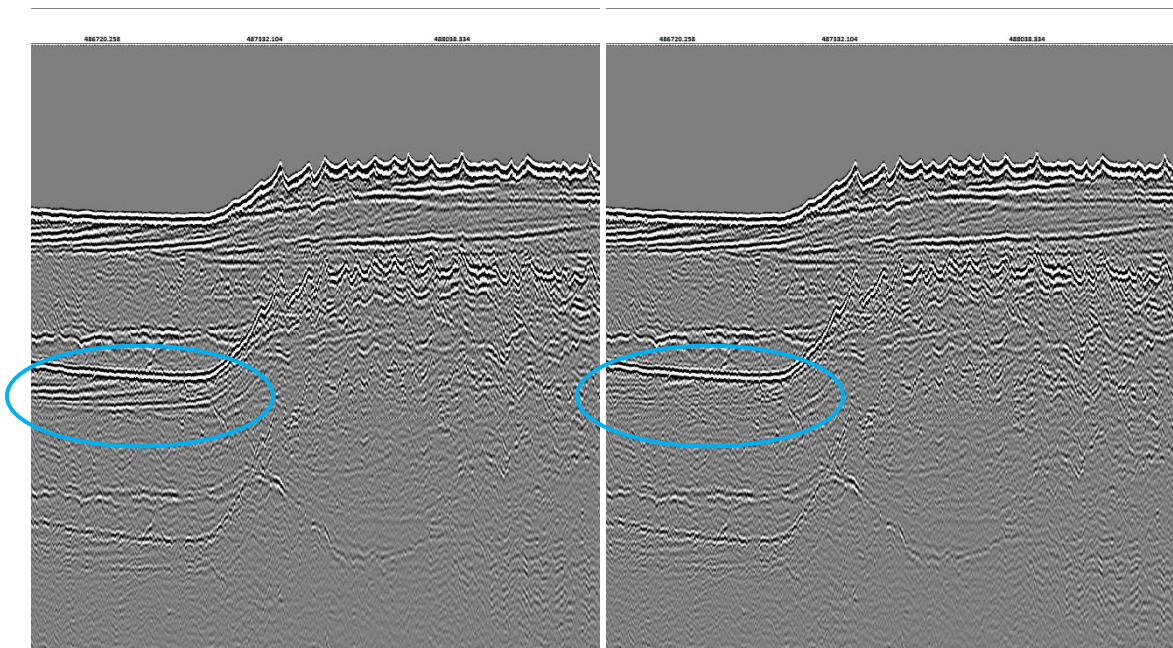


Figure B.4 – Centipede sparker profile, test line across the Ostend Valley. Before (left) and after (right) demultiple

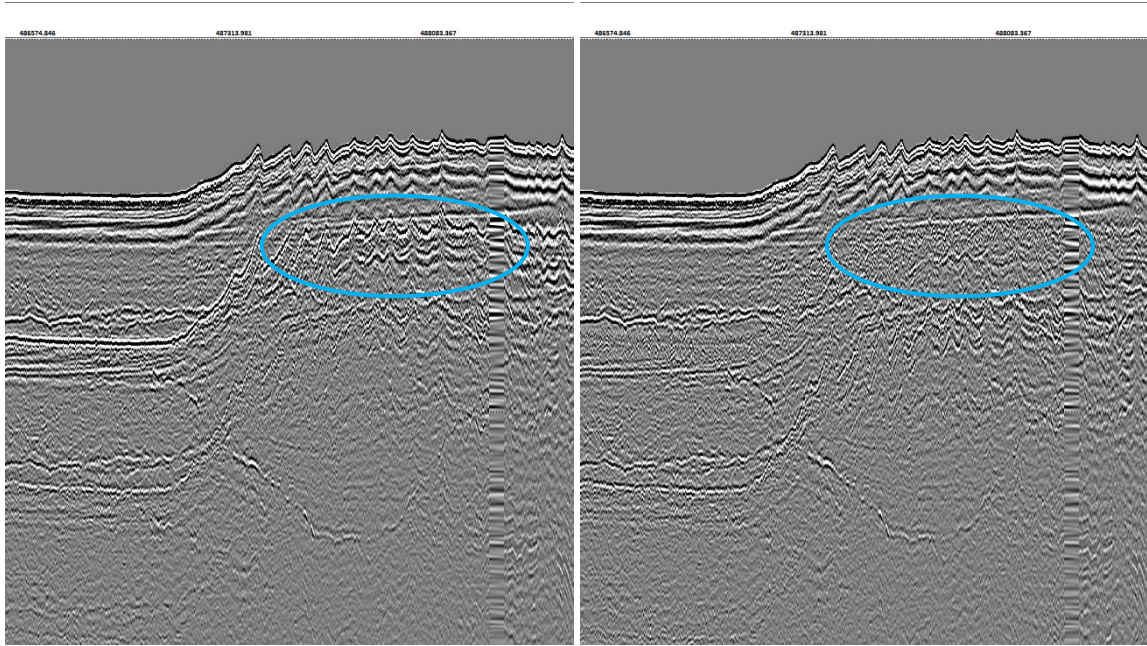


Figure B.5 – Seistec boomer profile, test line across the Ostend Valley. Before (left) and after (right) demultiple

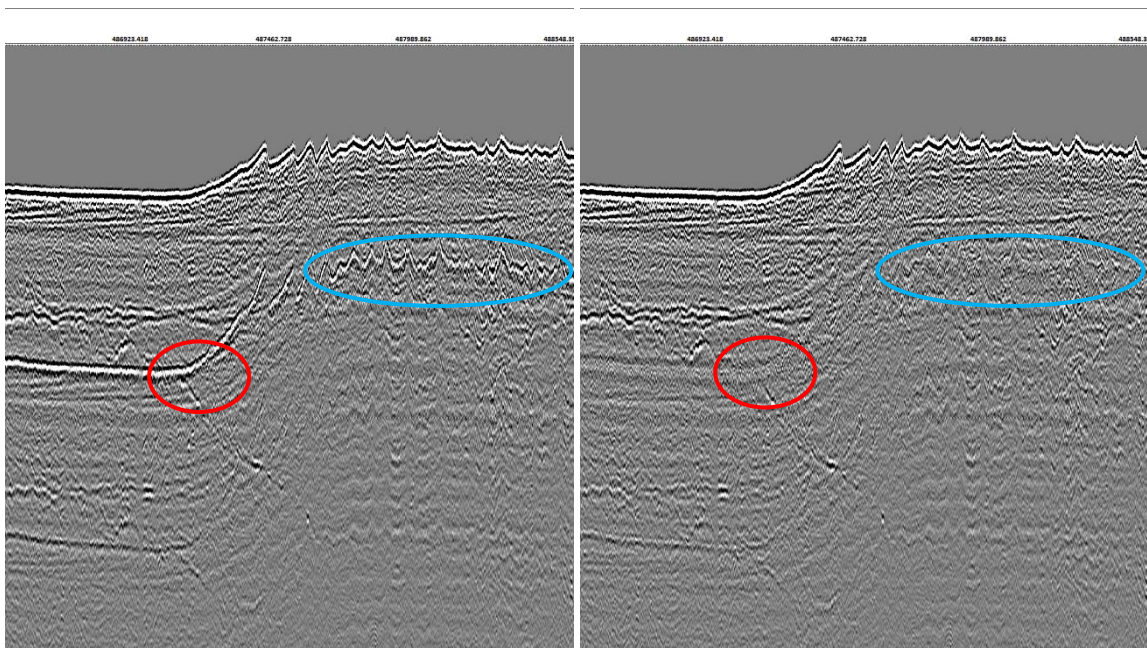


Figure B.6 – 500J boomer profile, test line across the Ostend Valley. Before (left) and after (right) demultiple

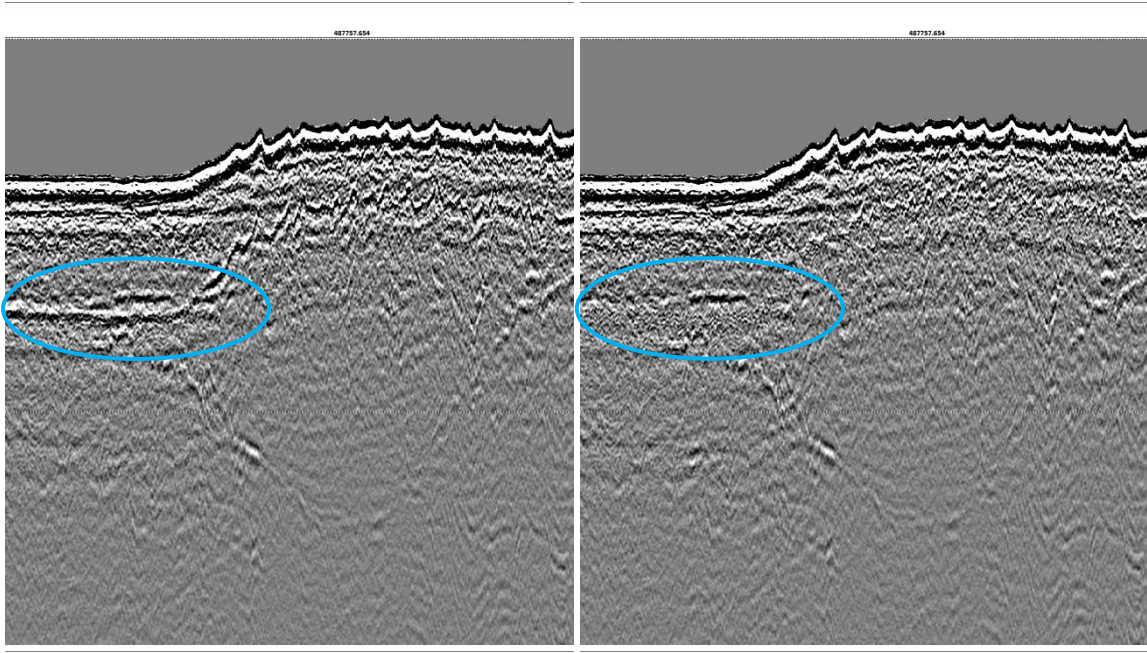


Figure B.7 – 300J boomer profile, test line across the Ostend Valley. Before (left) and after (right) demultiple

## Appendix C (Navigation systems specifications)

- Furuno GP-150 EGNOS DGPS receiver

**FURUNO**

GP-150/Dual

### SPECIFICATIONS OF GPS NAVIGATOR GP-150/Dual

|          |  |  |
|----------|--|--|
| <b>1</b> | <b>GPS RECEIVER</b>                    |  |
| 1.1      | Receiving frequency                    | 1575.42 MHz  |
| 1.2      | Tracking code                          | C/A code   |
| 1.3      | Number of channel                      | GPS: 12 channels parallel, 12 satellites                                     |
| 1.4      | Position fixing method                 | All-in-view, 8-state Kalman filter   |
| 1.5      | Accuracy                               |  |
|          | GPS:                                   | 10 m approx. (2drms)   |
|          | DGPS:                                  | 5 m approx. (2drms)  |
|          | WAAS:                                  | 3 m approx. (2drms)  |
| 1.6      | Ship's speed accuracy                  | 0.2kn (10kn or less), 2 % of ship's speed (more than 10kn)                   |
| 1.7      | Course accuracy                        | ±3° (within 1 to 17kn), ±1° (more than 17kn)                                 |
| 1.8      | Position fixing time                   | Warm start: 12 s typical, Cold start: 90 s typical                           |
| 1.9      | Tracking velocity                      | 999 kn   |
| 1.10     | Position update interval               | 1 s  |
| 1.11     | RAIM indicators                        | Safe, Unsafe, Caution  |
| 1.12     | Beacon receiver (internal kit, option) |  |
|          | Frequency range                        | 283.5 to 325.0 kHz   |
|          | MSK rate                               | 50, 100, 200 bps; select auto or manual                                      |
| <b>2</b> | <b>DISPLAY SECTION</b>                 |  |
| 2.1      | Display type                           | Monochrome LCD 122 x 92 mm, 320 x 240 dot matrix                             |
| 2.2      | Display modes                          | Plotter 1 (NU), Plotter 2 (CU), Highway, Navigation, Data                    |
| 2.3      | Projection                             | Mercator   |
| 2.4      | Track plotter display                  |  |
|          | Scale                                  | 0.02 to 320 NM, 14 steps   |
|          | Latitude limits                        | Between 85°N and 85°S  |
|          | Plot interval                          | By time 0 to 60m00s or by distance 0 to 99.99NM, sm or km, or halt           |
| 2.5      | Memory capacity                        |  |
|          | Track and Marks                        | 2,000 points   |
|          | Waypoints                              | 999 points with 12 characters comment each                                   |
|          | Route                                  | 30 (containing 30 waypoints/route) and 1 simplified route                    |
| 2.6      | Alarms                                 | Arrival and anchor watch, XTE, Speed, Trip, Water temperature*, Water depth* |
|          |  | *: external sensor required  |
| 2.7      | Satellite information                  | Satellite number, Bearing, Elevation, Signal level, DOP, Status              |

SP-1

E4440S01C-M

**3 INTERFACE**

|       |                 |   |
|-------|-----------------|---|
| 3.1   | Number of ports | 4   |
| 3.1.1 | Data format     | IEC61162-1 (JUL-2000), NMEA0183 Ver1.5/2.0  |
| 3.1.2 | IN:             | DATA 1 and 2*: AGFPA, DBT, DPT, MTW, TLL<br>HDG**, HDM**, HDT**, VBW**, VHW**   |
|       |                 | DATA 3: MOB from external device (contact closure),   |
|       |                 | DATA 4: DGPS correction data in RTCM SC-104 V2.0,<br>Waypoint data downloaded from YEOMAN plotter,<br>Waypoint data or nav aids information from conventional PC  |
|       | OUT:            | AAM, APA, APB, BOD, BWC, BWR, BWW, DTM, GBS, GGA, GLL,<br>GNS, RMB, RMC, Rnn, RTE, VTG, WCV, WNC, WNR, WPL, XTE,<br>ZDA (or LOGOUT depending on jumper setting for Port 3),<br>Waypoint data to conventional PC (Data 4 only) |
|       |                 | *GP-150-Dual: DATA 2 port is used for the system connection.  |
|       |                 | ** : GP-150 only  |

**4 POWER SUPPLY**

|     |                           |  |
|-----|---------------------------|--|
| 4.1 | Display unit              | 12-24 VDC: 0.8-0.4 A (w/ internal beacon receiver) |
| 4.2 | Rectifier (PR-62, option) | 100/110-115/220/230 VAC, 1 phase, 50/60Hz          |

**5 ENVIRONMENTAL CONDITION**

|     |                      |   |
|-----|----------------------|---|
| 5.1 | Ambient temperature  |   |
|     | Antenna unit         | -25°C to 70°C   |
|     | Display unit         | -15°C to 55°C   |
| 5.2 | Relative humidity    | 95 % at +40°C   |
| 5.3 | Degree of protection |   |
|     | Antenna unit         | IPX6  |
|     | Display unit         | IPX5 (USCG CFR-46)  |
| 5.4 | Vibration            | -2 - 5 Hz and up to 13.2 Hz with an excursion of $\pm 1$ mm $\pm 10\%$<br>(7 m/s <sup>2</sup> maximum acceleration at 13.2 Hz)<br>-13.2 - 100 Hz with a constant maximum acceleration of 7 m/s <sup>2</sup> |

**6 COATING COLOR**

|     |              |              |
|-----|--------------|--------------|
| 6.1 | Antenna unit | N9.5 (white) |
| 6.2 | Display unit | N3.0         |

- MGBTECH RTK GPS

### RTK-GPS



| General                        |  |
|--------------------------------|--|
| Product Name:                  | RTK-GPS                                    |
| Description:                   |  |
| Year of initial introduction : | 2007                                       |
| Height [m]:                    | 0.08                                       |
| Depth [m]:                     | 0.285                                      |
| Width [m]:                     | 0.215                                      |
| Total weight [kg]:             | 3.5  |
| Housing material:              | Powder coated thick aluminum               |
| Power                          |  |
| Operating power: min. [V]:     | 10   |
| Operating power: max. [V]:     | 30   |
| Typical consumption [W]:       | 4  |
| Internal power supply:         | 4 cell LiPo battery                        |
| External power supply:         | Wide input AC/DC adaptor or 10-30VDC power |

| Power   |                       |
|---|-----------------------|
| Operating time with internal power supply [hr]: | 8                     |
| Certifications:                                 | CE                    |
| Rechargeable with (auto)battery :               | Y                     |
| Direct car connection cable available :         | On request            |
| Environment                                     |                       |
| Operating temperature: min. [°C]:               | -20                   |
| Operating temperature: max. [°C]:               | 60                    |
| Humidity resistance:                            | 95% non-condensing    |
| Water sand and dust proof:                      | IP 65                 |
| Shock and vibration proof:                      | Y                     |
| ROHS compliance:                                | Y                     |
| WEEE compliance:                                | Y                     |
| Performance                                     |                       |
| No. channels:                                   | 136                   |
| Max. simultaneous tracked channels:             | 136                   |
| Tracked satellite signals:                      | GPS; GLONASS; GALILEO |
| SBAS differential signals:                      | EGNOS; WAAS           |
| Type of measurements:                           | full carrier          |
| Reacquisition time [s]:                         | 1.2                   |
| RTK Network Compatibility:                      | Y                     |
| MRS functionality:                              |                       |

| <b>Horizontal uncertainty</b>                           |   |
|---|---|
| code: DGNSS/RTC (constant part) [m]:                    | 0.35  |
| code: DGNSS/RTC (variable part) [ppm]:                  |   |
| phase: RTK rapid static (constant part) [m]:            | 0.002                                       |
| phase: RTK rapid static (variable part) [ppm]:          | 0.5   |
| phase: RTK kinematic (constant part) [m]:               | 0.006                                       |
| phase: RTK kinematic (variable part) [ppm]:             | 0.5   |
| phase: static post processing (constant part) [m]:      | 0.002                                       |
| phase: static post processing (variable part) [ppm]:    | 0.5   |
| phase: kinematic post processing (constant part) [m]:   | 0.006                                       |
| phase: kinematic post processing (variable part) [ppm]: | 0.5   |
| Initialization time on the fly [s]:                     | 7   |
| Range on the fly [km]:                                  | 25  |
| RTK network solution methods:                           | RTCM3                                       |
| <b>Recording</b>  |   |
| Memory medium :   | SD-Card                                     |
| Data capacity [MB]:                                     | 2000  |
| Type of data (on board recording):                      | SBF Raw data; NMEA                          |
| Data input :  | Depends on connected interface (Laptop/PDA) |

| <b>Communication: general</b>         |                            |
|---------------------------------------|----------------------------|
| Communication ports:                  | 4 RS232; 1 USB; 1 Ethernet |
| Simultaneous links:                   | Y                          |
| PPS Out:                              | Y                          |
| Bluetooth :                           | Y                          |
| <b>Communication: links</b>           |                            |
| Radio modems :                        | internal                   |
| GSM; UMTS phone modems:               | external                   |
| CDMA phone modems:                    | external                   |
| Landline modems:                      | external                   |
| <b>Communication: Protocols</b>       |                            |
| RTCM standards for differential data: | version 2.2; 2.3; 3.0; 3.1 |
| CMR standards for differential data:  |                            |
| Other formats for differential data:  | SBF                        |
| NMEA output format:                   | version 2.30               |
| other output formats:                 |                            |
| L-Band Compatible:                    | Veripos                    |
| Configuration method :                | PC software                |
| <b>More information</b>               |                            |
| Distinguishable features :            | Including heading output   |

- DGPS JRC JLR 7800

## (D)GPS navigator – specifications

| Model                     | JLR-7500  | JLR-7800  |
|---------------------------|---|---|
| IMO compliant             | ✓   | ✓   |
| <b>General</b>            |   |   |
| Display                   | 5.7-inch, white LED backlit, 320 by 240 pixels  |   |
| Dimmer                    | 4 stages (brightness, redshift, dark, off)  |   |
| Power supply              | 10.8V to 31.2V AC, <10W   |   |
| Serial data in/out        | output: 4 ch (IEC61162-1), input: 1 ch  |   |
| Contact signal in/out     | output: 2 ch, input 1 ch  |   |
| LAN                       | built-in 10/100 Mbps  |   |
| Data backup               | display: 2MB ROM, sensor: SRAM with battery   |   |
| Waypoint                  | 10,000 points, event memory 1000 points, WPT name: 16 characters  |   |
| Waypoint input            | LAT/LON, bearing/range, event, TD   |   |
| WPT/route data transfer   | via LAN and RS-232C   |   |
| Track/route               | 2000 points, 100 routes with 512 WPT per route  |   |
| Plot scale                | 0.2, 0.5, 1.2, 5, 10, 20, 50, 100, 200, 300 NM  |   |
| Plot interval             | 1 up to 60 min (1 sec) or 0.01 to 99.99 NM (0.01 NM)  |   |
| Navigation calculation    | select Great Circle and Rhumb line for each leg (total distance up to 99,999 nm)  |   |
| Screen mode               | LAT/LON, CDI (highway), trackplot, GPS sat. info, enter WPT/route planning, WPT info  |   |
| Alarms                    | arrival, anchor, boundary, off-course, no position fix, speed, trip, 1) temperature, 1) depth, HDOP   |   |
| Adjust magnetic variation | auto or manual  |   |
| Geodetic system           | 46 systems  |   |
| Units                     | NM/KTS, km/kPH, mi/miPH, m, ft, fm, °C or °F  |   |
| LORAN C/A convert         | convert LAT/LON to TD of LORAN C/A  |   |
| <b>GPS specs</b>          |   |   |
| Receiver/sensor type      | multichannel (12 ch), SBAS (1 ch)   | multichannel (12 ch), SBAS (1 ch), DGPS integrated    |
| Frequency                 | 1575.42 MHz ±1 MHz (C/A code)   |   |
| Satellite tracking        | up to 12 satellites   |   |
| SBAS                      | WAAS, MSAS, EGNOS   |   |
| Accuracy                  | 13 m (HDOP <= 5A off), 7 m (SBAS) 2dRMS   | 13 m (HDOP <= 5A off), 7 m (SBAS), 5 m (beacon) 2dRMS |
| Power supply              | 10.8V to 31.2V AC, <1.5W  | 10.8V to 31.2V AC, <2.5W                              |
| <b>NMEA</b>               |   |   |
| Version                   | 1.5, 2.1, 2.3   |   |
| Bit rate                  | 4800, 9600, 19200, 38400  |   |
| Output                    | GGA, RMC, GLL, VTG, GSA, GSV, DTM, GBS, GRS, GST, ZDA, GNS, 2) MSS, ALR, 3) VDR, 3) VHW, APB, BOD, BWC, BWR, RMB, XTE, ZTG, AAM, ALR, RTE, WPL, ACK |   |
| Input                     | HDT, THS, BDT, DPT, MTW, CUR, VBW, VHW, ACK, WPL, RTE ALR   |   |
| Interval                  | 1, 2, 3, 4, 5, 6, 7, 8, 9 sec and off   |   |
| <b>Environment</b>        |   |   |
| Operating temperature     | sensor -25° to 55°C, display -15° to 55°C   |   |
| Storage temperature       | sensor -40° to 70°C, display -25° to 70°C   |   |
| Operating humidity        | 0% to 93% non-condensing  |   |
| Water resistance          | sensor IEC60945 (ed.4), USCG CFR-46, display IP44   |   |
| <b>Optional items</b>     |   |   |
| Rectifier                 | NBG-320   |   |
| Printer (table mount)     | DPU-414   |   |
| Connection box            | CQD-10  |   |
| Data switching unit       | NCZ-777   |   |
| Junction box              | NQE-7700A   |   |
| Extension cable (15 m)    | CFQ-9000  |   |

1) Via external temp sensor/echo sounder 2) Only JLR-7800 3) Via external speed log/current meter  
For further information please contact:

All specifications are subject to change without notification.



**Japan Radio Co., Ltd.**

JRC  
Cessnalaan 40-42  
1119 NL, Schiphol-Rijk, The Netherlands  
T +31 20 6 580 750  
F +31 20 6 580 755  
E sales@jrceurope.com  
W www.jrceurope.com

**NAVTEAM**  
Professional Marine Electronics

NAVTEAM A/S  
Norgesvej 7 - DK-5700 Svendborg - Denmark  
Phone: + 45 63 21 80 80 - Fax + 45 63 21 80 81  
sales@navteam.com www.navteam.com

Copyright © 2009 JRC -09.01/35/1